

**JIMMA UNIVERSITY**  
**Jimma Institute of Technology**  
**Faculty of Mechanical Engineering**

**Thesis Title: Biomimetic structure-based parametric optimization design using a multi-objective algorithm of the crash box for passenger vehicle**

A thesis submitted to the School of Graduate Studies of Jimma University in Partial Fulfilment of the Requirements for the Degree of Master of Science in Mechanical Engineering (Design of Mechanical System)

**BY: ASHENAFI KENA DEFERSHA**

**Jimma, Ethiopia**  
**October 2021**



**JIMMA UNIVERSITY**  
**Jimma Institute of Technology**  
**Faculty of Mechanical Engineering**

Thesis Title: **Biomimetic structure-based parametric optimization design using a multi-objective algorithm of the crash box for passenger vehicle**

BY: [Ashenafi Kena Defersha](#)

Advisor: **Prof. Hirpa G. Lemu (Ph.D.)**.

Co-Advisor: **Mr. Abiyou Solomon (Ph.D. Candidate)**

**Jimma, Ethiopia**

**October 2021**

## DECLARATION

This research thesis entitled: **Biomimetic structure-based parametric optimization design using a multi-objective algorithm of the crash box for a passenger vehicle** is my original work and has not been presented for a dissertation, master's and bachelor's degree in any other university.

Researcher: Ashenafi Kena

Name

\_\_\_\_\_  
Signature

\_\_\_\_\_  
Date

**APPROVAL**

As a member of the examining board of open defense, we have checked and evaluated the Master's Thesis prepared and presented by Ashenafi Kena entitled “*Biomimetic structure-based parametric optimization design using a multi-objective algorithm of the crash box for passenger vehicle*”. Hereby we certify this work fulfilled the requirement of the Degree of Master of Science in Mechanical Engineering (Design of Mechanical System).

1. Mr. Iyasu Tafese (MSc):           Signature: \_\_\_\_\_ Date: \_\_\_\_\_

Chair person



Stavanger, Aug. 09, 2021

2. Prof. Hirpa G. Lemu (PhD):

Signature

Date

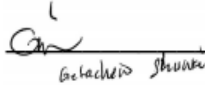
Main Advisor

3. Mr. Abiyou Solomon (Ph.D. Candidate):   Signature: \_\_\_\_\_ Date: \_\_\_\_\_

Co-Advisor

4. Mr. Ferew Tulu (MSc):           Signature: \_\_\_\_\_ Date: \_\_\_\_\_

Internal examiner

Signature:  Date: October 6, 2021

5. G. S. Tibba (Dr.-Ing.):

External examiner

## ABSTRACT

Associated with the popularity and wider use of vehicles as common means of transport there is a fundamental concern of safety during a journey. The risk of injuries and fatalities is severe when the vehicle structure is crashed during a collision accident, especially in a front collision where the bumper system, in which crash boxes play a great role to absorb impact load. Over the current global traffic accidents occurred by vehicle accidents are a very crucial problem in public health. Especially, during front collision accidents of passenger vehicle number of occupants get injured and die because of the crash box not absorb all impact load energy come from beam bumper. An adequate design and sufficient strength of the crash box superstructure for passenger vehicles can reduce the number of injuries and fatalities. During the crushing of the vehicle, it involves a complex interaction between body structure and interior system. Therefore, the energy absorption system design of the vehicle crash box should be in such a way that it should absorb the energy created during impact and should have blocked the shock transfer to the occupant area. To improve the crashworthiness and energy absorption performance of the crash box, this study was proposed eight hexagonal honeycomb structures reinforced by ribs connection of spider web and core woodpecker based on biomimetic structure design techniques (methods). The honeycomb configuration has been widely applied in the energy absorption structure design due to its energy-absorbing potential and advantage, which has been validated by some numerical and experimental studies. Spider orb-web frame silk structure is stronger per unit weight, compared to high tensile steel and has very high toughness capability equal to  $2.5 \times 10^8$  J/m<sup>3</sup> or usually expressed by  $1.5 \times 10^5$  J/kg. Also, the woodpecker is well known for the ability to absorb the strong shock from the process of drumming the hard trunk of trees and without any damage to its brain. After conceptual modeling, CAD modeling of these conceptual model structures is done in SOLIDWORK 2020 as a file of IGES. To evaluate the performances of models and compares each other the experimental simulation was carried out in LS-Prepost and post-process and LS-DYNA as a solver. As the ribs connection reinforcement increase with a constraint of mass to optimum point the crashworthiness of the crash box model was increased, as the P-5 (C2W) Multi-cell full quadrilateral and circular hexagonal tube and corner to wall ribs connection model result indicated. The result of P-5(C2W) was selected for validation and optimization, shows good agreement with three experimental results and improvement after parametric optimization in ANSYS 2020 R1 using a multi-objective genetic algorithm. After parametric optimization, the new optimized crash box of P-5(C2W) experimental simulation result shows good improvement of crashworthiness indicator than all other model and without optimization with the result of Peak Force 69.319 kN, mean crush force 25.99 kN, Total energy 9.060 kJ, Specific energy 6.864 KJ/Kg and crushing force efficiency (CFE) 0.375 respectively. The results of performance indicator for P-5(C2W) model after parameter optimization shows good increments specially in mean crush force which more countable for crashworthiness, with the result of 30.25 kN, peak crush force 69.13 kN, total energy 12.342 kJ and specific energy 9.35 kJ/Kg.

**Keywords:** Crash box, multi-objective optimization, biomimetic, structural bionics, honeycomb, spider web, and MOGA.

## ACKNOWLEDGMENT

Almighty God thank you for giving me such an opportunity. Next, it is my pleasure to express my deepest appreciation for his excellency to Prof. Hirpa G. Lemu (at the University of Stavanger, Norway) for exposing me to such indispensable work. Without his continuous support and guidance, as well as his encouragement during difficult periods the completion of this thesis work would not possible.

Then, I wish to express heartfelt thanks to my co-advisor Abiyou Solomon (Ph.D. Candidate), an instructor at the School of Mechanical Engineering, JiT, and. my Co-Advisor for his careful review, comments, and suggestions with regards to this thesis.

And I would like to acknowledge and appreciate all my friends and teachers who have been played a valuable role in my work by sharing supportive materials, data, information, and concrete ideas when I get confused and lost. Last, but not least, I thank my family, for all their help and understanding. Without your encouragement, love, and support, this work would never have been accomplished

## Table of contents

DECLARATION .....	I
APPROVAL.....	II
ABSTRACT .....	III
ACKNOWLEDGMENT.....	IV
TABLE OF CONTENTS .....	V
LIST OF FIGURES.....	IX
LIST OF TABLES .....	XII
ACRONYMS .....	XIII
SYMBOLS.....	XV
 CHAPTER ONE .....	 1
1. INTRODUCTION.....	1
1.1. Background .....	1
1.1.1. Safety Features in Automobiles and crashworthiness .....	2
1.1.2. Vehicle Safety Features.....	3
1.2. Statement of the problem .....	6
1.3. Objective .....	7
1.3.1. General objective.....	7
1.3.2. Specific objective .....	7
1.4. Research Questions /hypothesis .....	7
1.5. The motivation of the study .....	7
1.6. Scope and limitation.....	7
1.7. Methodology .....	8
1.8. The layout of the Thesis .....	10
 CHAPTER TWO .....	 11
2. LITERATURE REVIEW.....	11
2.1. Introduction .....	11
2.2. General Theoretical review/Conceptual Framework .....	11
2.3. General Characteristic for Energy Absorption Structure .....	13
2.3.1. Energy Absorption and performance indicators.....	13
2.4. Review on various factors affecting energy absorption of the crush box .....	14
2.4.1. Material of Crash Box .....	14
2.4.2. The shape of Crash Box .....	14

2.4.3.	Type of Analysis .....	14
2.4.4.	Impact Velocity .....	15
2.4.5.	The angle of Impact or loading .....	15
2.4.6.	Effect of Wall Thickness .....	15
2.4.7.	Effect of Width of Tube .....	16
2.5.	Approach and methodology for Biomimetic structure design .....	16
2.5.1.	Biomimetic approaches .....	16
2.6.	Biomimetic structure design methodology and tools .....	18
2.6.1.	TRIZ is a Primary Tool for Biomimetics for Geometrical structure modeling .....	18
2.6.2.	Morphological chart as a Primary Tool for Biomimetics for Geometrical structure modeling .....	20
2.7.	An integrated method of TRIZ, morphological chart, and biomimetics for product design concept generation .....	20
2.8.	Biomechanical characteristics and theoretical background of some biological structure .....	20
2.8.1.	Biomimetic Structure (bioinspired structure design) .....	20
2.8.2.	Impact load energy absorption characteristics of a honeycomb structure .....	21
2.8.3.	Impact load energy absorption characteristics of spider web structure .....	22
2.8.4.	Impact load energy absorption characteristics of woodpecker spongy tissue .....	22
2.9.	Analytical Energy absorption capability analyses and theoretical framework for a particular structure	23
2.9.1.	Bending dissipated energy ( $E_b$ ) .....	24
2.9.2.	Membrane deformation dissipated energy .....	25
2.10.	Computer-Aided Engineering (CAE) Tools used for Crash Analysis .....	29
2.10.1.	LS-DYNA .....	29
2.10.2.	MSC PATRAN .....	30
2.10.3.	MADYMO .....	30
2.10.4.	EASI CRASH DYNA (ECD) .....	30
2.10.5.	EASI-CRASH MAD .....	30
2.10.6.	Implicit and Explicit Philosophy .....	31
2.10.7.	Common Element used in Crash FE Analysis .....	31
2.11.	Research gap .....	31
2.12.	Summary .....	32
<b>CHAPTER THREE.....</b>		<b>34</b>
3.	<b>MATERIALS, CONDITIONS, AND METHODS.....</b>	<b>34</b>
3.1.	Material of Crash Box .....	34
3.1.1.	Energy absorbing materials and their characteristics .....	35
3.1.2.	Material modeling for theoretical (analytical) and numerical analysis .....	36
a)	Johnson-Cook strength and failure models .....	36
3.2.	Crash box design specification.....	39
3.3.	Structural and geometrical modeling of new crash box approach and methods .....	40
3.3.1.	Biomimetic structural modeling approach of new cashbox .....	40
3.3.2.	Biomimetic structural modeling methodology of new Crash Box .....	41
3.4.	The procedure of structural modeling of the crash box.....	43
3.4.1.	Develop TRIZ contradiction matrix from general TRIZ inventive solution principle .....	43
3.4.2.	Translate TRIZ recommended solutions to their specific ideas by the morphological chart .....	43



3.4.3.	Geometry specification using an integrated method of TRIZ, morphological charts, and biomimetics .....	44
3.5.	Biomimetics structure-based geometrical modeling of the crash box.....	45
3.5.1.	Structural modeling of the new crash box.....	45
3.5.2.	CAD Geometry modeling of the new crash box .....	46
3.6.	Analytical analysis of energy dissipation for developed conceptual design .....	46
3.6.1.	Bending dissipated energy (Eb) .....	46
3.6.2.	Membrane deformation dissipated energy .....	47
3.6.3.	Membrane deformation dissipated energy for design concept p-1 (SC-OHT) .....	48
3.6.4.	Membrane deformation dissipated energy for design concept p-2 (MC-FTHT) .....	48
3.6.5.	Membrane deformation dissipated energy for design concept p-3 (MC-ICHT) .....	49
3.6.6.	Membrane deformation dissipated energy for design concept p-4 (MC-DFHT).....	49
3.6.7.	Membrane deformation dissipated energy for design concept p-5 (MC-FQCHT C2C).....	49
3.6.8.	Membrane deformation dissipated energy for design concept p-6 (MC-FQCHT W2W).....	50
3.6.9.	Membrane deformation dissipated energy for design concept p-7 (MC-FQCHT (c2c&w2w)) ...	50
3.6.10.	Membrane deformation dissipated energy for design concept p-8 (MC-FQCHT C2W).....	51
3.7.	The mean crashing forces.....	51
3.7.1.	The mean crashing force of P-1, Single-cell original hexagonal tube (SC-OHT) .....	51
3.8.	Crashworthiness performance indicators .....	52
3.8.1.	Total energy absorption.....	52
3.8.2.	Specific energy absorption .....	53
3.8.3.	Mean crushing force.....	53
3.8.4.	Peak crushing force .....	53
3.8.5.	Energy absorption efficiency .....	53
3.8.6.	Crush force efficiency .....	53
3.8.7.	Fluctuation coefficient ( $\omega$ ) in plateau stage .....	53
3.9	Finite Element Method Computational Analysis Procedure .....	54
CHAPTER FOUR .....		59
4.	DESIGNXPLORER ANALYSIS AND PARAMETRIC OPTIMIZATION USING MULTI-OBJECTIVE ALGORITHM IN ANSYS .....	59
4.1.	Optimization and ANSYS.....	59
4.2.	Parameterization with Finite Element Analysis .....	59
4.3.	Parameter Optimization in ANSYS workbench.....	59
4.4.	Parametric optimization procedure .....	60
4.4.1.	Determine the design variables .....	60
4.4.2.	Approximate model of optimization objectives and constraints .....	61
4.4.3.	Defining Optimization modules .....	62
4.5.	Optimization Methods implemented.....	62
4.5.1.	DesignXplorer Implementation with Optimization.....	62
4.5.2.	Parametric Optimization Techniques .....	63
4.6.	Design of experiments and response surface modeling in optimization .....	65
4.6.1.	Set up generate for the response surface and response surface optimization. ....	65
4.6.2.	A MOGA optimization Setup .....	68
4.7.	Sensitivity analysis of parameters .....	69

CHAPTER FIVE.....	70
5. RESULTS AND DISCUSSION .....	70
5.1. Results and discussion of Biomimetic structure modeling of crash box.....	70
5.2. Analytical analysis result discussion.....	71
5.3. Experimental simulation result of the crash box .....	73
5.4. Model verification.....	74
5.4.1. Energy conservation.....	74
5.5. Crashworthiness Evaluation.....	76
5.5.1. Deformation mode.....	76
5.5.2. Performance indicators.....	78
5.6. Result and discussion in terms of performance indicator.....	78
5.6.1. Concept design p-1 (SC-OHT).....	78
5.6.2. Concept design P-2 (MC-FTHT) .....	79
5.6.3. Concept design P-3 (MC-ICHT).....	79
5.6.4. Concept design P-4 (MC-DFHT).....	80
5.6.5. Concept design P-5 (MC-FQCHT (C2C, W2W, C2C & W2W and C2W)).....	80
5.7. Summary of results and comparison discussion all model in one.....	82
5.8. Consistency of the numerical results with analytical solutions.....	83
5.9. Finite element model validation.....	84
5.10. Optimization results .....	87
5.10.1. DesignXplorer analysis results.....	87
5.10.2. Response surface modeling and optimization.....	87
5.10.3. Sensitivity of all maximum output parameter .....	89
5.10.4. Response surface local sensitivity curve of maximum total deformation.....	90
5.10.5. Comparison of local sensitivity of all output parameter .....	90
5.10.6. The candidate parameter design point suggested by DesignXplorer .....	92
5.11. Simulation Results of the crash box with optimized parameter.....	92
5.11.1. Deformation mode.....	93
5.11.2. Performance indicator result .....	93
CHAPTER SIX .....	94
6. CONCLUSION AND RECCOMENDATION .....	94
6.1. Conclusion.....	94
6.2. Recommendation and future work .....	94
REFERENCE.....	96
APPENDIX- A.....	101
APPENDIX-B.....	104
APPENDIX-C.....	105
APPENDIX D.....	109

## LIST OF FIGURES

Figure 1.1 Illustration of the crumple zone (orange line) and safety cell (blue line) in car design [5] .....	2
Figure 1.2 Relative distribution of crash positions for the passenger vehicle [7]. .....	4
Figure 1.3 Crash box positions in the frontal bumper system [7]. .....	5
Figure 1.4 The old automotive crash box [8]. .....	5
Figure 1.5 Model, Structural design and simulation of lightweight Crash Box flow chart .....	9
Figure 2.1 Most common loading/deformation modes of TW tubes used in automobiles .....	15
Figure 2.2 Biomimetics top-down and bottom-up approaches. ....	17
Figure 2.3 Natural hexagonal honeycomb structure [55]. .....	21
Figure 2.4 Natural reinforced spiderweb structure [57]. .....	22
Figure 2.5 Natural woodpecker skull and pecked wood structure [59]. .....	23
Figure 2.6 Energy dissipation in bending deformation: (a) extensional elements; (b) stationary hinge lines; (c) ideal completely folding; (d) actual folding [64]. .....	24
Figure 2.7 Basic structural forms of the crash box [63]. .....	25
Figure 2.8 3-panel element and Simplification: (a) Pattern-1; (b) Pattern-2; (c) Simplification of convex and concave T-shape elements [54]. .....	27
Figure 2.9 (a) Right corner element and (b) 4-panel angle element [68]. .....	28
Figure 2.10 (a) Collapse mode of 4-panel angle element and (b) extensional elements [72] .....	29
Figure 3.1 Schematic of the problem of the normal impact of a circular plate by a cylindrical punch with a hemispherical nose [73]. .....	37
Figure 3.2 Top-down approaches of biomimetics design of cashbox and its procedure.....	41
Figure 3.3 Approach, methods, procedure, and steps of biomimetics structure design of cashbox.....	42
Figure 3.4 Integrated method of TRIZ, morphological chart, and biomimetics for crash box concept design generation.....	47
Figure 3.5 Bio-inspired concepts and geometries of (a) SC-OHT (original hexagonal tube), (b) MC-FTHT (full triangular hexagonal tube); (c) MC-ICHT (internal clone hexagonal tube), (d) MC-DFHT (double fill hexagonal tube), (e) MC-FQCHT (Full quadrilateral and circle .....	45
Figure 3.6 Figure 3.5 Bio-inspired concepts and geometries of (a) SC-OHT (original hexagonal tube), (b) MC-FTHT (full triangular hexagonal tube); (c) MC-ICHT (internal clone hexagonal tube), (d) MC-DFHT (double fill hexagonal tube), (e) MC-FQCHT (Full quadrilateral and circle.....	47
Figure 3.7 Importing IGES file crash box into LS-Prepost.....	54
Figure 3.8 The meshing of the crash box in LS-Prepost.....	55
Figure 3.9 Assigning boundary condition for crash box in LS-Prepost.....	55
Figure 3.10 Assigning material types and property for crash box in LS-Prepost.....	56
Figure 3.11 Defining connection and contact part for crash box in LS-Prepost.....	57

Figure 3.15 Assigning setting analysis for crash box in LS-Prepost.....	58
Figure 3.9 Finite element models of integrated bionic structures with the mesh size of 4 mm × 4 mm with its overall setup for modeling and simulation (a) SC-OHT (original hexagonal tube), (b) MC-FTHT (full triangular hexagonal tube); (c) MC-ICHT (internal clone hexagonal tube) .....	58
Figure 4.1 The crash box optimization process.....	60
Figure 4.2 Design variables of parameter optimization .....	61
Figure 4.3 MOGA method workflow.....	64
Figure 4.4 The outline of the project schematic window .....	65
Figure 4.5 The outline of the parameter set in the design of the experiment module .....	66
Figure 4.6 Outline schematic of the response surface set-up .....	68
Figure 4.7 Set-up demonstration for surface response optimization.....	68
Figure 4.8 Optimization Methods selection setup.....	69
Figure 5.1 Conceptual design CAD model based on the biomimetic structure .....	71
Figure 5.2 Mean crushing force comparison of theoretical result for all mode .....	72
Figure 5.3 Specific energy absorption comparison of theoretical result for all model .....	73
Figure 5.4 Deformation modes of representative lobes folding (a) SC-OHT, (b) MC-FTHT, (c) MC-ICHT and (d) MC-DFHT (e) MC-FQCHT (C2C) (f) MC-FQCHT (W2W) (g) MC-FQCHT (C2C & W2W) (h) MC-FQCHT (C2W). More lobes mean shorter fold length contributing to higher.....	77
Figure 5.5 deformation modes of representative lobes folding (a) SC-OHT, (b) MC-FTHT, (c) MC-ICHT and (d) MC-DFHT (e) MC-FQCHT (C2C) (f) MC-FQCHT (W2W) (g) MC-FQCHT (C2C & W2W) (h) MC-FQCHT (C2W) .....	77
Figure 5.6 Force vs. displacement curve for model p-1 .....	79
Figure 5.7 Force vs. displacement curve for model P-2.....	79
Figure 5.8 Force vs. displacement curve for model P-3.....	80
Figure 5.9 Force vs. displacement curve for model P-4.....	80
Figure 5.10 Force vs. displacement curve for model P-5(c2c) .....	81
Figure 5.11 Force vs. displacement curve for model P-5(w2w) .....	81
Figure 5.12 Force vs. displacement curve for model P-5(w2w and c2c).....	82
Figure 5.13 Force vs. displacement curve for model P-5(c2w) .....	82
Figure 5.14 Force vs displacement curve for all model specimens.....	83
Figure 5.15 SEA comparison between all model structure .....	83
Figure 5.16 (a) Agreement of mean force between experiment and simulation, only 4.53% error in representative MC-FQCHT (C2W) (P-5 C2W); (b) deformation modes also agree to some extent. ....	86
Figure 5.17 Validation comparison of J. Wang, Y. Zhang, N. He, and C. H. Wang experiment result with a present experimental simulation of model P-5 MC-FQCHT (C2W).....	87

Figure 5.18 Validation comparison of X. Xu, Y. Zhang, J. Wang, F. Jiang, and C. H. Wang experiment result with a present experimental simulation of model P-5 MC-FQCHT (C2W) .....	87
Figure 5.19 SEA increasing ratio comparison (validation)between a theoretical and numerical result.....	84
Figure 5.20 Plot of minimum safety factor vs design point .....	88
Figure 5.21 The 3-D response chart maximum total deformation .....	89
Figure 5.22 Sensitivity of input parameter vs. output parameter .....	89
Figure 5.25 Local sensitivity curve for the maximum total deformation.....	90
Figure 5.24 Local sensitivity of input parameter vs. output parameter.....	91
Figure 5.25 The spider chart of the maximum all output parameter.....	91
Figure 5.26 Optimum parameter candidates suggested by design explorer.....	92
Figure 5.27 Deformation mode of simulation optimized model .....	93

**LIST OF TABLES**

Table 2.1 List of general TRIZ inventive solution of principles .....	18
Table 2.2 Summary of factors that have a significant influence on the energy absorption.....	32
Table 3.1 Aluminum alloys properties .....	35
Table 3.2 Aluminum tempers .....	36
Table 3.3 Aluminum 7075-T651 reports for Automotive Crash Box material by using Johnson-Cook Model Parameters. ....	39
Table 3.4 Summary of product design specification for ACB [23, 74, 57].....	40
Table 3.5 Steps for top-down biomimetic approaches for crash box .....	41
Table 3.6 TRIZ contradiction matrix for ACB design .....	43
Table 3.7 ACB design strategy based on TRIZ recommended solutions.....	43
Table 3.8 Number of energies absorbed elements for all structures.....	48
Table 3.9 The formulated formula of mean crushing force for all structure .....	52
Table 4.1 design variable of parameter selected for optimization.....	61
Table 5.1 The summary result of mean crush force, total and specific energy from analytical analysis	72
Table 5.2 Meshed statistics for the parts model .....	73
Table 5.3 Simulation Results of a different conceptual design model of the crash box.....	78
Table 5.4 Information of the experiments for validation.....	85
Table 5.5 The three-option candidate value of optimized crash box parameters .....	92
Table 5.6 Simulation Results of the parametrically optimized crash box .....	93

## ACRONYMS

ACB: Automotive crash box,  
CAE: Computer-Aided Engineering  
CF: Crush force  
CFE: Crush force efficiency  
EA: Energy absorption  
ESC: Electronic stability control  
ETB: Ethiopian Birr  
FEA: Finite element analysis  
FSAE: Formula Society of Automotive Engineering  
GNP: Growth national product  
GSI: Gadd Severity Index  
GTRS: global technical regulations  
HIC: Head Injury Criterion  
MC-DFHT: Multi-cell double fill hexagonal tube  
MC-FQCHT: Multi-cell full quadrilateral and circular hexagonal tube  
MC-FTHT: Multi-cell full triangular hexagonal tube  
MC-ICHT: Multi-cell internal close hexagonal tube  
MCL: Mean crushing load  
MCL: Mean Crushing Load  
MOGA: multi-objective genetic algorithm  
NHTSA: National Highway Traffic Safety Administration  
NPR: Negative poisson ratio  
PCF: Crash Load Efficiency  
PCF: Peak Force  
PCF: photonic crystal fibers/peak crushing force  
PDS: product design specifications  
PET: Polyethylene terephthalate  
RCAR: Research Council for Automobile Repairs  
RCAR: Research Council for Automobile Repairs

SAE: Society of Automotive Engineering  
SC-OHT: Single-cell original hexagonal tube  
SEA: Specific energy absorption  
SEA: Specific Energy Absorption  
SSFE: Simplified Super Folding Element  
TPMS: Tire Pressure Monitoring System  
TRIZ: Theory of inventive problem solving  
TRL: Transport Research Laboratory  
TTI: Thoracic Trauma Index  
VIR: Viscous Injury Response  
VMT: Vehicle's miles traveled  
WHO: World Health Organization?



## SYMBOLS

\$: Dollars,

=: Percent

### **Greek letters**

$\nu$ : Poisson's Ratio

$\rho$ : Density

$\varepsilon$ : Equivalent plastic strain

$\sigma_u$ : Ultimate Tensile strength

$\sigma_y$ : Yield Strength or Yield Tensile Strength

G or  $\mu$ : Shear Modulus

### **Latin letters**

K: Bulk Modulus or Modulus of Rigidity

A: Elastic limit or Initial yield stress

B: Modulus of strain hardening or hardening constant,

C: Strain rate sensitivity index/constant

hr.: hours

Km: kilometer

Kg: kilogram

m: Meter

min: minutes

mm: millimeter

T: Current temperature

$T_m$ : Melting temperature

$C_p$ : Heat capacity of the material

Vol: Volume of element

t: Time

E: Young's Modulus or Modulus of Elasticity

C's: Material-dependent elastic constants

n: Exponent of strain hardening

N: Number of elements

m: Exponent of thermal weakening

## CHAPTER ONE

### 1. INTRODUCTION

#### 1.1. Background

Advances in technology have led not only to increasing numbers of vehicles and vehicles miles traveled (VMT), but also to higher speeds and more massive vehicles (e.g., large trucks, buses, and aircraft). This means that the vehicles themselves are costly structured and that, if they are involved in traffic accidents, the damage to people and the environment will be more serious. Motor vehicle-related accidents are a major worldwide health problem and constitute a great economic loss to society [1].

Nowadays, a road traffic accident is a major but neglected public health challenge. The World report on road traffic accident prevention has indicated that worldwide, an estimated 1.2 million people died in road traffic accidents each year and as many as 50 million are being injured and died, and injuries are a global problem of massive proportions [1]. In recent years, some important and major studies on the subject of road accidents and fatalities carried out by World Bank, World Health Organization (WHO), Transport Research Laboratory (TRL), and others have highlighted the growing significance of road crashes as a cause of death particularly in developing and transitional countries.

In developing countries, although they own only 32% of the motor vehicles in the world, the annual fatality per 10,000 vehicles ranges from 20 to 200 in low- or middle-income countries like African countries [2]. On the other hand, it varies between 1.5 and 5 in industrialized countries. Economically, the cost of road accidents is estimated at 1% of the Gross National Product (GNP) in low-income countries, 1.5% in middle-income countries, and 2% in high-income countries, estimates that global economic losses due to road traffic injuries are close to US\$ 518 billion annually [2]. From all those, the current and projected trends in motorization indicated that the problem of road traffic accidents will get worse, leading to a global public health crisis.

Africa is one of the highest road traffic death rates in the world, with little difference in rates between those countries categorized as low-income. Whereas the range of fatalities per 100,000 populations in countries of African region is not very wide, 70% of all the deaths occurred in ten countries that account for 70% of the regional population: Democratic Republic of Congo, Ethiopia, Ghana, Kenya, Madagascar, Mozambique, Nigeria, South Africa, and Tanzania [3]. But this incident was more affecting countries in sub-Saharan Africa.

Like many African countries, Ethiopia is facing an enormous road safety crisis. A road traffic accident was a probable cause for the loss of 36796 lives, 54731 serious injuries, 58987 light injuries, and 141063 property damage in the past eleven years [3]. The result of the study also introduces that a total of 291577 road traffic accidents were registered in Ethiopia in the past twelve years i.e., since 2007/2008. In Ethiopia, more than 276491 road traffic accidents, 912956km road network, and 681000 number of motorized vehicles were newly introduced since 2007/08 year [4]. This implies that as road traffic accident increases concerning motorized vehicle growth in this year except for the remaining study period.

### 1.1.1. Safety Features in Automobiles and crashworthiness

Millions of people throughout the world are killed due to road accidents. With the increase in vehicles, the number of collisions and fatalities has also increased. Given this, higher demand has been advocated to ensure higher standards of safety in vehicles. This has led to continuous research in designing efficient energy absorbers to dissipate energy during an accident and protecting the occupant in the vehicle using, among others, energy absorbers when a car crash occurs.

In crushes, many variables affect the outcome of the crush. When the car crash by another car or an obstacle the impact will destroy the car and kill the passenger because of the large equal and opposite forces acting on the car. To make the crush survivable it must be reduced below the human body limits. As Newton stated in his second law  $F=ma$ , to decrease the force acting on the car the acceleration must be reduced. In other words, the time of the impact must increase. The crumple zone or also known as crush space as shown in Figure 1.1 is designed to take the impacts of the crush and move the force away from the passenger. The Crumple zone is carefully designed to fail predictably to help stretch out the time of the impact. This can be done by using varying and construction techniques.

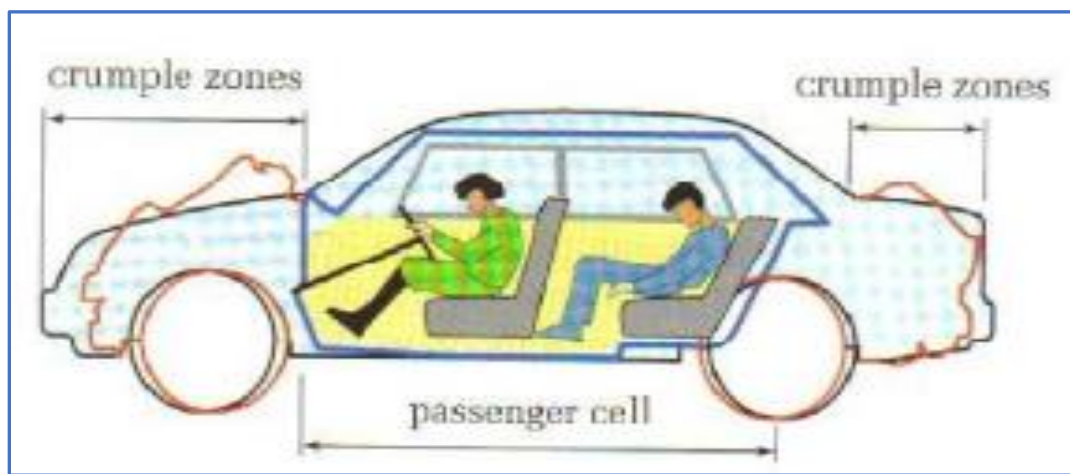


Figure 1.1 Illustration of the crumple zone (orange line) and safety cell (blue line) in car design [5]

The crumple zone is normally built in a shape of a honeycomb design because this shape gives stiffness under normal conditions, but can collapse and crumple in the crash. This results in the crumple zone becoming a great shock absorber through its failing events. In a normal crash setting the crumple of the car will channel the impact force around the vehicle making the front or the back of the car deformed. The only thing that is left is the passenger cell or safety cell. This means that the crumple zone has done its job but the crumple zone is also designed to work most effectively with other features in a car, like an airbag, seatbelt, etc. When all the features work together the driver will come out unhurt from the collision. Crumple zone has a great impact on people and company economically. The reason for this is that now people that are looking to buy a car would like to have a built-in safety feature to protect them from an accident that might happen at any time. This will give the automobile industry good business. So, the better the safety features the more people will buy them.

### *1.1.2. Vehicle Safety Features*

In the event of a collision, the vehicle safety cage protects occupants by maintaining survival space and dissipating collision forces that otherwise the occupants would be exposed to. Safety cages work in conjunction with seatbelts and airbags to slow occupants over the longest possible time and distribute crash forces over the largest area possible. When these systems function correctly, they effectively decrease the loads exerted upon occupants in a crash and reduce the severity of any resulting injury. The safety features that are introduced into vehicles can be of two categories (I) active and (II) passive safety features. While the former features are for proactive measures to avoid the crash completely, the latter is for reactive measures to reduce the severity of injury after the crash has occurred.

occurred.

I. Active Safety features include:

1. ABS: anti-lock braking system
2. ESC: electronic stability control
3. Adaptive cruise control
4. Automatic braking system
5. Daytime running lights
6. Tire Pressure Monitoring System (TPMS)
7. On-board breathalyzer

II. Passive Safety features include:

1. Seat belts
2. airbags
3. Energy absorbers
4. Pre-tensioners
5. Load limiters
6. Crumple zones

In general, vehicle safety must have the following features to protect occupants:

1. Minimize crush to maintain survival space.
2. Provide proper restraint throughout the entire accident event.
3. Prevent ejection from the vehicle and nominal seating positions.
4. Distribute energy and dissipate crash forces.
5. Prevent post-crash fires.

In crashworthiness optimization, vehicle safety is significantly reducing the impact of accidents and save both occupants and other traffic partner's life. Within the discipline of vehicle safety, the area of passive safety aims to reduce the severity of impact through structural design and it is the area where novel materials, such as composites and novel structural geometry may yield improved vehicle performance.

Car accidents are the major accidental collisions between automobiles. It can damage one or more autos, people, and structures. Anonymous terms for car accidents used in the literature are traffic accidents, auto accidents, road accidents, and motor vehicle accidents. Types of car accidents fall into several major categories:

- Rear-end collisions
- Side collisions
- Rollovers
- Head-on collisions

For every crash (collision) different crash severity causes the risk of injury to the occupants. But based on a survey of different studies most accidents happen by the frontal impact which causes severe head and pelvis injuries to the occupants in which the front bumper system plays an important role in the passive safety of the car [5]. Therefore, to avoid or reduce the injuries caused due to accidents due to the front impact, the front vehicle structure should be crashworthiness. Crashworthiness is the science of optimizing vehicle structures that can absorb crash energy. Vehicular passive energy absorption plays an important part during a frontal crash for passenger safety, the optimization of the frontal components is the key to increasing energy absorption due to large parameters [6].

When evaluating real-world crashes involving at least one car, about 50.5% of all crash events are frontal impacts, while side impacts account for 33.7% of all accidents, and rear impacts make up 15.9% of accidents, as shown in Figure 1.2 [7]. Frontal impact with full coverage amounts to only 31.1% of all typical frontal crash accidents, while the majority of crashes cover only a small proportion of the vehicle front. This makes it necessary not only to design the frontal section of the vehicle to absorb the kinetic energy of the vehicle in an accident but also, to design different zones into the vehicle front which can cope with various crash cases.

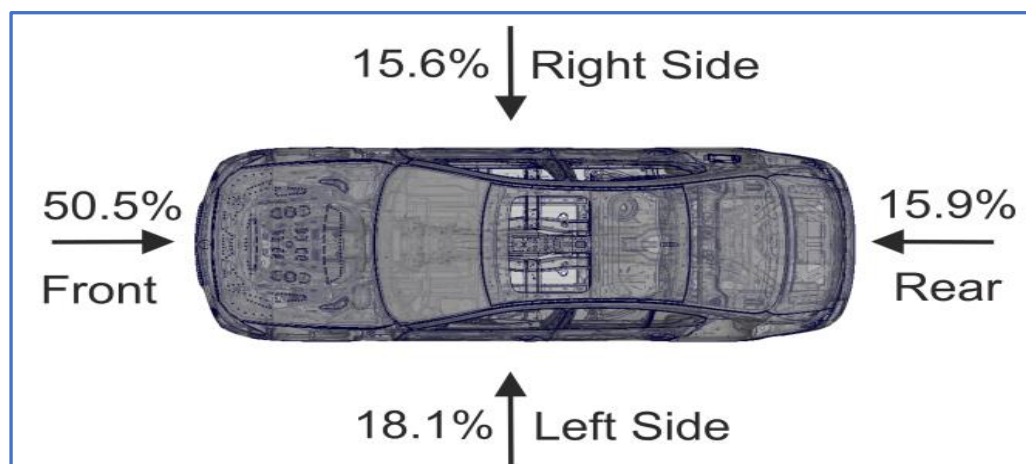


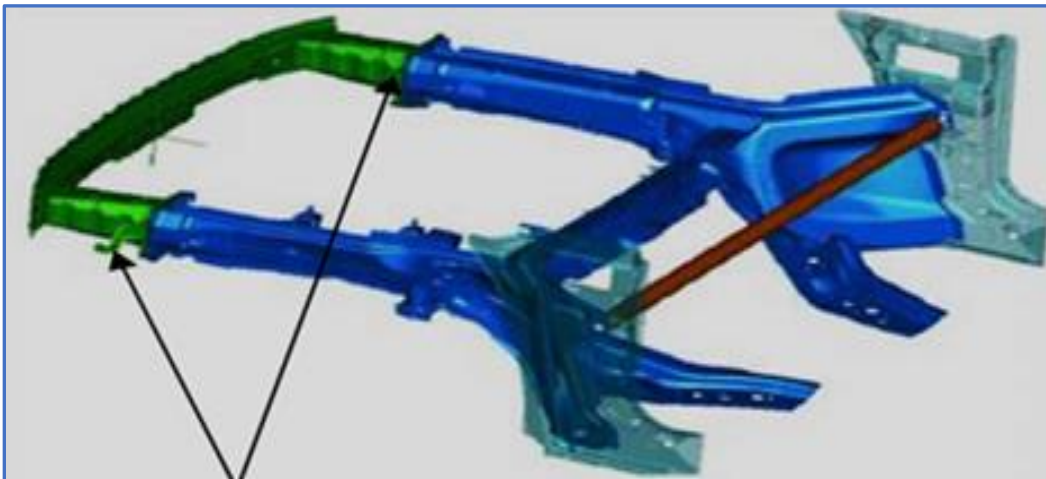
Figure 1.2 Relative distribution of crash positions for the passenger vehicle [7].

Therefore, to ensure passenger safety, there are various crashworthiness requirements like deformable and yet stiff, front structure with crumple zones to absorb the crash, properly designed side structures, strong roof structure, properly designed restraint systems, etc. Out of all the above requirements, one option is that the vehicle's front structure should be deformable to absorb energy. This is the reason

why the recent studies focus on the front structure from the reality that head-on collision or front collision is the most frequent accident of all the types of traffic accidents.

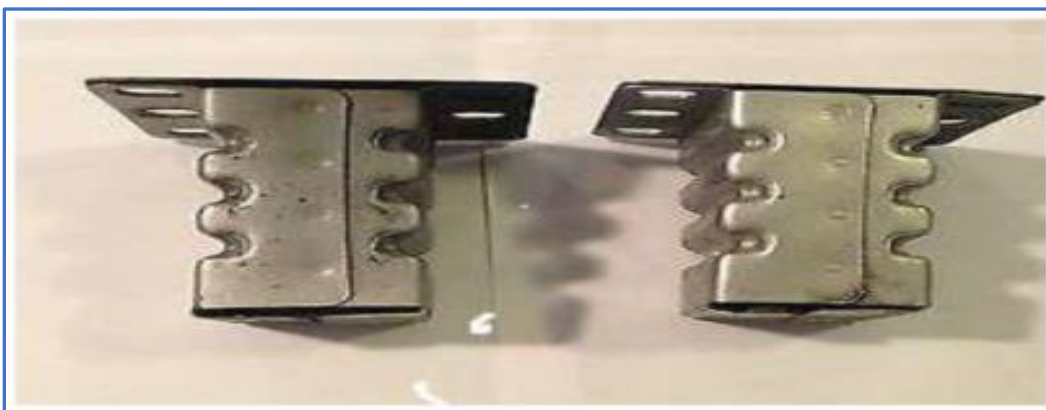
When a frontal crash occurs, the bumper system that consists of a bumper beam, crash box, and front rail absorbs about 70% of the total impact force [7]. That means the crash box plays a great role in saving occupants by transmitting the crushing force to the stringer and disperse it during a collision, to improve the passive safety performance of the vehicle. It absorbs the energy in the low-speed and high-speed impact through deformation to reduce the damages to the car and the casualties of the passengers.

The crash box is the most important device mounted between the front bumper and mainframe of a car, as it is shown in Figure 1.3 to absorb impact energy during a collision crash to minimize the damage to passenger and automobile parts damage. The crash box will absorb the impact energy by deforming itself. On the one hand, it can absorb the energy from the beam as much as possible, to reduce the collision damage to the front part of the car body and protect the safety of passengers. It buckles when the axial compressive force exceeds the limit and energy is absorbed during buckling and damage to the mainframe is avoided



*Figure 1.3 Crash box positions in the frontal bumper system [7].*

Also, the old crash box is shown separately as the following Figure 1.4.



*Figure 1.4 The old automotive crash box [8].*

Therefore, the design of the crash box has a great influence on the energy absorption performance of the bumper system and the collision force distribution of the vehicle. Generally speaking, the energy absorption effect of the crash box is closely related to the shell's shape, structure, and inner filling material [3]. As for the shape and structure, the traditional crash box mostly adopts the column shape with a rectangular section or a certain taper shape and improves the low-speed anti-collision performance by improving the shape, thickness, and section structure.

Recent attempts to improve crashworthiness are the use of the biomimetic approach, a word derived from the Greek word biomimetic, which is a highly interdisciplinary field. It involves the understanding of biological functions, structures, and principles of various objects found in nature and the design and fabrication of various materials and devices of commercial interest. The word biomimetic first appeared in Webster's dictionary in 1974 and is defined as 'the study of the formation, structure or function of biologically produced substances and materials (as enzymes or silk) and biological mechanisms and processes (as protein synthesis or photosynthesis) especially to synthesize similar products by artificial mechanisms which mimic natural ones' [8].

In general, the structural design and energy absorption characteristics of current bio-inspired structures with different configurations such as multi-cell and multi-corner tubes, hybrid tubes, frusta, sandwich panels, composite plates, honeycombs, and other specific structures. But there have some limitations, that some do not consider loading condition, some do not consider bending character during the condition, some are only considering low-speed impact in contrast nowadays front car accident is due to high speed. Besides, bio-inspired structural design is a new research area and not more study done on and there is money biological structure to be researched for energy absorption structure. From the spider, web and honeycomb are the major. Therefore, depending on indicated gap this thesis introduces the structural biomimetic to the structural design of the crash box and proposes a new structure design, by taking (imitating) the honeycomb for outer structure and one-layer spider web structure that reinforce at the center by fiber foam as a biometric object.

## 1.2. Statement of the problem

The motor vehicle-related accidents are a major worldwide health problem and constitute a great economic loss to society. The World report on road traffic accident prevention has indicated that worldwide, an estimated 1.2 million people died in road traffic accidents each year and as many as 50 million are being injured road deaths and injuries are a global problem of massive proportions [1]. When evaluating real-world crashes involving at least one car, about 50.5% of all crash events are frontal impacts [7]. Hence, the automobile industry is trying to improve three themes which are energy conservation, safety, and comfort.

Further, due to this humongous increase of vehicles on the road, and that traditional structure of the crash box is unable to efficiently solve the problem of bending during the collision process and not ensure passenger safety many research universities are focusing on improving vehicle safety standards [9]. The safety and performance of Crash Box are also similar for impact Attenuators, as they all are affected by the weight, geometry, and boundary conditions used in the structure of the vehicle.

Past research and experiences had indicated that during collision of vehicle important role played by crash box, which absorbs maximum impact energy. Size and shape of crash box affects its impact energy absorption. Hence problem statement is “to find out optimum shape of crash box for maximum energy absorption and minimum critical deformation.”

### 1.3. Objective

#### 1.3.1. General objective

The general objective of this study is to develop a new structural optimized crash box for passenger vehicles by imitating the honeycomb, spider web, and woodpecker structure.

#### 1.3.2. Specific objective

The specific objectives of the study include:

- Conceptual design of crash box geometric structure using biomimetics techniques
- CAD modeling of conceptually designed crash box
- Experimental simulation and crush analysis of the conceptual designed crash box
- Crashworthiness comparison of crash box by performance indicator result from simulation
- Parametric optimization using multi-objective Algorithm in ANSYS

### 1.4. Research Questions /hypothesis

The research questions of this study are:

- How is the problem related to the crashworthiness of the vehicle?
- Is crash box, the major vehicle crashworthiness component?
- What are the factors (variables) that affect the performance of crashworthiness?
- What method is used to redesign and optimize the crash box?
- How is a new crash box evaluated and validated?

### 1.5. The motivation of the study

The application of biological systems to design engineering systems and structures has been practiced since the time human beings understood that nature generates good solutions. The transfer of knowledge from natural life forms to synthetic constructs is attractive because the living organisms and plants are optimized and efficient thanks to natural selection. Engineering structure functionality could thus be increased by mimicking the qualities of biological organisms. Bearing in mind all these over the current global traffic accidents occurred by vehicle accidents are a very crucial problem in public health. Especially, during front collision accidents of passenger vehicle number of occupants get injured and die because of the crash box not absorb all impact load energy come from beam bumper. Therefore, using the biological structure that has good mechanical structure to engineering structure, is a very important design of efficient crash box for passengers to reduce these problems.

### 1.6. Scope and limitation

This study will cover the structural optimization design and validation of the result with the latest and that have a similar structure to previous experimental work results. Thus, the scope of the study includes:



- Structural optimization design and simulation of lightweight Crash Boxes.
- Achieve the structural (Crash Box) prerequisites of lightweight ACB.
- Improve the structural geometry of ACB.
- Structure design dynamic loading condition (impact/energy absorption).
- Multi-objective optimization
- Validation of the results with the published experimental test result.

As experimenting is demanding and costly, however, the comparison may be limited to theoretical analysis and experimental results that are available in published sources.

### 1.7. Methodology

There are two ways of modeling the structure of Crash Box, which are physical, and software modeling analysis. The physical model analysis of the Crash Box is not recommended because it is not economical, therefore the software modeling of the frame structure was performed by seating different approximate boundary conditions by following the SAE rules.

Structural design and simulation of lightweight Crash Box were performed by using SOLIDWORKS modeling from the conceptual design of the biomimetic structure. The finite element analysis was performed by using LS-PREPOST and LS-DYNA solver. Then the best model was chosen for optimization in ANSYS and further investigation.

The secondary data collection method is grazing different published papers, journals, looking up general vehicle's crash box and visiting the existing automotive company. Finally, Crash Box design and simulation with appropriate structural material that would have lightweight, better stiffness, and crashworthy properties used.

SOLIDWORKS Modeling and Finite Element Analysis by using LS-PREPOST and LS-DYNA solver

The finite element method (FEM) is a computational technique used to obtain approximate solutions for boundary value problems in engineering. There are different modeling and simulation software to perform the structural design and simulation of lightweight Crash Box. SOLIDWORKS software was used for creating a three-dimensional model of Crash Box structure by complying with Formula Society of Automotive Engineering rules. In addition, LS-PREPOST and LS-DYNA solver software was applied for finite element analysis of the lightweight crash box structure by applying a wide range of boundary conditions. The following procedures are used:

1. Data collection (Secondary data collection method which is grazing different published papers, journals, looking up general vehicles crash boxes, and visiting existing automotive companies).
2. By using SOLIDWORKS software, a three-dimensional structure of the Crash Box was created, by adopting the Formula Society of Automotive Engineering (FSAE) rules.
3. Model generation from SOLIDWORKS to LS-PREPOST:
  - Simplifications, idealizations.
  - Define materials/material properties.

- Generate a finite element model (mesh) or meshing software.
4. Solution generation stage:
- Specify boundary conditions by following SAE rules and other standard books.
  - Obtain the solution.
5. Review the results
- Plot/list results by seeing the total deformation, equivalent stress, equivalent elastic strain, and strain energy) and impact load (by examining the energy absorption of the Crash Box for the front impact case by seeing force, acceleration, total energy absorption, and displacement concerning time))
  - Check the validity comparing with SAE rules.
- Note: Figure 1.5 shows how the structure design and simulation of lightweight Crash Box is performed by using finite element method steps.

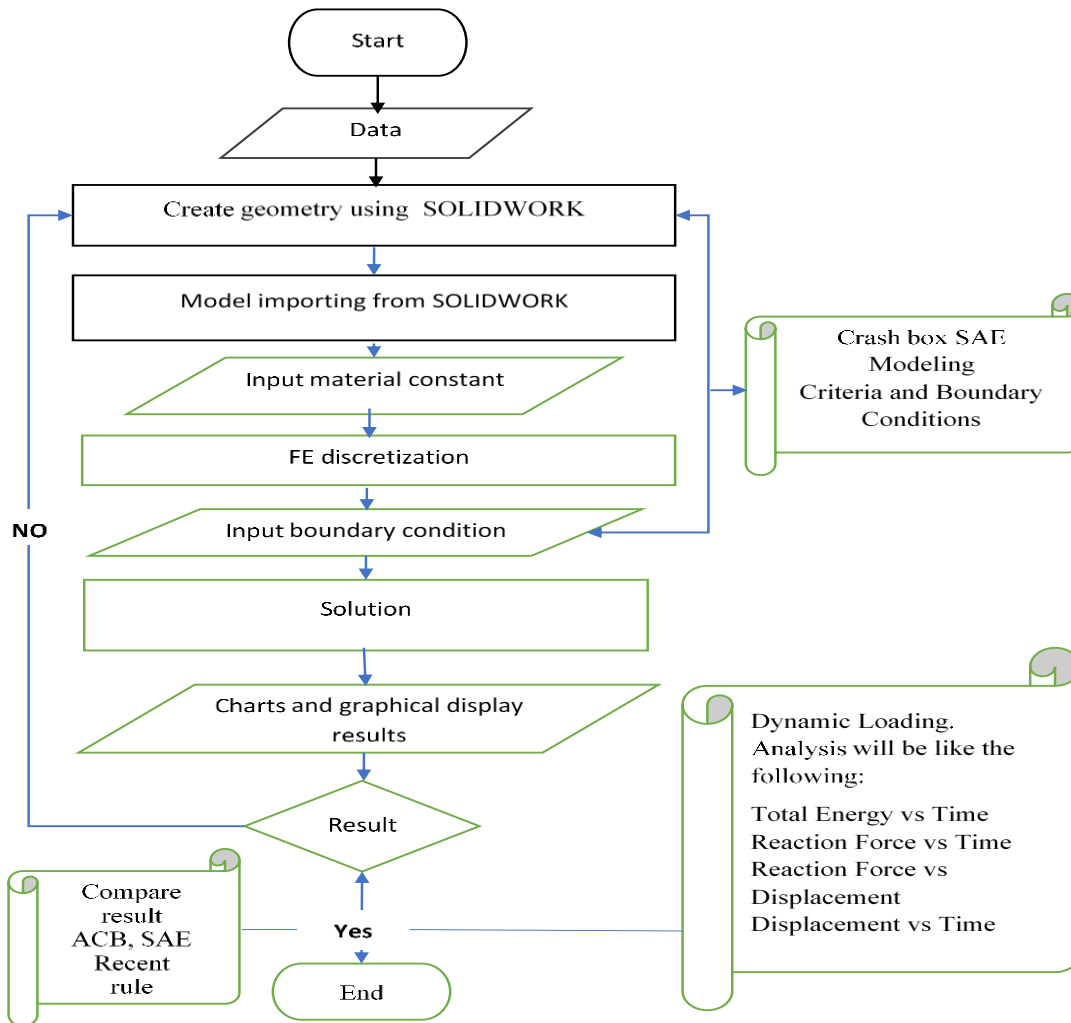


Figure 1.5 Model, Structural design and simulation of lightweight Crash Box flow chart

### 1.8. The layout of the Thesis

This “Structural Design, Simulation, and optimization of Lightweight automotive crash box” research paper is organized into five chapters:

In chapter one, introduction background, statement of the problem, the motivation of the research, objectives, scope, and methodology discussed, other than of Crash Box types, loading condition.

In chapter two, the survey of literature related to the research investigated, going through journals, articles, publications, and 2017-21 crashworthiness Rules books for Crash Box.

In chapter three, material modeling for Crash Box, geometrical modeling, finite element modeling, and analysis for Crash Box are discussed in detail.

In chapter four, the parametric optimization in the ANSYS workbench and variable sensitivity analysis can be carried out under this chapter.

In chapter five, the conceptual design based on biomimetic structure CAD developed in SOLIDWORK is displayed. Also, the finite element analysis results are displayed and discussed in detail for the best model of Crash Box using different figures, charts, and tables.

In chapter six, conclusions, recommendations, and future work for “Structural Design optimization and Simulation of Lightweight of the automotive crash box” are discussed, concerning weight reduction, geometrical improvement, and another main point.

## CHAPTER TWO

### 2. LITERATURE REVIEW

#### 2.1. Introduction

In the past years, many types of research have been carried out on the design and optimization of vehicle crashworthiness. Vehicle crashworthiness is a vital issue to ensure passenger's safety and reduce vehicle costs in the early design stage of vehicle design. The crashworthiness design aims to provide an optimized structure that can absorb the crash energy by controlled vehicle deformations while maintaining enough space in the passenger compartment. Optimization techniques have been used to reduce the vehicle design cycle. The traditional structure of the crash box is unable to efficiently solve the problem of bending during the collision process and not ensure passenger safety. Because of that, nowadays, researches on the crash box structure with good energy absorption characteristics mainly focus on the optimization design of the structural geometry and the cross-section shape. However, there are many organisms with fine mechanical properties in nature, which may provide new ideas for the design of the energy-absorbing structure with high efficiency. This chapter presents a review of the literature to address the problem of the crashworthiness of vehicle structures of crash boxes.

#### 2.2. General Theoretical review/Conceptual Framework

National Highway Traffic Safety Administration (NHTSA) recorded the first motor vehicle fatal accident that occurred in 1889 in New York City [10]. An early period of safety awareness regards to vehicle accidents initiated by the United States government started from the turn of the century to the year 1935 which is a period of genesis, growth, and development to understanding the extremely complex process of vehicle collisions. The second period started from the year 1936 to 1965, which was called an intermediate safety period with crash avoidance devices. After that period, numerous researchers studied and investigated deeply structure crashworthiness in enhancing the crash box capability. Energy-absorbing devices have been extensively used in all vehicles and moving parts such as road vehicles, railway coaches, aircraft, ships, lifts, and machinery. The aim is to protect these structures from serious damages while subjected to impact load or to minimize human injuries while collision has occurred in transportation systems. These energy-absorbing devices can dissipate kinetic energy in a wide variety of ways like friction, fracture, plastic bending, crushing, cyclic plastic deformation, and metal cutting [11].

As one of the most typical energy absorbers, thin-walled structures have been widely used in automobile, aerospace, and transportation engineering for their high ratio of energy absorption induced by progressive axial folding to structural weight. The early investigations of thin-walled structures were concentrated on the straight columns with circular, square, rectangular, and/or multi-corner cross-sections using analytical, numerical [12], and experimental methods [13]. In addition to straight columns, experimental and numerical studies were also conducted for tapered structures under axial or oblique loads [14]. Compared with straight tubes, taper tubes have been considered more preferable because they can more likely provide a desired constant mean load-deflection response and are capable of withstanding oblique and axial loads [15]. Furthermore, tapered tubes are less likely to fail in a global buckling, thereby avoiding an undesirable crushing.

Also, various structures like circular and square tubes, octagonal cross-section tubes, spherical shells, frusta, taper tubes, s-shaped tubes, composite tubes, honeycomb cells, foam-filled and wood-filled tubes may be used as collapsible energy absorbers. Amongst them, metallic cylindrical tubes have attracted much more attention due to their high stiffness and strength combined with the low weight and ease of manufacturing process, which leads to the low cost of the energy dissipating device [11]. Therefore, several theoretical and experimental investigations have been performed so far to introduce different methods of plastic collapsing in these structures. Axial crushing of tubes between two flat plates, external and internal inversion of tubes against the shaped die, and axial splitting and curling of cylindrical tubes against canonical dies are the most common energy dissipating methods, which have been realized and studied by several researchers so far [16]. However, investigation on the progressive folding process of thin-walled structures under axial load has been the subject of most of the researches.

Favorable crashworthiness characteristics for energy dissipation purposes can be achieved from the axial collapse of tubes while they crush progressively. Experimental and theoretical results have shown that depending on various parameters such as tube geometry, material properties of tube, boundary and loading conditions, circular tubes buckle in different modes of deformation, namely concertina, diamond, and Euler collapsing modes [11]. It is shown that when the tube length is greater than the critical length, the tube deforms in overall Euler buckling mode, which is an inefficient mode of energy absorption and needs to be avoided in crashworthiness applications. Different modes of deformation and load compression curves of round aluminum tubes of various geometric parameters were studied experimentally by [18, 19].

Having two types of collision i.e., low-speed and high-speed collision, most researchers investigated the crashworthiness of vehicle structures by considering only low impact speeds. Low-speed collision generally does not cause casualties and the primary absorbing energy is to reduce maintenance costs. High-speed collision is the main cause of occupant injuries, death, and high damage of property, which attracts the attention of the Government and researchers [19]. Hence to avoid all these Couse, improve the crashworthiness of the crash box further different researcher-made investigation by considering different types of factors. SBKIM et al. [20] investigated the different cross-section shapes on the effect of the crash-box crashworthiness. The study showed that the octagonal crash-box showed better crashworthiness, but the average cross-section force of the octagonal crash-box was larger.

Nowadays there are several types of research done biologically inspired design, adaptation, or derivation from nature or by 'biomimetics' to increase the performance of impact energy absorber devices. Wan et. al [21] study negative Poisson's ratios in auxetic honeycombs based on a large deflection mode and found that negative Poisson's ratios of auxetic honeycombs give a complete estimation of negative Poisson's ratios. In similar topic, Boria & Forasassi [22] made the investigation of honeycomb sandwich material modeling for dynamic simulations of a crash-box for a racing car through experiment as well as numerical approaches, to optimize the energy-absorbing capabilities of a thin-walled crash-box, made of sandwich material, for a racing car. In the study, [23] to develop a conceptual design of oil palm polymer composite automotive crash box (ACB) choose the model of honeycomb structure for the outermost profile and reinforced by spider web structure

inside the part. Because of the natural reality that Spider orb-web silk structure is stronger per unit weight, compared to high tensile steel and has very high toughness capability equal to  $2.5 \times 10^8 \text{ J/m}^3$  or usually expressed by  $1.5 \times 10^5 \text{ J/kg}$  [24] and taking advantage of the honeycomb structure which could provide very low weight, high stiffness, durability and production cost savings [22]. This means that spider web structures honeycomb structures can absorb very high shock impact energy during collision.

### 2.3. General Characteristic for Energy Absorption Structure

#### 2.3.1. Energy Absorption and performance indicators

The most popular form of collapsible energy absorbers, that are widely used to absorb the kinetic energy and to improve the crashworthiness behavior of a structure, is TW (thin-walled) components. The common use of TW components as energy-absorbing devices is due to many important aspects including superior performance under dynamic loading, cost-effectiveness, high efficiency, ease of manufacturing, and installation. Thin-walled energy absorbers were employed in many applications including aircraft subfloor structures [25], front structures of cars and trains [26], Rollover Protective Structures (ROPS) of heavy equipment used in agriculture and construction, such as earthmoving machinery and tractors [27].

Energy cannot be created or destroyed, but it can be changed from one form to another form. During an impact or crash, energy absorption occurs, in which the energy is changing form or converts into the internal potential energy of a system. Theoretical calculation of energy absorption can be calculated using impact theory [28]. The terms widely used to calculate and quantify the crashworthiness thin-walled crash box are Energy absorption (EA), Specific Energy Absorption (SEA), Mean Crushing Load (MCL), the Peak Force (PCF), and Crash Load Efficiency (CFE) Taking an axial crushing of crash box for calculation, the energy absorption is the integration of the crushing force concerning displacement  $x$  as below:

$$E(L) = \int F(X)dx \dots\dots\dots (2.1)$$

Where  $L$  denotes deformed length and  $F$  is the axial crushing force. A practical force  $V/s$  deformation curve of a crash box is illustrated in Fig-1 above. Mean load is an appropriate criterion to find the energy absorption capacity of an absorber. It is obtained by dividing the measured absorbed energy by the total crushing distance

$$P_{mean} = \frac{1}{\delta} \int Pd\delta \dots\dots\dots (2.2)$$

The specific energy absorption (SEA) is the ratio of energy absorbed to the structural mass  $M$  is the more specific criterion to measure the energy absorption capability of the crash box per unit mass, higher SEA numbers indicate the higher capacity of energy absorption per unit mass

$$SEA = (E_{Total} / M) \dots\dots\dots (2.3)$$

Crush force efficiency is defined as the ratio of mean crushing force to maximum crushing load. Crush force efficiency (CFE) =  $M_{ean} / P_{max}$ , Maximum the crushing force efficiency for energy absorbers used in crashworthiness design when the protection of occupants is a priority.

## 2.4. Review on various factors affecting energy absorption of the crush box

Factors that have a significant influence on the energy absorption such as shapes of tubes, materials, method of analysis, angle of impact, the velocity of the impactor, the most important thickness of the tube, and the cross-sectional width of the tube, etc. are listed in Table 2.2 as obtained from different sources.

### 2.4.1. Material of Crash Box

A crash-worthy material should absorb the kinetic energy of the impacting vehicle and also prevent the transfer of peak loads to the occupant cell. The use of appropriate material, geometrical shape, and features have the potential for major payoffs such as lower weight, design of higher stiffness areas which are stable energy absorption processes. Much research has studied either aluminum/aluminum alloy and steel [29, 30, 31]. Other materials like Glass Reinforced Composite, Kevlar Reinforced Composite have also been studied by some researchers [32]. Also, foam-filled aluminum is taken for the study [33]. Foams are used to improve energy absorption of the thin-walled crash box without increasing volume and weight too much, materials such as honeycombs and metal foams are often used as fillers for such structures. Filling of the column with moderate or high strength aluminum foam gives better Specific Energy Absorption (SEA, absorbed energy per unit mass as compared to steel, aluminum/ aluminum alloy has low density; hence it is widely used in lightweight applications. The maximum load-carrying capacity and energy absorbing capacity of the steel tubes were higher than those of the reinforced and Composite tubes due to the high strength rigidity of steel [32] and the energy absorbing capacity of steel tubes is 2 to 3 times higher than that of composite tubes.

### 2.4.2. The shape of Crash Box

Different shapes of tubes have been used for the study of energy absorption. The cross-sectional shapes of the tubes are Square, Rectangle, Circle, Hexagon, Octagon. Most of the research is based on square tubes [34, 35, 32, 36]. The circular profile is also studied by many scientists to prove as it is the most standard shape [29, 37, 38]. The elliptical shape is also considered for energy absorption [29] and the same is true for hexagonal. Another shape octagon is studied by few researchers [12]. For constant thickness and same perimeter, significantly lower energy absorption is found in square and rectangular profiles when compared with circular, hexagon, and octagon profiles at the time of axial crushing [20] and justify that octagonal profile absorbs slightly more energy during deformation than circular and the hexagonal profiles, which absorb nearly the same amount of energy.

### 2.4.3. Type of Analysis

Energy absorption can be determined using a real-time test, but due to the high cost of conducting real-time tests, finite element analysis (FEA) is used in the automotive industry before conducting a real-time test. By using FEA, industries have reduced the cost and time of the product development process while increasing the safety, comfort, and durability of the vehicles manufactured.

Quasi-static and dynamic analysis, are two types of analysis that are widely used to study the crushing behavior, mode of crush, and calculation of the energy absorber. Quasi-static analysis of tubes is preferred by some researchers [22, 39], while others have opted for dynamic analysis [36, 40].

However, loading in real-world accidental cases is primarily dynamic or impulsive [19]. Software is used for analysis in many cases, [22, 34]. Some are using ABAQUS [16, 22], while other researchers have used ANSYS-LS-DYNA [21, 41] and one researcher has used PAM-CRASH [18]. Few researchers have used both experimental and software, rest have compared their results with experimental results published by earlier researchers.

#### 2.4.4. Impact Velocity

For studying dynamic impact cases velocity of impact is varying widely. The impact velocity has a limitation of the experimental facility; the impact velocity was not higher than 10 m/s [34]. But the maximum of all frontal collisions takes place at speeds up to 56 km/hr. [42]. Few researchers have used the impact velocity range from 5 to 20 km/hr. with some increment value, to represent the range of low-speed impacts using which vehicle crash box is designed [28].

#### 2.4.5. The angle of Impact or loading

The most common loading situations of the thin-walled tubes used in the protection system of a road vehicle are axial, oblique, lateral, and bending loading, Figure 2.1. As an example, during a full-frontal collision scenario, the front longitudinal rails including the crash boxes undergo axial deformation mode and absorb around 50% of the total kinetic energy where the crash box itself accounts for around 15% of the total absorbed energy [43].

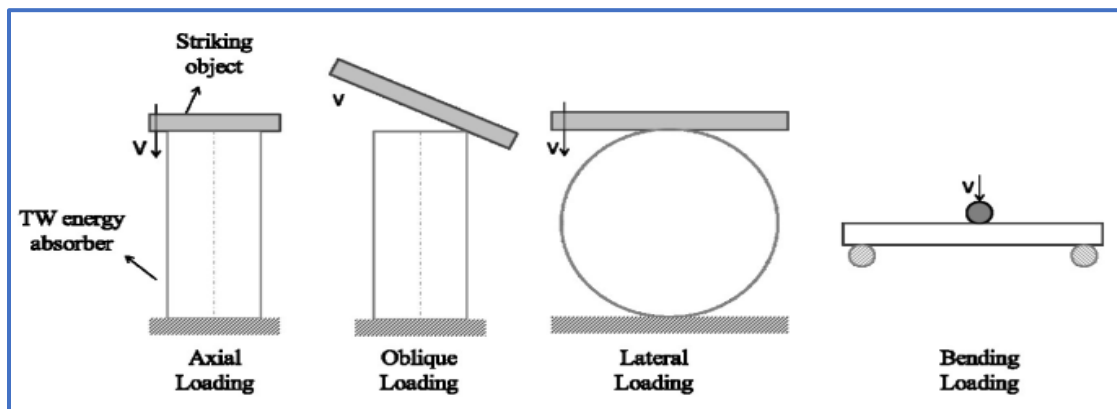


Figure 2.1 Most common loading/deformation modes of TW tubes used in automobiles

Some researchers have studied the axial crushing of the columns [44]. But oblique impacts are much more common in real crash events [45]. Oblique loading is considered by some researchers [14, 33]. Despite extensive research on axial crushing, crash boxes in real crash scenarios are usually subjected to oblique loading, i.e., the impact is not in the direction of the axis of the crash box. Research in this area is relatively limited [45]. Energy absorption drops drastically when global bending mode is initiated instead of progressive buckling, and it decreases further with increasing load angle. The mean load also decreases with increasing load angle. With an increase in load angle, peak crushing force (PCF) also decreases [21].

#### 2.4.6. Effect of Wall Thickness

With an increase in wall thickness energy absorption also increases [22, 34]. There is a subsequent increase in energy absorption of the crash box with increasing the thickness of the wall, because it



has more material to deform plastically. Hence, the energy absorption of a crash box if the length is kept constant increases with an increase in the wall thickness [19]. Referring to the mean force formula, we can say that width and thickness of the crash box are the most influential factor in energy absorption. Thickness affects energy-absorbing efficiency more strongly [46]. The down gaging of wall thickness also helps to reduce the peak crushing force because it leads to decreases of stiffness [22]. Wierzbicki’s & Abramowitz analyzed the crushing of a thin-walled multi-corner structure [25]. Mean crushing load for the symmetrical Crushing for square tube crash box under axial loading made of rigid-plastic material is given by:

$$P_m = 9.56 \times \sigma_0 \times (t^{5/3} \times W^{1/3}) \dots\dots\dots 2.4$$

Where t is the crash box thickness,  $\sigma_0$  is yield stress, W is the width of the square crash box. For an arbitrary angle between the adjacent faces of the crash box. Also, [13] further provided an improved model to predict mean crushing load previously defined for the average static crushing force for the asymmetric collapse of a square tube crash box to as:

$$P_m = 13.06 \times \sigma_0 \times (t^{5/3} \times W^{1/3}) \dots\dots\dots 2.5$$

**2.4.7. Effect of Width of Tube**

The response of energy absorbers is majorly influenced by their geometry parameters, such as cross-sectional dimensions [19]. With the increasing width of the crash box more material is available per fold for deformation and hence energy absorption also goes up. Also increasing the width of the crash box leads to an increase in the crushing load, since large impact loads are required to compress a high gauge crash box and which results in decreasing the number of tube folds in plastic deformation [22, 28]. The same is also evident from the above formula derived by Abramowitz. An increase in wall thickness also implies higher crash box mass and thus reduces specific energy absorption [21]. The profiles with large wall thickness and small profile width give a low relative fluctuation of the crushing force (i.e. a more stable folding process), while profiles with small wall thickness and large profile width give a large relative fluctuation of the crushing force (i.e. a less stable folding process) [18].

**2.5. Approach and methodology for Biomimetic structure design**

**2.5.1. Biomimetic approaches**

In the realm of biological organisms, the abundance of shape is a direct consequence of the evolutionary process that living beings undergo to constantly meet changing environmental conditions. The morphological features of each individual are the result of the constant interaction between the organism and its environment, under the influence of which populations of living beings adapt through selection and breeding, thus enhancing their probability of survival. The result is a compromise satisfying partially conflicting requirements which limit the potential of natural selection as an optimizing agent [47]. Moreover, typical optimization tasks in engineering science primarily focus on the determination of a set of parameters that produce the fittest outcome chosen from an array of different solutions by implementing deterministic algorithms that assure the convergence to the problem. The same cannot be said about biological systems, which achieve a high level of structural performance through redundancy and local differentiation of their constituent features.

Approaches to biomimetics as a design process typically fall into two categories: Defining a human need or designing problem and looking to the ways other organisms or ecosystems solve this, termed here Design looking to biology (Top-Down approach), or identifying a particular characteristic, behavior or function in an organism or ecosystem and translating that into human designs, referred to as Biology influencing design (Bottom-Up approach) [47].

**a) Design looking to biology (Top-Down approach)**

Throughout the literature review, this approach has different names as “Design looking to biology” (Top-down Approach) [47] and “Problem-Driven Biologically Inspired Design” [48], “challenge to biology” (Biomimicry Institute). They all have the same meaning and they also point to the way designers look to nature and organisms for solutions, where designers must recognize exactly their design problems and match their problems with organisms and creatures that have solved similar problems. This kind of approach is a result of the designer’s knowledge of the aims and triggers of their design.

**b) Biology influencing design (Bottom-Up approach)**

Just like the previous approach, this approach has different names and expressions such as “Biology Influencing Design”, “Bottom-Up Approach”, “Solution-Driven Biologically Inspired Design”, and “Biology to design”. They all refer to the same meaning, where this approach depends on the previous knowledge of biological research and solutions not to search for a solution in nature, then applying this knowledge to the design problem you already have (Figure 2.2).

TOP-DOWN	BOTTOM-UP
1. Design problem	6. design solution
2. Search for biological analogies	5. Technical implementation
3. Identification of appropriate principles	4. Abstraction, detachment from biological model
4. Abstraction, detachment from biological model	3. Understanding the principles
5. Testing analysis and feedback	2. Biomechanics, functional morphology and anatomy
	1. Biological research

*Figure 2.2 Biomimetics top-down and bottom-up approaches [47, 48].*

## 2.6. Biomimetic structure design methodology and tools

### 2.6.1. TRIZ is a Primary Tool for Biomimetics for Geometrical structure modeling

TRIZ was developed to support engineers and natural scientists in solving inventive problems by using the knowledge of former inventors. For this purpose, TRIZ offers a comprehensive set of methods to analyze and solve problems by considering different perspectives. The basic approach and central demand of TRIZ are solving inventive problems by its abstraction instead of approaching direct problem-solving. The abstracted problem is solved on an abstract level, which offers possible concrete solutions for the specific problem [49]. The abstract solutions are finally converted into concrete solutions. TRIZ was used as a set of procedures and tools to generate technical systems imitated from nature and developed the Bio-TRIZ matrix derived from the TRIZ Matrix of Contradictions.

Table 2.1 List of general TRIZ inventive solution of principles [49].

No	Engineering parameters	Inventive principles
1	Weight of mobile object	Segmentation
2	Weight of a stationary object	Extraction
3	Length of a mobile object	Local quality
4	Length of a stationary object	Asymmetry
5	Area of a mobile object	Consolidation
6	Area of a stationary object	Universality
7	Volume of a mobile object	Nesting
8	Volume of a stationary object	Counterweight
9	Speed	Prior counteraction
10	Force	Prior action
11	Tension/pressure	Cushion in advance
12	Shape	Equipotential
13	Stability of composition	Do it in inverse
14	Strength	Spheroidal
15	Time of action of a moving object	Dynamicity

16	Time of action of a stationary object	Partial or excessive action
17	Temperature	Another dimension
18	Brightness	Mechanical vibration
19	Energy spent by moving object	Periodic action
20	Energy spent by a stationary object	Continuity of useful action
21	Power	Rushing through
22	Loss of energy	Convert harm into benefit
23	Loss of substance	Feedback
24	Loss of information	Mediator
25	Loss of time	Self-service
26	Amount of substance	Copying
27	Reliability	Dispose
28	Accuracy of measurement	Mechanics substitution
29	Accuracy of manufacturing	Pneumatics or hydraulic construction
30	Harmful factors acting on an object from outside	Thin and flexible
31	Harmful factors developed by an object	Porous materials
32	Manufacturability	Changing the color
33	Convenience of use	Homogeneity
34	Repairability	Rejecting and regenerating part
35	Adaptability	Transformation properties
36	The complexity of a device	Phase transitions
37	Complexity of control	Thermal expansion

38	Level of automation	Accelerated oxidation
39	Capacity/productivity	Inert environment
40	Engineering parameters	Composite materials

### ***2.6.2. Morphological chart as a Primary Tool for Biomimetics for Geometrical structure modeling***

A morphological chart is a visual way to capture the necessary product functionality and explore alternative means and combinations of achieving that function. For each element of the product function, there may be several possible solutions. The chart enables these solutions to be expressed and provides a structure for considering alternative combinations. This can enable the early consideration of the product 'architecture' through the generation and consideration of different combinations of sub-subs that have not previously been identified. Used appropriately, it can help to encourage a user-driven approach to the generation of potential solutions [50].

### **2.7. An integrated method of TRIZ, morphological chart, and biomimetics for product design concept generation**

The TRIZ-based biomimetic part design possesses a great potential regarding part complexity and adaption for an innovative part design due to a layer-wise buildup offering multiple geometry variants from a broad design solution space. Thus, design optimization is a complex challenge for the designer that requires systematic design approaches. A methodology for a function-oriented systematic part design was used in this study besides the biomimetics method which partially integrated with TRIZ and morphological charts.

The TRIZ method provided a general solution that still needed to be interpreted further by the designers using several techniques [49]. Thus, the usage of a morphological chart could help to translate TRIZ recommended solutions to their specific ideas. Besides, the usage of the biomimetics method is based on the recommended solution. Combined (integrated) geometry was used in different design generations by the combination of two concepts of energy absorption from woodpeckers and spider webs. The integration approach between the three tools or methodology towards a more effective and efficient inventive design methodology. The paper used systematic a comparison between the tools based on functional modeling used during the process of problem-solving within TRIZ and Biomimetics.

### **2.8. Biomechanical characteristics and theoretical background of some biological structure**

#### ***2.8.1. Biomimetic Structure (bioinspired structure design)***

Nature has already found answers to all problems that we face today. It has developed systems and various modifications in itself to adapt to the different changes that happen all around us. It has been there before us and continues its life. Designs in nature ensure the greatest productivity for the least number of materials and energy. To create an architecture of meaning and beauty we need to return to the source - nature. We should make use of the materials and innovation provided by the natural

world and put them to good use according to their true nature, not merely to imitate the appearances of the past [51].

Biological structural or Bio-inspired materials are especially of interest to engineers and material scientists because of their hierarchical structures as well as mechanical properties superior to man-made counterpart materials and with a good energy absorption ability this makes them important to the Crash Box structure of the vehicle [52]. The ways by which nature can be inspired, in this study “Nature as the model” Biomimicry is a new science that studies nature's models and then imitates or takes inspiration from these designs and processes to solve human problems.

### *2.8.2. Impact load energy absorption characteristics of a honeycomb structure*

Honeycomb cellular structures, due to their lightweight and high energy-absorbing capability, have been used extensively as energy absorbers or cushions to resist external loads. A natural honeycomb consists of numerous hexagon cells as shown below Figure 2.3, which is prepared for multiple functions of honey storing, living, and reproduction. The honeycomb configuration has been widely applied in the energy absorption structure design due to its energy-absorbing potential and advantage, which has been validated by some numerical and experimental studies in comparing different section tubes [53]. The section of a cell is constituted as a hexagon with minimum material, withstanding external loads and foreign invasion to protect the population's safety from destroying.

Lured by the exceptionally high stiffness-weight to ratio, honeycomb-like configurations made of hexagonal thin-walled cells have been extensively utilized in engineering to play a role in absorbing a substantial amount of crashing energy when the impact occurs. Hence recent novel new design of the crash box, the single-cell hexagon honeycomb was chosen (picked) as an external geometry profile, taking advantage of the honeycomb structure which could provide very low weight, high stiffness, durability, and production cost savings [41, 54 55].



*Figure 2.3 Natural hexagonal honeycomb structure [55]*

### 2.8.3. *Impact load energy absorption characteristics of spider web structure*

The orb-web spider has evolved over the last 180 million years. This long period of evolution has made the present spider web, an elegant, natural, lightweight structure that efficiently resists different loads, such as wind and insect impact. It can function as a net for catching prey even if several elements are broken. Nature has accomplished these tasks by optimizing its form of construction, and by making spider silk a biopolymer with superior elasticity and tensile strength. Spider webs are one of the most efficient structures engineered by nature [56].

Spider webs are known for their high strength and damage tolerance. A spider web can maintain its performance even when it is damaged by wind or other insects. The spider's web is a highly efficient network of natural fibers where geometry plays a major role in unique properties such as significant strength, toughness, and reversible extensibility.

Spider orb-web frame silk structure is stronger per unit weight, compared to high tensile steel and has very high toughness capability equal to  $2.5 \times 10^8$  J/m<sup>3</sup> or usually expressed by  $1.5 \times 10^5$  J/kg [57]. This means that spider web structures can absorb very high shock impact energy during a collision. When the spider orb-web stops a prey Figure 2.4, the web dissipates impact energy by three routes: internal dissipation within the radial silk, internal dissipation within the spiral silk, and aerodynamic dissipation [24]. Therefore, by taking all advantage of the mechanical structure characteristics of the spider web, the cross-section of the new design crash box had been imitated based on all its physical and mechanical properties. The dynamic response and energy dissipation of single spider silk under transverse impact had been studied analytically and numerically.



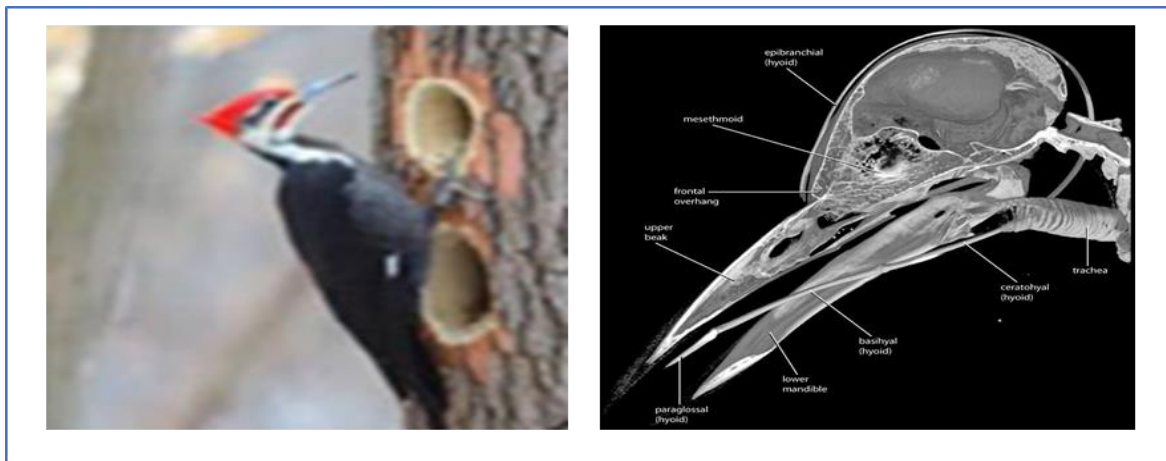
Figure 2.4 Natural reinforced spiderweb structure [57]

### 2.8.4. *Impact load energy absorption characteristics of woodpecker spongy tissue*

Most woodpeckers drum on trees to obtain food, and their skulls are functionally designed to withstand this impact. During this function, the woodpecker is well known for the ability to absorb the strong shock from the process of drumming the hard trunk of trees and without any damage to its brain.

This bony structure aids the woodpecker in extending its tongue extremely long distances to spear insects beneath bark or leaf litter. It was known as an impact-proof system, in Woodpeckers that was located at the unique hyoid bone inside the skull. It has been proven to be an original mechanism to absorb shock impact [58]. The most striking feature of the skull of the woodpecker is the hyoid apparatus which rigidly supports the tongue, in which the Trachea is located, which extends from its usual position just ventral to the lower mandible and wraps posteriorly around the skull to end between the orbits immediately dorsal to the base of the upper beak. This musculotendinous tissue serves as an attachment site for the muscles around the throat and tongue.

The unique anatomical structure of the woodpecker's head has been another important consideration. The woodpecker has special macro-morphology such as strong neck muscles, along the hyoid bone, and a stout sharply pointed, and unequal upper/lower beak [59]. The hyoid bone of the woodpecker has unique strength and flexibility owing to its unique micro/nano hierarchical composite structures. It consists of a flexible cartilage and bone skeleton covered with a thin tissue layer having high strength of 136 MPa and elasticity of 3.74 GPa. Woodpeckers have an impact-proof system, located at the unique hyoid bone inside the skull. It has been proven to be an original mechanism to absorb shock impact. At the interface between the cartilage bone skeleton and the tissue layer, there is a hierarchical fiber connection [59]. Also, the strong neck muscles have the character of compression and stretch repeatedly during the drumming process. These stretching and deformed function is the most important behavior for crash box during crushing to absorb or resist the sudden impact load [60]. Therefore, the nature-inspired design consideration is the structure of the Trachea from wood pecking head structure Figure 2.5 to increase the strength of the new crash box.



*Figure 2.5 Natural woodpecker skull and pecked wood structure [59]*

## 2.9. Analytical Energy absorption capability analyses and theoretical framework for a particular structure

Analytical frameworks provide the basic vocabulary of concepts and terms that may be used to construct the kinds of causal explanations expected of a theory. Besides, analytical-based approaches are applied as a way of dealing with the complexity that arises in situations involving interactions with the different factors. Although numerical simulation technology is widely used to simulate the collision behavior of thin-walled structures, theoretical prediction is still a key method,



which can directly analyze the structure's crashworthiness without test and numerical simulation. Therefore, this section analyzes the axial crushing of integrated and hybrid tubes by the Simplified Super Folding Element (SSFE) theory [25].

Then, the mean crushing force of the element can be determined by considering the energy conservation of the system in one folding wavelength  $2H$ . According to the energy balance of the system, the external work done by compression is dissipated by the plastic deformation in bending and membrane: Suppose that each folded wave has a wavelength of  $2H$  and is consistent and the wall thickness of the structure is uniform in the SSFE theoretical model.

According to Wierzbicki's theory [25], it is assumed that, as multiple lobes develop during the progressive collapse, the folding distance or wavelength within each fold stays constant. The mean crushing force can be calculated based on a basic folded component, including three stationary hinge lines, extensional and compressional elements (as shown in Figure 2.6 (a) and (b)) [61].

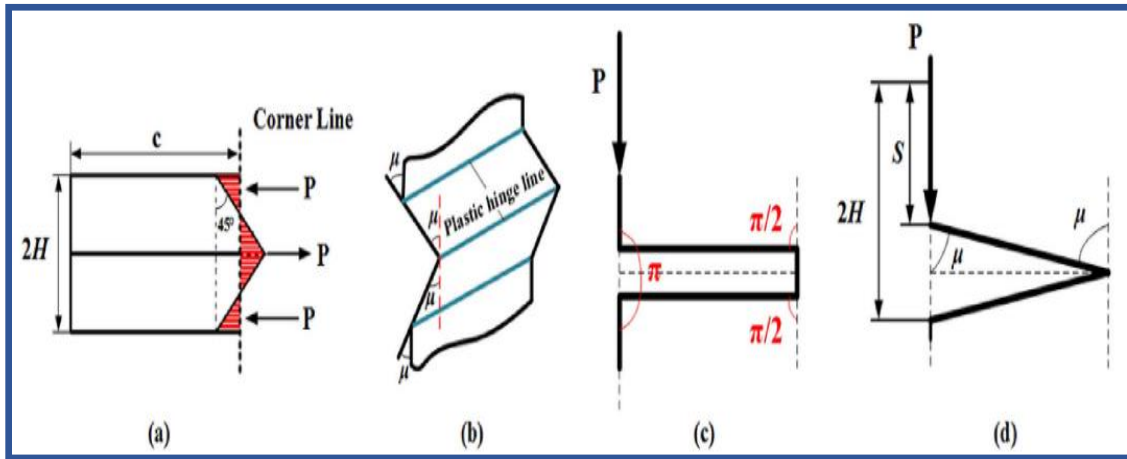


Figure 2.6 Energy dissipation in bending deformation: (a) extensional elements; (b) stationary hinge lines; (c) ideal completely folding; (d) actual folding [64].

Therefore, during the whole collapse process of a folded layer ( $2H$ ), the energy balance equation of the system is:

$$P_m \cdot 2H \cdot K = E_b + E_m \dots\dots\dots 2.6$$

where  $P_m$  represents the mean crushing force;  $E_b$  and  $E_m$  are energy consumed by bending and membrane deformation, respectively. Figure 2.6 (c) shows the ideal status of the folding element for the flange. Regarding the practical status, effective crushing coefficient  $k$  which is the ratio of effective crushing distance  $S$  (see Figure 2.6 (d)), and the wavelength  $2H$  is introduced,  $k$  is taken as 0.7 here [61].

**2.9.1. Bending dissipated energy ( $E_b$ )**

The energy dissipated by bending ( $E_b$ ) can be calculated by integrating the energy dissipation at three stationary hinge lines:

$$M_b = \sum_1^3 M_o \cdot \mu \cdot L_c \dots\dots\dots 2.7$$

where,  $M_o = \frac{1}{4} \sigma_o \cdot T^2$  is the completely plastic bending moment of the flange;  $\mu$  is the rotation angle of each static hinge line, and  $L_c$  is the total length of all flanges.  $\sigma_o$  is denotes the flow stress of material with power-law hardening and can be approximate as the average value of yield stress  $\sigma_u$  and ultimate stress  $\sigma_\mu$  and which can be calculated by the following formula [62]:

$$\sigma_o = \frac{\sigma_y + \sigma_\mu}{2} \dots\dots\dots 2.8$$

**2.9.2. Membrane deformation dissipated energy**

To analyze the membrane energy dissipation under compression, the multi-cell tubes with hexagonal outer profiles with different sectional area configurations were divided into different kinds of basic elements as shown in above Figure 2.6. Furthermore, internal arcs of the circular cross-section at the center have the obvious strain in the compressive process (elliptical frame), so it is necessary to consider the membrane deformation of the circular element [63].

Therefore, dividing hybrid structures into several basic elements to analyze the membrane energy dissipation under axial crushing: namely Circular element, 2-panel element, 3-panel element, 4-panel element, Concave T-shape element, Crisscross element, and T-shape element, as shown in Figure 2.7.

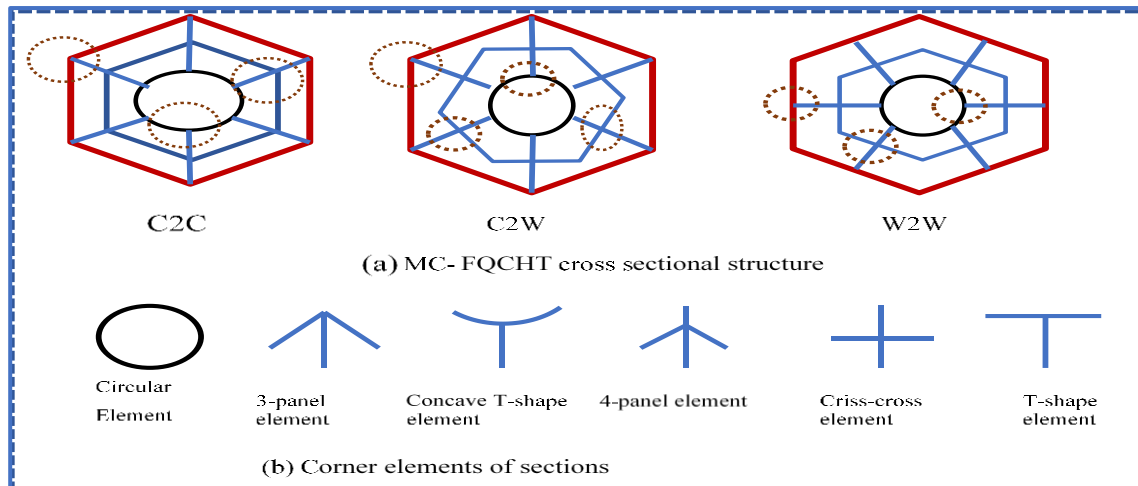


Figure 2.7 Basic structural forms of the crash box [63]

According to [64], the web to web (W2W) configurations performed best of all these different multi-cell configurations for energy absorption. But for more comparison, under this analysis is consider all the geometrical configurations shown as above Figure 2.7 (a) which have one circular element, 6 T-shape elements, 6 crisscross elements, and 6 concave T-shape elements for all structures.

Therefore the membrane energy is generated by compressing or expanding the shell element for the Circular element, which can be calculated during a whole fold formation as [63]:

$$E_m^{circular} = 8\pi \frac{M_o H^2}{T} \dots\dots\dots 2.9$$

But here in circular, there is foam reinforced for increasing energy dissipation capability and strength of the structure. Hence the crushing force energy dissipation by foam material is separately calculated as:

$$P_f = \sigma_p \frac{\pi D^2}{4} = 0.3Y_s \left( \frac{\rho^*}{\rho^s} \right)^{1.5} \frac{\pi D^2}{4} \dots\dots\dots 2.10$$

Where;  $\rho^*$  is the density of the foam

$\rho^s$  is the density of the solid from which the foam walls are made

D mean diameter of a circular tube,

$Y_s$  is the yield stress of the solid cell wall of the foam.

The corner of the normal hexagonal tube is considering as a 2-panel element that angles by 120°. According to the previous studies [65], the membrane energy of the corner element with central angle  $\theta$  can be evaluated as:

$$E_{membrane}^{corner}(\theta) = \frac{4M_o H^2 \tan(\theta/2)}{(\tan(\theta/2) + 0.05 / \tan(\theta/2))t / 1.1} \dots\dots\dots 2.11$$

For a normal hexagonal tube, the interior angle is 120, hence the formula for membrane energy for the extensional mode, the membrane can be calculated by the following formula:

$$E_{membrane}^{Corner}(\theta = 120^0) = \frac{4.328M_o H^2}{T} \dots\dots\dots 2.12$$

For Concave T-shape elements, since the membrane energy is mainly dissipated in the intersection region [66], a simplified method by replaced arc-panel with the tangent plane which is formed from the intersection point of the panels is taken to calculate its membrane energy as shown in Figure 2.8 (c); Therefore, the Concave T-shape element is simplified as T-shape element. Then

$$E_m^{concave.T-shape} = E_{T-shape} \dots\dots\dots 2.13$$

The T-shape element is a special case for  $\alpha = 90^0$  of 3-panel element I. Therefore, the membrane energy of the T-shape element is expressed as:

$$E_{T-shape} = E_m^{3-panel.element.I}(\alpha = 90^0) = \frac{12.3M_o H^2}{T} \dots\dots\dots 2.14$$

The deformation modes of the 3-panel elements are divided into two types: Pattern-1 and Pattern-2 (shown in Figure 2.8 (a) and (b)), in which the broken lines indicate the deformation directions of the panel elements. According to SAFE theory: when included angle  $\alpha < 90^0$ , the 3-panel element tend to deform in Pattern-1; when  $\alpha > 120^0$ , the 3-panel element tend to deform in Pattern-2; when  $90^0 \leq \alpha$

$\leq 120^\circ$ , both types of deformation are likely to occur. When the 3-panel element experiences Pattern-1 deformation, its membrane energy is expressed as [54], 67, 65, 67].

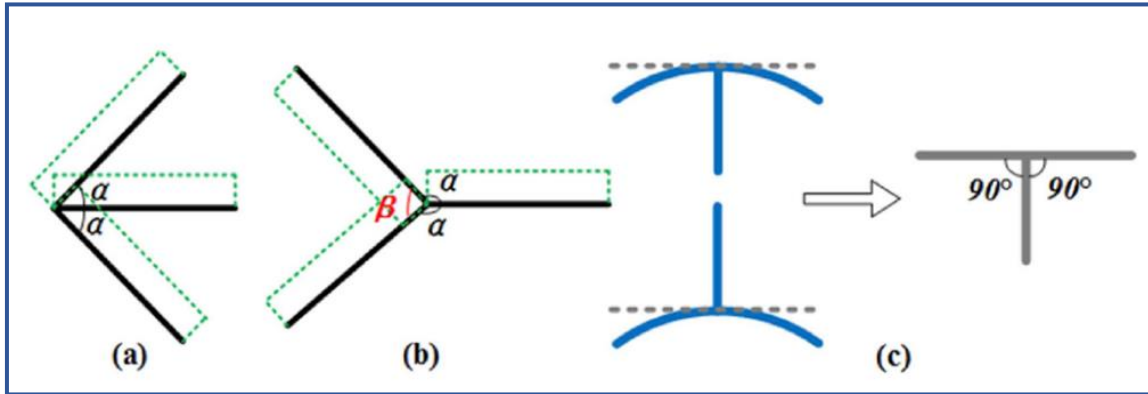


Figure 2.8 3-panel element and Simplification: (a) Pattern-1; (b) Pattern-2; (c) Simplification of convex and concave T-shape elements [54].

$$E_m^{3\text{-panel-element-I}}(\alpha) = \frac{4M_o H^2}{T} \left( \frac{\tan(\alpha)}{(\tan(\alpha) + 0.05 / \tan(\alpha) / 1.1)} + 2 \tan(\alpha) \right) \dots\dots\dots 2.15$$

When the 3-panel element undergoes Pattern-2 deformation, its membrane energy is expressed as [54, 65, 67].

$$E_m^{3\text{-panel-element-II}}(\beta) = \frac{2M_o H^2}{T} \left( 4 \tan\left(\frac{\beta}{4}\right) + 2 \sin\left(\frac{\beta}{2}\right) + 3 \sin \beta \right) \dots\dots\dots 2.16$$

where  $\beta = 2(\pi - \alpha)$ ,  $\alpha$  and  $\beta$  are the included angle of the two panels in the 3-panel element, their position relationships are shown in Figure 2.8. The value of  $\alpha$  and  $\beta$  for the 3-panel element I and 3-panel element II referred to herein are  $60^\circ$  and  $120^\circ$ , respectively, which can be seen from Figure 2.8 (a). Therefore, their membrane energy dissipation is:

$$E_m^{3\text{-panel-element-I}}(\alpha = 60^\circ) = \frac{8.946M_o H^2}{T} \dots\dots\dots 2.17$$

$$E_m^{3\text{-panel-element-II}}(\beta = 120^\circ) = \frac{13.279M_o H^2}{T} \dots\dots\dots 2.18$$

The membrane energy at the crisscross of three panels is also estimated by three times the three-panel element one.

$$E_m^{3\text{-panel-crisscross}} = 3E_m^{3\text{-panel-element-I}}$$

$$E_m^{3\text{-panel-crisscross}}(\alpha = 60^\circ) = 3 \frac{8.946M_o H^2}{T} \dots\dots\dots 2.19$$

*The membrane energy of 4-panel and crisscross angle element.*

The 4-panel angle element was asymmetric structure and created by a combination of one right corner element and two additional panels. Due to the similarity in deformation mode, it was assumed that

the independent right-corner element was equivalent to the corresponding right corner element in a 4-panel angle element (Figure 2.9) [68]. Simultaneously, the deformation mode of the right-corner element is asymmetric. The independent right-corner element has a similar geometric parameter as the 4-panel angle element with  $\beta = 60^\circ$  excepting the latter had two additional panels at top of the right corner element. Therefore, the dissipated membrane energy of the 4-panel angle element was calculated by the sum of the right corner element's membrane energy in the case of symmetric mode and two additional panels' membrane energy. The  $E_m$  of the right corner element in the case of symmetric mode is:

$$E_m^{Right-corner} = 8M_o \frac{H^2}{T} \dots\dots\dots 2.20$$

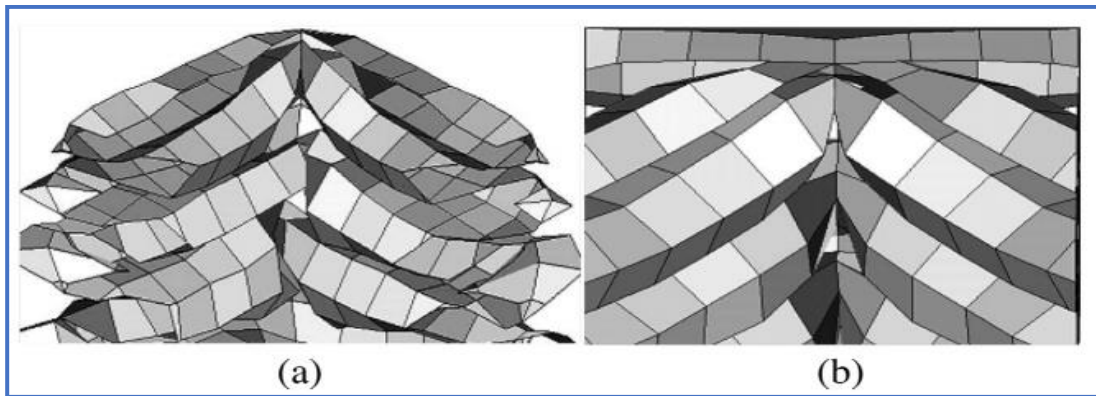


Figure 2.9 (a) Right corner element and (b) 4-panel angle element [68].

It was not easy or quite impossible to give a precise calculation of the membrane energy of the additional panel. In this case, the SFE theory was too complicated to apply. In consequence, a simplified deformation model of the additional panels was suggested and the SSFE theory was used to deal with this problem [68]. Represented in Figure 2.10 (b), the areas of ABC and ABF are defined as extensional elements of two additional panels. Thus, the membrane energy of one additional panel, during one wavelength crushing, was evaluated by integrating the triangular areas:

$$E_m^{a-panel} = \int_s \sigma_0 T ds = \sigma_0 T \frac{H^2}{\cos \beta} = 4M_o \frac{H^2}{T \cos \beta} \dots\dots\dots 2.21$$

Then, the dissipated membrane energy of the 4-panel angle element is:

$$E_m^{4-panel-element} = E_M^{right-corner-element} + 2E_m^{a-panel-element} = 8M_o \frac{H^2}{T} \left( 1 + \frac{1}{\cos \beta} \right) \dots\dots\dots 2.22$$

Being asymmetric structure and formed by four panels, the energy dissipation in the membrane of a crisscross element was determined by the sum of membrane energy absorbed by all four panels (Figure 2.10 (a)). It is assumed that the angle elements contributed similar roles in structure, the four panels create two right-corner elements, and that the deformation mode of the right-corner element is symmetric. Consequently, the membrane energy of crisscross element, during one wavelength crushing, was calculated by the sum of membrane energy absorbed by two right-corner angle elements in the case of symmetric mode as follow:

$$E_m^{Right-corner} = 16M_o \frac{H^2}{T} \dots\dots\dots 2.23$$

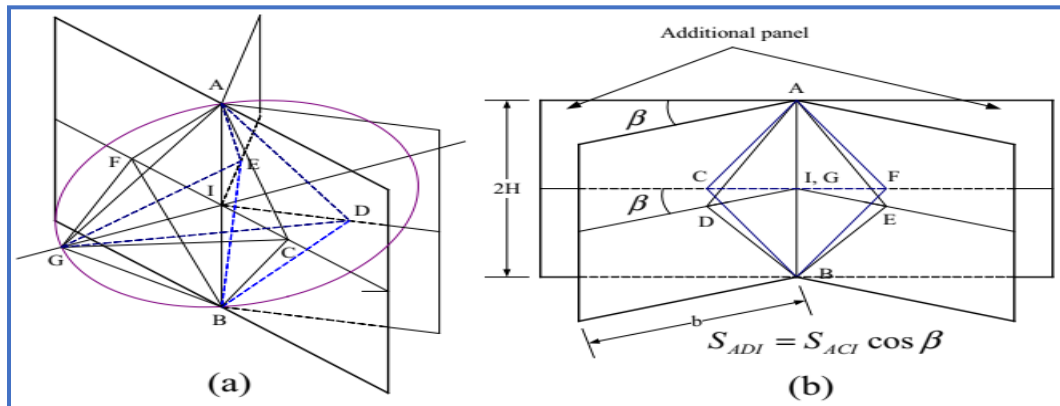


Figure 2.10 (a) Collapse mode of 4-panel angle element and (b) extensional elements [72]

## 2.10. Computer-Aided Engineering (CAE) Tools used for Crash Analysis

Due to the increasing cost of conducting real-time crash simulations, CAE tools are very widely used in the auto industry. As a result, automakers have reduced product development costs and time while improving the safety, comfort, and durability of the vehicles they produce. The predictive capability of CAE tools has progressed to the point where much of the design verification is now done using computer simulations rather than physical prototype testing. Tools used in this study are briefly explained below.

### 2.10.1. LS-DYNA

LS-DYNA is a general-purpose, explicit finite element program used to analyze the nonlinear dynamic response of three-dimensional inelastic structures. Its fully automated contact analysis capability and error-checking features have enabled users worldwide to solve successfully many complex crashes and forming problems.

An explicit time integration scheme offers advantages over the implicit methods found in many FEA codes. A solution is advanced without forming a stiffness matrix (thus saving storage requirements). Complex geometries may be simulated with many elements that undergo large deformations. For a given time, step, an explicit code requires fewer computations per time step than an implicit one. This advantage is especially dramatic in solid and shell structures. In an extensive car crash, airbag, and metal forming benchmark analyses, the explicit method is faster, more accurate, and more versatile than implicit methods. LS-DYNA has over one hundred metallic and nonmetallic material models like Elastic, Elastoplastic, Elasto-viscoplastic, Foam models, Linear Viscoelastic, Glass Models, Composites, etc.

Some of the prime application areas of LS-DYNA are as follows:

- Crashworthiness simulations: automobiles, airplanes, trains, ships, etc.
- Occupant safety analyses: airbag/dummy interaction, seat belts, foam padding, etc.

- Biomedical applications.
- Bird strike
- Metal forming: rolling, extrusion, forging, casting, spinning, ironing, superplastic forming, sheet metal stamping, profile rolling, deep drawing, hydroforming (including very large deformations), and multi-stage processes.

### ***2.10.2. MSC PATRAN***

It is a finite element modeler used to perform a variety of CAD/CAE tasks including modeling, meshing, and post-processing for FEM solvers LS-DYNA, NASTRAN, ABAQUS Etc. Patran provides direct access to geometry from the world's leading CAD systems and standards. Using sophisticated geometry access tools Patran addresses, many of the traditional barriers to shared geometry, including topological incompatibilities, solid body healing, mixed tolerances, and others. MSC. Patran provides an open, integrated, CAE environment for multi-disciplinary design analysis. This feature can be used to simulate product performance and manufacturing processes early in the design-to-manufacture process.

### ***2.10.3. MADYMO***

MADYMO (Mathematical Dynamical Models) is a general-purpose software package, which can be used to simulate the dynamic behavior of mechanical systems. Although originally developed for studying passive safety, MADYMO is now increasingly used for active safety and general biomechanics studies. It is used extensively in industrial engineering, design offices, research laboratories, and technical universities. It has a unique combination of fully integrated multi-body and finite element techniques. MADYMO offers in addition to standard output quantities, the possibility to calculate injury parameters like femur and tibia loads, Head Injury Criterion (HIC), Gadd Severity Index (GSI), Thoracic Trauma Index (TTI), and Viscous Injury Response (VC). Special output can be obtained through user-defined output routines. Results of the simulation are stored in several o/p files, to be accessible by post-processing programs.

### ***2.10.4. EASI CRASH DYNA (ECD)***

EASI CRASH DYNA is the first fully integrated simulation environment specially designed for crash engineering requiring large manipulation capability. It can directly read files in IGES, NASTRAN, PAM-CRASH, MADYMO, and LS-DYNA data. ECD has unique features, which enable the crash simulation more realistic and more accurate.

### ***2.10.5. EASI-CRASH MAD***

EASI-CRASH is based on EASIs 20+ years of practical experience in crash simulations. It greatly enhances the simulation process by allowing concurrent access to the model and simulation results. Animation, visualization, and synchronized curve plotting make EASi-CRASH MAD a high-performance CAE environment.

This study applied the Ls-Dyna explicit finite element since it has a capability for crashworthiness simulation and is also available in the ANSYS workbench and free separately.

### 2.10.6. *Implicit and Explicit Philosophy*

Most software would normally solve the dynamic equilibrium equation in an implicit approach however the foremost widespread approach that ought to be used for highly non-linear issues is to use explicit(specific) time integration schemes like a central difference scheme.

**Implicit:** A global stiffness matrix is computed, inverted, and applied to the nodal out-of-balance force to obtain a displacement increment. The advantage of this approach is that time step size may be selected by the user. The disadvantage is the large numerical effort required to form, store, and factorize the stiffness matrix. Implicit simulations therefore typically involve a relatively small number of expensive time steps.

**Explicit:** Internal and external forces are summed at each node point, and a nodal acceleration is computed by dividing by nodal mass. The solution is advanced by integrating this acceleration in time. The maximum time step size is limited by the Courant condition, producing an algorithm that typically requires many relatively inexpensive time steps. There are several benefits of such a procedure and therefore the most significant is that it results in an algorithmic program that may be simplified programmed, does not need any matrix operation procedure, and is very appropriate for a quick parallel computing methodology.

Comparison of explicit and implicit

The explicit method requires a short time step for an accurate solution, whereas the implicit method can give reliable results with large time steps. The implicit methods are unconditionally stable, whereas the explicit methods are mostly conditionally stable. In an implicit method, contact cannot be easily controlled.

### 2.10.7. *Common Element used in Crash FE Analysis*

- Shell element- Quadrilateral, Triangular, and mixed, Belytschko-Tsay-Lin-Tsay shell element
- Beam element- Hughes-Liu beam element
- Hexahedron element
- Solid element

## 2.11. **Research gap**

The ultimate goal of the research work in the crashworthiness domain is to develop a lightweight design that has efficient fuel consumption while maintaining effective crashworthiness performance under a crash scenario. It was shown in this review the axially loaded components, that absorb energy through progressive deformation, are very effective energy absorption devices. However, the progressive deformation is very challenging as the axially loaded components may develop an inefficient deformation mode, known as global bending mode, for certain dimensions.



The complete energy-absorbing structures used in the automotive industry consist of components that deform axially and laterally. The lateral collapsing of thin-walled structures has received relatively less attention than axial deformation. It is recommended that more attention should be dedicated to investigating the lateral and bending collapse of innovative structures such as those with multi-cell configuration and graded thickness that exhibited a superior performance under axial loading.

From reviewing the optimization researches, it was found that most of the studies have focused on the behavior of a solo thin-walled and a little attention was directed towards analyzing a complete energy absorbing system. However, to provide reliable design recommendations, the effectiveness of an optimized TW component should be verified when it is assembled with other structural components to build a complete energy absorbing system.

Finally, it was demonstrated in this review that the response of cellular materials to dynamic loading is a complicated behavior and the microstructure constituents of the foam including the shape, size of cells, and biomimetic structure have a significant effect on this behavior. Thus, to attain a comprehensive understanding of the collapse mechanisms of such materials during an impact scenario, the microstructure evolution must be captured and understood. The recent micromechanical computational models are capable of reproducing all aspects of the microstructural deformation behavior and could assist in understanding the mechanical properties of cellular materials when subjected to dynamic loading. Thus, it is suggested that such techniques should receive more attention in future crashworthiness studies to understand the dynamic behaviors of such structures.

## 2.12. Summary

In general, the study on material's effect, types of analysis, method of analysis, the structure of crash box and size of the crash box, on energy absorption is summarized in the following Table 2.2

*Table 2. 2 Summary of factors that have a significant influence on the energy absorption*

Ref. No.	Material of tube	Shape of tube	Analysis Method	Impact Velocity	Angle of Impact	Thickness, of a tube (mm)	Width of tube (mm)
[29]	Steel, Aluminum	Square, Circle, Ellipses	Dynamic	33.825 km/hr.	--	1.25, 1.5	Side- 30, Side- 50
[32]	Mild Steel, Glass & Kevlar Reinforced Composite	Square	Quasi-static	10 mm/min	--	1	100

[34]	Aluminum alloy	Square	Dynamic	18.792 to 25.812 km/hr.	--	1.25	44.3
[35]	Aluminum	Square	Quasi-static	80 mm/min	7,14,21	1.5	35
[69]	Aluminum alloy	Circle	Quasi-static	5 mm/min	--	1.3	OD-50.5
[30]	Aluminum alloy	Square Tapered straight	Dynamic	36 km/hr.	0 to 40 in step of 5	2	80
[13]	High strength steel	Circle	Dynamic	19.2 to 88.16 km/hr.	--	0.5 to 1	Dia. 31 to 62
[18]	Aluminum alloy & Al Foam filled.	Square	Dynamic	36 km/hr.	0-10-20-30	1.4 to 3	64 to 98
[8]	Annealed M.S	Square	Dynamic	36 km/hr.	0-10-20-30	1.2 to 3	80
[22]	Aluminum alloy	Square	Quasi-static	700 mm /hr.	5,15, 30	1.9, 2.46	Side-80
[17]	Aluminum alloy	Circle	Quasi-static	10 mm/min	--	0.8, 1, 1.2	ID-30, 39,44
[70]	Steel	Square, Rectangle, Circle, Hexagon	Dynamic	56 km/hr.	0, 15, 30	2	75 ,60/90 ,95 Dia. 50 Side 45/30 Side
[40]	Aluminum alloy	Rectangle	Quasi-static & Dynamic	54 km/hr.	0-10-15-20-25 30-35-4	1.5,2,2.5	60 x 100 80 x100 100 x100
[12]	Steel	Octagon	Dynamic	3.6 km/hr.	--	1.52	Side 31.8

## CHAPTER THREE

### 3. MATERIALS, CONDITIONS, AND METHODS

#### 3.1. Material of Crash Box

At the beginning of the design phase, it is important to study the benefits of the available materials and choose a suitable one for the structure. The needs of materials are among considerations for crashworthiness enhancement. Lighter materials are being developed to reduce vehicle's weight, cost, and running energy consumption. At the same time, these lighter materials should maintain the safety of the vehicle's stiffness desires, according to the standard requirements. Significant research work has been conducted to achieve these objectives.

Crash box material plays a critical role in the selection of a material for crash energy absorption. The performance of the crash box during the crash will determine the injury level of the occupants. A crash-worthy material should absorb the kinetic energy of the impacting vehicle and also prevent the transfer of peak loads to the occupant cell. The use of appropriate material, geometrical shape, and features have the potential for major payoffs such as lower weight, design of higher stiffness areas which are stable energy absorption processes.

Though the most common solution being used in the automotive industry is steel, as referred to in the previous studies, there are other better options in terms of cost and weight savings. Aluminum is used for the crash box design because the density of aluminum is approximately less than three times that of steel. This means the mass of aluminum is three times lighter than steel of the same volume, which will reduce the crash box weight by three times compared with that of steel. Similarly, the modulus of elasticity of aluminum is three times less than that of steel, and this directly affects the flexibility of the crash box by three times for Aluminum as the Crash Box needed and it can absorb the maximum amount of energy at maximum deformation, that is why Aluminum has low stiffness so it has high weight- stiffness ratio [71]. And comparing to carbon fiber reinforced composite material to Aluminum both are safe, light, stiff, and bodywork with better adaptability to change in circumstances, but carbon fiber reinforced composite material has a high cost of production and needs advanced manufacturing technology [72].

There are different criteria to describe the material property when a crash or impact scenario takes place. According to these criteria's the material property when impact scenario takes place is beyond the elastic limit, different and have a high amount of kinetic energy will be generated, therefore the energy will be converted to another form of energy (deformation, sound, heat, and friction energy), hence Johnson-Cook strength and failure model that predict/anticipate more accurate result focusing on these energies created [73].

In any collision between vehicles, kinetic energy has to dissipate in a controlled manner that will protect the occupants in the vehicle from bodily injuries or fatalities. Thin-walled tubular metallic structures are very efficient as energy absorbers and can be easily designed into a vehicle's frontal protection system. These metallic thin-walled structures can convert the kinetic energy to strain energy by irreversible plastic deformation. Most of the reported works in the literature on such tubes have used mild steel as the base material for understanding the energy absorption efficiency.

### 3.1.1. Energy absorbing materials and their characteristics

The energy-absorbing materials that are used in crash box design and their characteristics can be listed as follows:

1. Steel: lower strength to weight ratio compared to Al & composites.
2. Aluminum: Higher strength to weight ratios compared with steel
3. Composites: Highest strength to weight ratio compared with other potential materials
4. Honeycombs & Metal Foams: Higher strength to weight ratio compared with other materials

Composite materials in particular have been studied as good options to crash box applications. This type of material can be even better than metal alternatives but the properties are more difficult to reproduce in the numerical model and failure models are less accurate. Being the focus of this work, an impact-focused structure, complex deformations are expected so the model should have the best possible correlation with reality.

Aluminum is also being used in many automotive applications. The versatility of this metal is the existing variety of alloys and mechanical and thermal treatments that can be done to this metal to make it serve a wide range of purposes. Following European standards, the different alloys can be designated by chemical composition or by a 4-digit designation. The first digit defines the alloy group, as listed in Table 3.1. The second indicates modifications of the original alloy or impurity limits and the last two digits define the alloy [74].

Table 3.1 Aluminum alloys properties [74].

Definition of Alloy Group	group	*
Aluminum 99.00 percent and greater	1XXX	(H)
Aluminum alloys grouped by major alloying elements		
Copper (Cu)	2XXX	(T)
Manganese (Mn)	3XXX	(H)
Silicon (Si) .3	4XXX	(H/T )
Magnesium (Mg)	5XXX	(H)
Magnesium and Silicon (Ma + Si)	6XXX	(T)
Zinc (Zn)	7XXX	(T)
Other elements (e.g., Fe, Li...)	8XXX	(H/T )
Unused series	9XXX	(-)
* H = work hardening (non-heat-treatable), T = heat-treatable		

For automotive structural purposes, the most used alloys are the 6 and 7 series because they have high stiffness and are heat treatable [75]. The heat treatment makes possible a change in the mechanical properties of the metal to fulfill the demands of the design. Some types of heat treatment are listed in Table 3.2 below.

*Table 3.2 Aluminum tempers [75].*

Temper	Process
T4	Solution heat treated and naturally aged to a stable condition
T6	Solution heat-treated and artificially aged to maximum strength
T7	Solution heat treated and naturally overaged
T8	Solution heat treated, cold worked and artificially aged
T9	Solution heat treated, artificially aged, and cold worked

Therefore, in the present work, a T6 (Al 7075-T651) heat treatment will be used, because it is more suitable for energy absorption structures due to its maximizing strength [75].

### **3.1.2. Material modeling for theoretical (analytical) and numerical analysis**

#### **a) Johnson-Cook strength and failure models**

An Aluminum 7075-T651 plate is used for the crash box design. According to Johnson-Cook strength and failure models, the material must satisfy the criteria to absorb the energy that will be generated due to impact velocity, therefore the kinetic energy generated due to impact will be converted to deformation, sound, heat, and friction energy. Plasticity and failure model Johnson and Cook (1985) proposed that the material is loaded with shock and impacts the environment in the plastic range by the factors include large strains, large strain rates, high pressures, and high temperatures [73].

According to Johnson-Cook strength and failure models, different constants predicate the energy absorption propriety of the material. Therefore, to find these constants the following procedure was followed. A schematic experimental setup of the Aluminum 7075-T651 plate considered is shown in Figure 3.1 and the plate clamped around its periphery and a cylindrical punch with spherical nose and attached to a relatively mass, impact velocity of the mass with the plate. The prediction of the velocity threshold between impact with penetration and without penetration of the plate. The test specimen dimensions are  $D=171.45$  mm and  $t=12.7$  mm, while the punch had a diameter of  $d=12.7$  mm and mass was 138.8 kg as shown in Figure 3.1 [73].

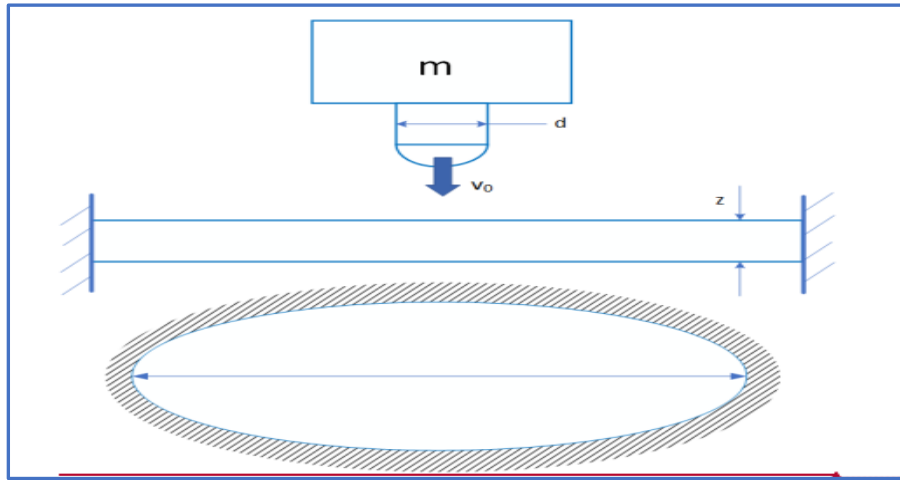


Figure 3.1 Schematic of the problem of the normal impact of a circular plate by a cylindrical punch with a hemispherical nose [73].

*B) Basics of the Johnson-Cook Strength Model*

The expression for the equivalent stress-plastic strain ( $\sigma_e$ - $\epsilon_e^p$ ) curve of the material depends on the current plastic strain rate and the temperature. Therefore, these parameters are decomposed in a multiplicative manner as seen in Equation 3.1 [73].

$$\sigma_e = [A + B(\epsilon_e^p)^n][1 + c \ln(\frac{\dot{\epsilon}_e^p}{\dot{\epsilon}_e^p})][1 - \tilde{T}^m] \dots\dots\dots 3.1$$

$$\tilde{T} = \frac{T - T_r}{T_m - T_r} \dots\dots\dots 3.2$$

Where  $\dot{\epsilon}_e^p$  = Reference strain rate

- A - Elastic limit or Initial yield stress
- B – Modulus of strain hardening or hardening constant
- C – Strain rate sensitivity index/constant
- n – Exponent of strain hardening
- m – Exponent of thermal weakening
- $\dot{\epsilon}_e^p$  - The non-dimensional speed of plastic strain
- $\epsilon_e^p$  - Equivalent plastic strain
- T - Homological temperature
- T - Current temperature
- Tr - Reference (usually room temperature)
- Tm - Melting temperature.

Finally, the five parameters A, B, C, n, m are approximated to match material test data obtained from an experiment (quasi-static, dynamic conditions, and as well as at temperature are needed to fit this model) [73].

**c) Failure Models**

The failure model is also constructed using a multiplicative decomposition of the effect of triaxiality, which is the ratio of the mean hydrostatic stress to the equivalent stress ( $\eta = \frac{\sigma_m}{\epsilon_e}$ ), strain rate, and temperature on the equivalent plastic strain at failure as seen in equation 3.3 [73].

$$\epsilon_{ef}^p = [d_1 + d_2 e^{d_3 \eta}] \left[ \left( 1 + d_4 \ln \left( \frac{\dot{\epsilon}_e^p}{\dot{\epsilon}_{e0}^p} \right) \right) \right] [1 - d_5 \hat{T}] \dots\dots\dots 3.3$$

Here  $d_1$ - $d_5$  adjusted to best represent the experimentally obtained material failure data on dependent of the equivalent plastic strain at failure on triaxiality has an exponential form, as suggested by Rice and Tracey (1969) for the enlargement of spherical voids [76]. Since the triaxiality, strain rate, and temperature at a material point can change during the loading history, a cumulative damage variable is defined as [73].

$$\bar{D} = \int \frac{d\hat{\epsilon}_e^p}{\hat{\epsilon}_e^p \left( \frac{\eta, \dot{\epsilon}_e^p}{\dot{\epsilon}_e^p, T} \right)} \dots\dots\dots 3.4$$

With failure occurring when  $\bar{D} = 1$

To calculate the temperature, rise in the material generated in response to plastic deformation and calculated on the assumption of adiabatic heating. It is assumed that the impact event is so fast that enough time is not available to conduct heat away from the regions with large plastic deformation. Under these conditions, the rise of temperature  $\Delta T = T - T_r$  is directly related to the plastic work done at a material point by using equation 11 [31].

$$\Delta T = \frac{\beta W^p}{\rho C_p} \dots\dots\dots 3.5$$

Where  $\beta$  - Represents the fraction of plastic work that is converted into heat,  
 $\rho$  - Density of the material and  
 $C_p$  - Heat capacity of the material.

The parameter  $\beta$  is generally taken to be a constant in the order of 0.90 to 0.95, but it can depend on strain and strain rate, and assuming constant values in the order of 0.90 to 0.95 is a good approximation, especially as the strains become larger [31].

**d) Calibration of the Johnson-Cook Model Parameters**

The data presented provides information that allows the determination of the parameters of the Johnson-Cook model for the Al 7075-T651 material of the plate specimens used in the impact tests. The material used for the Crash Box has the following property  $\rho=2810 \text{ kg/m}^3$ ,  $C_p=960 \text{ J/(kg K)}$ ,  $T_m=750 \text{ K}$  (1350OR),  $T_r=293 \text{ K}$  (527OR) and  $\dot{\epsilon}_{p0}^{\epsilon} = 0.00016 \text{ 1/s}$  from the Aerospace Specification Metal website [73].

From the quasi-static uniaxial tension test at room temperature to evaluate the coefficient of  $A=517$  MPa,  $B=405$  MPa, and  $n=0.41$  from the stress-strain curve, by using high-temperature test the value of  $m$  was determined and picked to match the experimental result by considering the temperature generated at the time interval and the stress-induced in the material, thus  $m=1.1$ . And finally, to calibrate the constant  $C$  in the strength model, a first estimate was made based on the ratio of the flow stresses in the quasi-static and dynamic tests. Therefore, it becomes  $C=0.0075$  from the stress-strain curves of the predictions and test results [73]. A summary of all the parameters that include the material model is shown in Table 3.3.

*Table 3.3 Aluminum 7075-T651 reports for Automotive Crash Box material by using Johnson-Cook Model Parameters [73].*

Strength Model Parameters		Failure Model Parameters	
Elastic limit or Initial yield stress, A	517 MPa	D1	0.025
Modulus of strain hardening or hardening constant, B	405 MPa	D2	0.15
Strain rate sensitivity index/constant, C	0.0075	D3	-1.5
Exponent of strain hardening, n	0.41	D4	-0.039
Exponent of thermal weakening, m	1.1	D5	8.0
Other Parameters		Thermal parameters	
Density, $\rho$	2810 Kg/m <sup>3</sup>	Heat capacity of the material, $C_p$	960 J/(Kg-K)
Reference strain rate, $\dot{\epsilon}_p$	0.00016/s	Melting temperature, $T_m$	750 K
Young's Modulus, E	71.7 GPa	Reference (usual room temperature), $T_r$	293 K
Poisson's ratio, $\nu$	0.33	$\beta$	0.95

### 3.2. Crash box design specification

The importance of existing studies is to provide a guideline for the researchers in satisfying the standards and regulations stated in ACB product design specifications (PDS). The other important element of PDS is to provide geometry limitation guidelines to ACB geometry profiles.

This is very important to determine the dimensions of a crash box, which should be long enough to offer sufficient deformation to dissipate more energy collisions, but should not occupy too much space before the deformation as it would gain more weight and reduce the product value from an economical point of view [30]. Apart from that, the information from PDS can be used as a reference to produce a product density lower than 0.19 g/cm<sup>3</sup>; material selection must be environmentally friendly and have biodegradable capability. Additionally, the ACB design must also fulfill the



requirements regarding pedestrian protection as stated in National Highway Traffic Safety Administration (NHTSA) regulations, which propose strength requirements of the frontal structure in FMVSS Part 581 tests and FMVSS Part 208 mandatory testing for frontal impact. Hence, the design must also consider the standards launched by the East European Constitutional Review (ECER) 42 and United Nation Economic Commission for Europe/Working Party 29 (UNECE/WP29) and Research Council for Automobile Repairs (RCAR) test, which have established global technical regulations (GTRS) for frontal impact structure and pedestrian safety [75].

Finally, the new ACB design must be able to absorb more than the minimum energy of 1826 J, the plate thickness must be between 1 mm and 3 mm, the length of each side of hexagonal geometry must be 140 mm and the length of other shapes must be in the range of 120 mm to 300 mm as shown in Table 3.4.

*Table 3.4 Summary of product design specification for ACB [23, 74, 57].*

Specification	Description
Square/Rectangle/Hexagonal	140 mm×140 mm
Length	$120 \text{ mm} \leq L \leq 300 \text{ mm}$
Thickness	$1 \text{ mm} \leq t \leq 3 \text{ mm}$
Circular	(diameter) $\theta=90 \text{ mm}$
Density	$0.15 \text{ g/cm}^3 \leq \rho \leq 2.81 \text{ g/cm}^3$
Energy absorption capacity	$1826 \text{ J} \leq E \leq 5704 \text{ J}$

### 3.3. Structural and geometrical modeling of new crash box approach and methods

#### 3.3.1. Biomimetic structural modeling approach of new cashbox

Innovations inspired by nature have stimulated attempts of systematization of the biologically inspired design processes and studies [77] indicate that there is “no general approach developed for biomimetics. From the analysis of the biomimetic design process as a whole (from the initial concept to product development), one from two directions were identified and can be used in any kind of biomimetic design. Hence the main objective of this study is to design the optimized crash box to absorb maximum axial impact load energy, the top-down biomimetic design approach would apply by marking that the existing crash box is not absorbing enough impact load energy as an engineering problem and starting points of the approach. The major procedures are given in Figure 3.2 with an approach diagram. The top-down process may also indicate some areas of biology where there may be some lack of fundamental data.

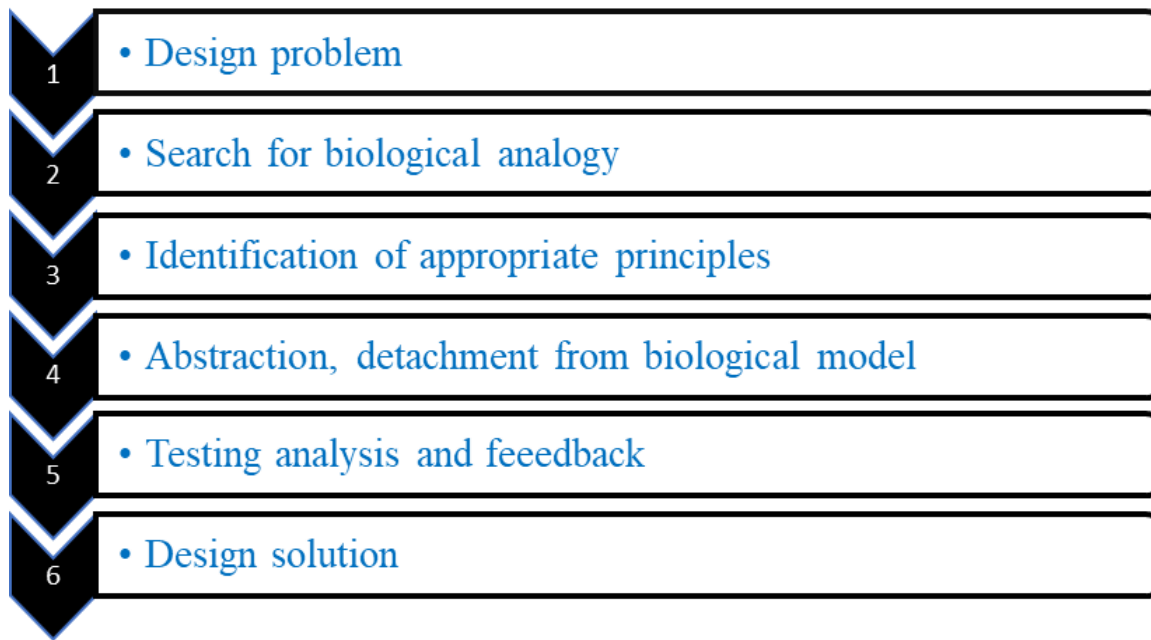


Figure 3.2 Top-down approaches of biomimetics design of cashbox and its procedure

In this approach process of conceptual design, there are several steps and sub-activities as shown in Table 3.5.

Table 3.5 Steps for top-down biomimetic approaches for crash box

Top-down steps and activities	
Starting point	An engineering problem
Search for analogies for the problem	Search for analogies in biological knowledge
Selection of the suitable principles	Suitable principles of one or more biological models analyzed
Abstraction	Transforming the biological principles in a solution neutral form and reframe the solution for the engineer
Technical implementation	Product development using the biological extracted

### 3.3.2. Biomimetic structural modeling methodology of new Crash Box

The present methodology will focus mostly on the domain of the bio-inspired formal features taken by nature to solve problems related to the efficient use of energy, resources, and information. This methodology aims to select the most used and effective geometrical features from biological systems, that can exceed in performances, and connect those with part of TRIZ principles and design requirements of sustainability. From the brief survey of Chapter two, can turn to the modern movements that look like the work of nature to produce biological and mechanical analogies, (terms suggested in “Biological and Mechanical Fallacies by Geoffrey Scott) such as the series of comparisons of mechanical structures with plant stems and with animal skeletons of D’Arcy Thompson [78].

Hexagons were chosen as an external geometry profile, taking advantage of the honeycomb structure which could provide very low weight, high stiffness, durability, and production cost savings [20]. The cross-section area was derived from the structure of the spider web and reinforced at the center by bioinspired woodpecker head, Trachea, and hyoid bone structure by fiber foam. Lastly, the new proposed designs of ACB could be developed by using a hybrid and integrated method of TRIZ, morphological charts, and biomimetics at the following stage. Three main approaches emerge in literature among the possible strategies to allow designers and technicians to access and use natural solutions, and more in general, the knowledge about nature contained in the models of natural systems described in the biological literature. There is no general or specific approach and methodology that has been developed for biomimetics structure design development, who went design the engineering product based on biomimetics principles can use any integration of approach, tools, and methods. In general, the approach, methodology, and steps shown in Figure 3.3 are used for biomimetics structure design modeling of cashbox in this study.

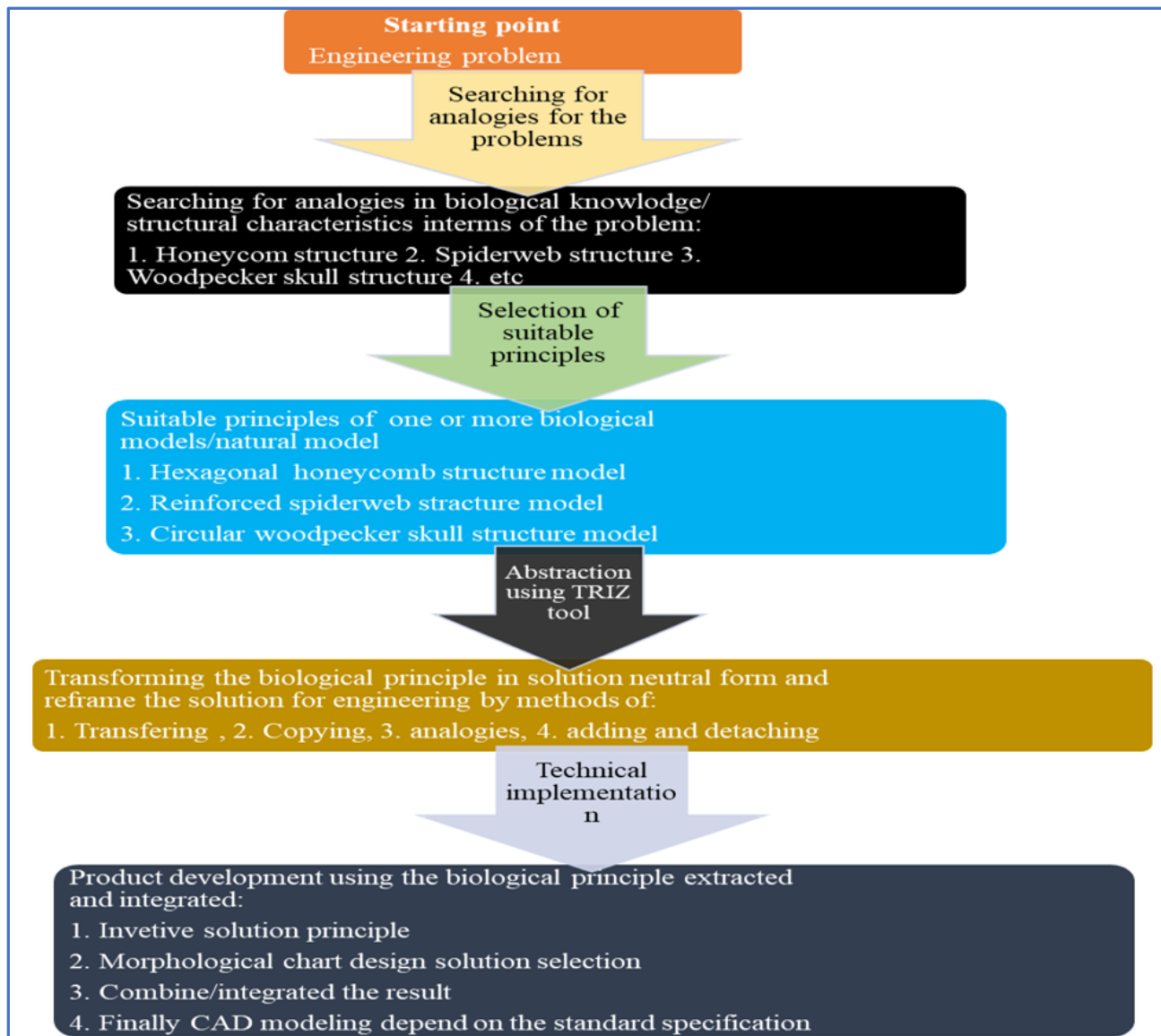


Figure 3.3 Approach, methods, procedure, and steps of biomimetics structure design of cashbox

### 3.4. The procedure of structural modeling of the crash box

#### 3.4.1. Develop TRIZ contradiction matrix from general TRIZ inventive solution principle

The first major step is to develop a specific TRIZ contradiction matrix concerning the design goal of this study from general TRIZ as given in Table 3.6. The study aimed to build a new optimized design of an automotive crash box with high energy absorption capability. Therefore, this design needs to be a product with higher toughness and this could be achieved by reducing the weight of stationary objects (#2 in the table). Thus, the inventive principles selected to be applied were #3. Local Quality, #26. Copying, #39. and #28. Mechanics substitution.

The TRIZ-based biomimetic part design possesses a great potential regarding part complexity and adaption for an innovative part design due to a layer-wise buildup offering multiple geometry variants from a broad design solution space. Thus, design optimization is a complex challenge for the designer that requires systematic design approaches. A methodology for a function-oriented systematic part design was used in this study besides the biomimetics method which partially integrated with TRIZ and morphological charts.

Table 3.6 TRIZ contradiction matrix for ACB design

39 Engineering parameters		TRIZ principal solutions to 40 inventive principles
Improving features	Worsening features inventive principles	
#2. Weight of the stationary object	#13. Stability of the object	#26. Copying
		#10. Preliminary action
		#28. Mechanics substitution
	#27. Reliability	#8. Anti-weight
		#3. Local quality
		#18. Mechanical vibration
#20. Use of energy by stationary	#28. Mechanics substitution	
	#19. Periodic action	

#### 3.4.2. Translate TRIZ recommended solutions to their specific ideas by the morphological chart

TRIZ method provided a general solution that still needs to be interpreted further by the designers using several techniques [49]. Thus, usage of a morphological chart as Table 3.7 developed for this study could help to translate TRIZ recommended solutions to their specific ideas.

Table 3.7 ACB design strategy based on TRIZ recommended solutions

TRIZ solution principle	TRIZ recommended solution	Strategy of design
#26. Copying	Use simpler and inexpensive copies (virtual reality, natural); Replace an object or process with optical copies	Biomimetics techniques generate conceptual ideas based on nature (how animals or plants absorb energy during collisions to survive and save their lives)

#28. Mechanics substitution	Change from static to movable fields, from unstructured fields to those having the structure	Improve the part by adding grooves, ribs, multiple layers of cross-section, crash bead, and various shape profiles. Creating the most optimum cross-section by using a hybrid approach, to strengthen structure (combination of two or more biomimetics elements)
#3. Local quality	Make each part of an object function in conditions most suitable for its operation; Make each part fulfill a different and useful function	Optimize the thickness of the component area according to the Stress location point. Thicker the component at higher stress location points and thinner component at crash bead

Besides, the usage of the biomimetics method is based on the recommended solution. Combined (integrated) geometry was used in this design generation by the combination of two concepts of energy absorption from woodpeckers and spider webs.

**3.4.3. Geometry specification using an integrated method of TRIZ, morphological charts, and biomimetics**

The integration approach between the three tools or methodology towards a more effective and efficient inventive design methodology (Figure 3.4). The paper used systematic a comparison between the tools based on functional modeling used during the process of problem-solving within TRIZ and biomimetics. 26#Copying” as shown the Figure 3.4 it would solve engineering problems with the help of nature’s wisdom approach [79].





TRIZ Solutions principle and design strategy	Design feature	Solution			
		1	2	3	4
<b>#3. Local quality</b> 1. Creating the most optimum cross section by using a hybrid approach to strengthen structure (combining two or more biomimetics elements) 2. Crush box designed with ribs to reinforce and strengthen crash box structure	Geometry profile	Octagon	Rectangular	Circular and Cone	Hexagonal
	Body type	Shell	Foam	Combined geometry	Multilayer
	Sectioning	symmetrical	Non-symmetrical		
<b>#26. Copying</b> Biomimetic techniques generate conceptual ideas base on nature (how animals or plants absorb energy during a collision to survive and save their life.	Cross section concept	Woodpecker 	Honeycomb 	Muskox 	Spiderweb 
	Absorb E by	Repeated collision	Strong structure	Protected by Strong and stiff thumbs	Suddenly impact
<b>#.28 Mechanics substitution</b> Improve the part by adding grooves, ribs, multiple layers of cross-section, crash bead, and various shape profiles.	Ribs and groove pattern	Screw join I	Rivet join V	Casting manufact <sup>n</sup>	Welding 1+x

Figure 3.4 Integrated method of TRIZ, morphological chart, and biomimetics for crash box concept design generation.

### 3.5. Biomimetics structure-based geometrical modeling of the crash box

#### 3.5.1. Structural modeling of the new crash box

In this study, five patterns of biomimetic prismatic tubes were established based on original hexagonal tubes, named and coding as Single-cell original hexagonal tube (SC-OHT), multi-cell full triangular hexagonal tube (MC-FTHT), multi-cell internal clone hexagonal tube (MC-ICHT), multi-cell double fill hexagonal (MC-DFHT), and multi-cell full Quadrilateral and circular hexagonal tube (MC-FQCHT) tube respectively. Accordingly, SC-OHT was associated with the bee honeycomb as shown in Figure 3.5 (a), while MC-FTHT in Figure 3.5 (b) followed the concept of marsh horsetail with strong resistance. Similarly, MC-ICHT, MC-DFHT, and MC-FQCHT were constructed by absorbing the merits of tortoiseshell, spider-web, and woodpecker null, as shown in Figure 3.5 (c), (d), and (e).

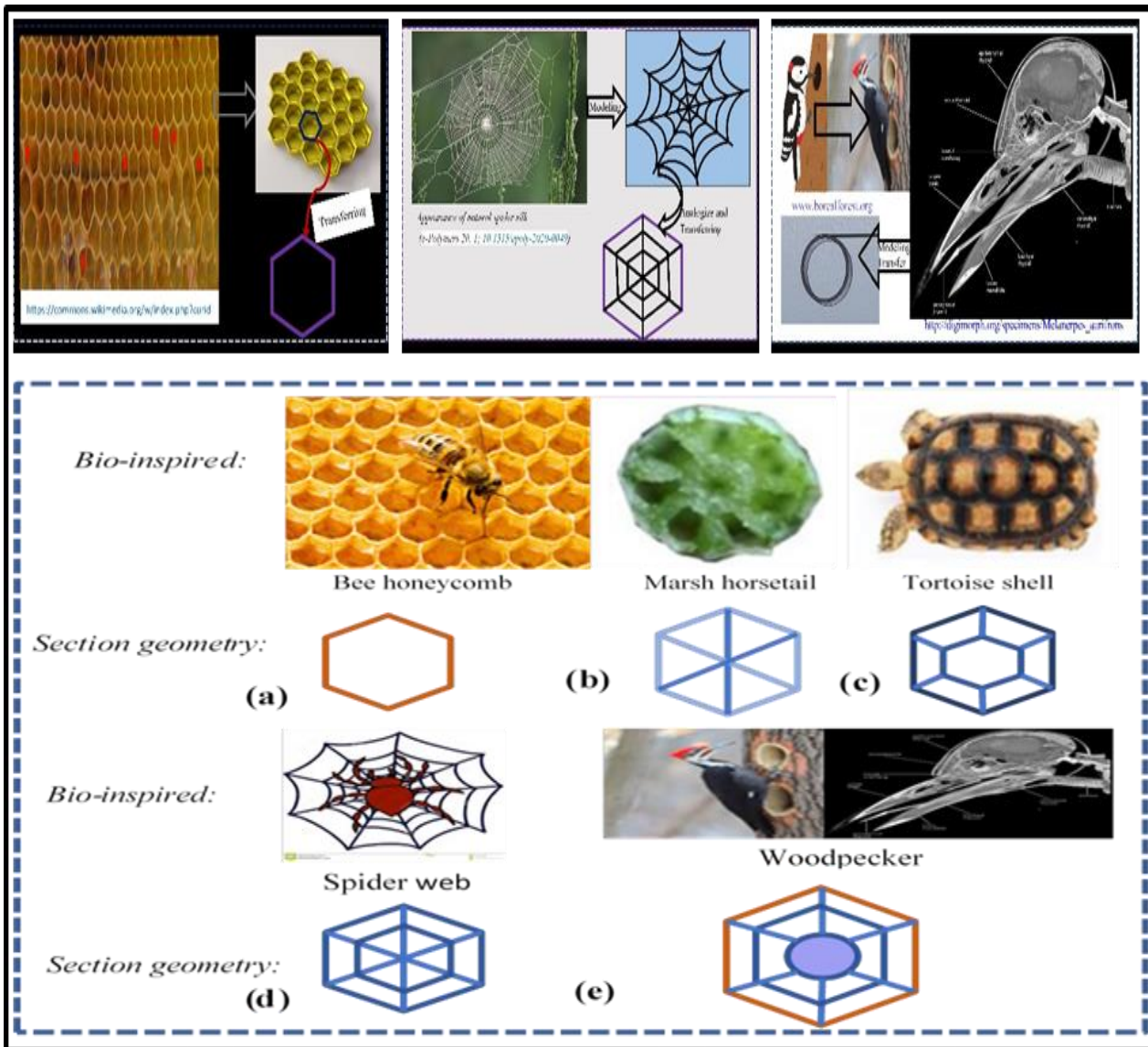


Figure 3.3 Bio-inspired concepts and geometries of (a) SC-OHT (original hexagonal tube), (b) MC-FTHT (full triangular hexagonal tube); (c) MC-ICHT (internal clone hexagonal tube), (d) MC-DFHT (double fill hexagonal tube), (e) MC-FQCHT (Full quadrilateral and circle

**3.5.2. CAD Geometry modeling of the new crash box**

The 3D model was developed on a 1:1 scale for better visualization of product design features in SOLIDWORK. The first concept idea labeled by P1 was copying the single hexagonal honeycomb structure tubes, the second concept P-2 is simply connecting all the parallel corners, which is similar to the horsetail structure, P3 is the concept that created by self-hierarchize of the hexagonal tube and connecting both hexagonal corners. The fourth (P-4), the model still used a honeycomb structure for the outermost profile, self-hierarchize, and reinforced by spider web structure inside the part. The last concept (P-5) is also modeled by reinforced a spider web structure inside the part and with a multi-layer of fiber foam acting like a sponge in a woodpecker’s skull to protect its brain during a collision and fiber foam at the center to optimize the energy absorption capability. All concept designs were equipped with straight slot profiles as a crash bead to initiate the axial collapse during the collision.

By considering the concept generated above and the design parameter specification crash box from the works of literature review, the newly developed crash box 3-D CAD modeling, Figure 3.6 was done in SOLIDWORK 2020 using the following parameter: L=240 mm, B=100 mm, b=70 mm, D=60 mm and T=0.8 mm. where, L is the length of the crash box, H and h are the side lengths of external and inner hexagonal tube respectively, and T is the shell tube wall thickness of hybrid structures initially.

**3.6. Analytical analysis of energy dissipation for developed conceptual design**

To further reveal the difference in crashworthiness of different structures, the theoretical models of eight-representative structures based on bio-inspired concepts and geometries of (a) SC-OHT (original hexagonal tube), (b) MC-FTHT (full triangular hexagonal tube); (c) MC-ICHT (internal close hexagonal tube), (d) MC-DFHT (double fill hexagonal tube), (e) Corner to corner connection of ribs MC-FQCHT (Full quadrilateral and circular hexagonal tube) (f) web to web connection of ribs MC-FQCHT (g) Both C2C & W2W connection of ribs MC-FQCHT and (h) C2W Connection of ribs MC-FQCHT, were proposed and established, including the equations of mean crushing force and half-wavelength. For axisymmetric structures, they are often viewed as a combination of multiple regular units. In general, during folding of the structure due to axial impact load can be dissipated in two forms, bending forms and in structure membrane.

**3.6.1. Bending dissipated energy ( $E_b$ )**

The energy dissipated by bending ( $E_b$ ) can be calculated as Eqn. (2.7) and in this study, case substitutes the value of  $\sigma_0$  calculated from the mechanical properties of aluminum A7075-T651 as 537.5 MPa. The flanges are ideally completely flattened Figure 2.6 (c) according to the SSFE theory in the axial deformation in the  $2H$  wavelength, and the angles of rotation of the three hinge lines are  $\pi/2$ ,  $\pi$ , and  $\pi/2$ , respectively. So:

$$E_b = 2\pi M_o \cdot L_c \dots\dots\dots 3.9$$

**3.6.2. Membrane deformation dissipated energy**

To analyze the membrane energy dissipation under compression, the multi-cell tubes with hexagonal outer profiles with different sectional area configurations were divided into different kinds of basic elements and units. The constituent elements of cross-sectional and unit numbers are the main factor for membrane deformation energy dissipation of structure under impact load, it needs series attention and deep analysis.

Therefore, dividing eight hybrid structures into seven basic elements to analyze the membrane energy dissipation under axial crushing: namely Circular element, 2-panel element, 3-panel element, 4-panel element, Concave T-shape element, Crisscross element, and T-shape element, as shown in Figure 3.8 or type (I, II, III, IV, V, VI, VII, and type VIII).

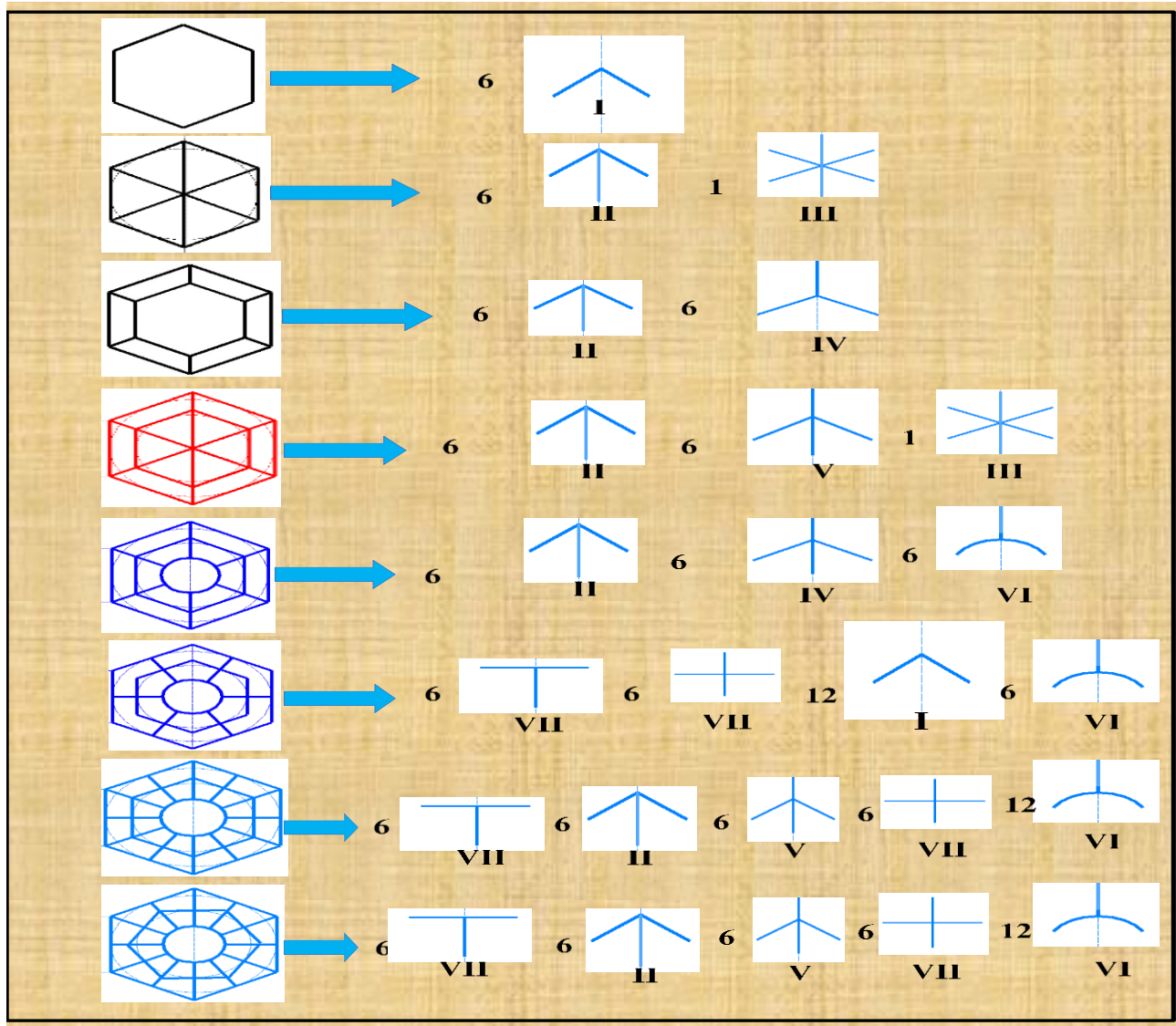


Figure 3.6 Constituent elements of cross section (a) SC-OHT, (b) MC-FTHT, (c) MC-ICHT, (d) MC-DFHT, (e) C2C MC-FQCHT, (f) W-W MC-FQCHT (g) C2C & W2W MC-FQCHT (h) C2W MC-FQCHT.



The number of energies absorbed elements, which help to calculate the mean crush force for each structure are also extracted, summarized, and listed in Table 3.8.

Table 3.8 Number of energies absorbed elements for all structures.

Energy absorbs elements	Structures							
	SC-OHT	MC-FTH	MC-ICHT	MC-DFH	MC-FQCHT (C2C)	MC-FQCHT (W2W)	MC-FQCHT (c2c&w2w)	MC-FQCHT (C2W)
Circular element					1	1	1	1
2-panel element	6					6		
Concave T-shape					6	6	12	12
3-panel element-I		6	6	6	6		6	6
3-panel element-II			6					
4-panel element				6	6		6	6
3-panel crisscross		1		1				
2-panel crisscross						6	6	6
T-shape element						6	6	6

**3.6.3. Membrane deformation dissipated energy for design concept p-1 (SC-OHT)**

The constituent elements in single-cell original hexagonal tube section have corner elements ( $\theta = 120^\circ$ ). Substitute the specific angles into Eqn. (2.11) and multiply by the number of corners written in above Table 3.8, the membrane energy of these constituent elements can be obtained as:

$$E_{membrane}^{Corner} (120^\circ) = \frac{4.328M_0H^2}{T} \dots\dots\dots 3.10$$

But single-cell original hexagonal tube section view has six (6) corners, hence the total membrane energy in this structure can be calculated as:

$$E_{Total.membrane}^{SC-OHT} = N_c E_{member}^{corner} = 6 \frac{4.328M_0H^2}{T} \dots\dots\dots 3.11$$

Where  $N_c$  is the number of constituent element corners.

**3.6.4. Membrane deformation dissipated energy for design concept p-2 (MC-FTHT)**

The constituent elements in multi-cell full triangular hexagonal tube section have corner elements 3-panel element-I ( $\theta = 60^\circ$ ) and 3-panel crisscross-III ( $\theta = 60^\circ$ ). Substitute the specific angles into Eqn.

(2.15) and (2.19), and multiply by the number of element units written in above Table 3.8, the membrane energy of these constituent elements can be obtained by adding the two equations.

$$E_{Total.membrane}^{MC-FTHT} = N_c E_{membrane}^{3-panel-element-I} (\alpha = 60^0) + N_c E_{membrane}^{3-panel-crisscross-III} (\alpha = 60^0) \dots\dots\dots 3.12$$

Substitute the parameter and value of mathematics trigonometry:

$$E_{Total.membrane}^{MC-FTHT} = 6 \frac{8.946M_oH^2}{T} + 1x3 \frac{8.946M_oH^2}{T}$$

$$E_{Total.membrane}^{MC-FTHT} = 9 \frac{8.946M_oH^2}{T} \dots\dots\dots 3.13$$

**3.6.5. Membrane deformation dissipated energy for design concept p-3 (MC-ICHT)**

In a similar fashion with the former structure concept design, identify and get an equation for constituent element unit from the literature review part. Hence this concept design structure has six 3-panel element-I and element-II, substitute the specific angle and numbers of element units in equations (2.17) and (2.18), and multiply with its constituent element unit numbers, adding the result.

$$E_{Total.membrane}^{MC-FTHT} = N_c E_{membrane}^{3-panel-element-I} (\alpha = 60^0) + N_c E_{membrane}^{3-panel-crisscross-III} (\alpha = 60^0) \dots\dots\dots 1.14$$

Then substitute the value and symbol of each element unit:

$$E_{Total.membrane}^{MC-FTHT} = 6 \frac{8.946M_oH^2}{T} + 1x3 \frac{8.946M_oH^2}{T}$$

$$E_{Total.membrane}^{MC-FTHT} = 9 \frac{8.946M_oH^2}{T} \dots\dots\dots 1.15$$

**3.6.6. Membrane deformation dissipated energy for design concept p-4 (MC-DFHT)**

This design concept has a corner element, six 3-panel element units, six 4-panel elements, and one three-panel crisscross as listed in above Table-13. Therefore, by a substitute, the value of angle and number of corner elements into equations (2.15), (2.19), and (2.22), the membrane energy absorbed by this structure can be obtained as the following.

$$E_{Total.membrane}^{MC-DFHT} = N_c E_{membrane}^{3-panel-element-I} (\alpha = 60^0) + N_c E_M^{4-panel-element} (\beta = 60^0) + N_c E_{membrane}^{3-panel-crisscross} \dots\dots\dots 3.16$$

Substitute the value:

$$E_{Total.membrane}^{MC-DFHT} = 6 \frac{8.946M_oH^2}{T} + 6 \frac{12.189M_oH^2}{T} + 1x3 \frac{8.946M_oH^2}{T}$$

$$E_{Total.membrane}^{MC-DFHT} = 153.648 \frac{M_oH^2}{T} \dots\dots\dots 3.17$$

**3.6.7. Membrane deformation dissipated energy for design concept p-5 (MC-FQCHT C2C)**

The fifth design concept structure is with the addition of some features like a circle at the center and ribs connection arrangement which are helping to increase the capability of membrane deformation

dissipated energy for the structure. It has the membrane element unit of one circular element, Concave T-shape, 3-panel element-I, and 4-panel element types respectively. Hence from the equation developed for each element of membrane energy, (2.9), (2.14), (2.15), and (2.22), and their summation is the membrane deformation dissipated energy for this structure.

$$E_{Total.membrane}^{c2c.MC-FQCHT} = N_c E_{membrane}^{circular} + N_c E_{membrane}^{Concave.T-shape} + N_c E_{membrane}^{3-panel-element-I} (\alpha = 60^0) + N_c E_M^{4-panel-element} (\beta = 60^0) \dots\dots\dots 3.18$$

$$E_{Total.membrane}^{c2c.MC-FQCHT} = 1 \times 8\pi \frac{M_o H^2}{T} + 6 \frac{12.3 M_o H^2}{T} + 6 \frac{8.946 M_o H^2}{T} + 6 \frac{12.189 M_o H^2}{T}$$

$$E_{Total.membrane}^{c2c.MC-FQCHT} = 208.61\pi \frac{M_o H^2}{T} \dots\dots\dots 3.19$$

**3.6.8. Membrane deformation dissipated energy for design concept p-6 (MC-FQCHT W2W)**

This structure is different from the p-5 only by ribs connection, which can change the types and numbers element units. It has one circular element, six 2-panel elements, six concave T-shape, six 2-panel crisscross, and six T-shape element membrane units. Hence from Eqn. (2.9), (2.12), (2.14), and (2.23), and their sum will be the total membrane energy dissipated during the axial impact of this structure.

$$E_{Total.membrane}^{w2w.MC-FQCHT} = N_c E_{membrane}^{circular} + N_c E_{membrane}^{2-panel} (\theta = 120^0) + N_c E_{membrane}^{Concave.T-shape} + N_c E_{membrane}^{N-crisscross} + N_c E_{membrane}^{T-shape} \dots\dots\dots 3.20$$

$$E_{Total.membrane}^{w2w.MC-FQCHT} = 1 \times 8\pi \frac{M_o H^2}{T} + 6 \frac{4.328 M_o H^2}{T} + 6 \frac{12.3 M_o H^2}{T}$$

$$E_{Total.membrane}^{w2w.MC-FQCHT} = 277.568\pi \frac{M_o H^2}{T} \dots\dots\dots 3.21$$

**3.6.9. Membrane deformation dissipated energy for design concept p-7 (MC-FQCHT (c2c&w2w))**

This structure has one circular element, twelve concave T-shape, six 3-panel element-I, six 4-panel elements, six 2-panel crisscross, and six T-shape element membrane units. Hence from Eqn. (2.9), (2.12), (2.14), and (2.23), and their sum will be the total membrane energy dissipated during the axial impact of this structure.

$$E_{Total.membrane}^{c2c\&w2w.MC-FQCHT} = N_c E_{membrane}^{circular} + N_c E_{membrane}^{Concave.T-shape} + N_c E_{membrane}^{3-panel-element-I} (\alpha = 60^0) + N_c E_{membrane}^{4-panel-element} (\beta = 60^0) + N_c E_{membrane}^{N.crisscross} + N_c E_{membrane}^{T-shape} \dots\dots\dots 3.22$$

$$E_{Total.membrane}^{c2c\&w2w.MC-FQCHT} = 1 \times 8\pi \frac{M_o H^2}{T} + 12 \frac{12.3 M_o H^2}{T} + 6 \frac{8.946 M_o H^2}{T} + 6 \frac{12.189 M_o H^2}{T} + 6 \frac{16 M_o H^2}{T} + 6 \frac{12.3 M_o H^2}{T}$$

$$E_{Total.membrane}^{c2c\&w2w.MC-FQCHT} = 452.21\pi \frac{M_o H^2}{T} \dots\dots\dots 3.23$$

**3.6.10. Membrane deformation dissipated energy for design concept p-8 (MC-FQCHT C2W)**

This last concept design structure has the same membrane element unit as the seventh one, which means they have the same theoretical membrane deformation dissipated energy value. Hence the total membrane energy for this structure is also the same as P-7, Eqn. (3.23) above.

**3.7. The mean crushing forces**

From the energy balance principal Eqn. (2.6), the mean crushing force can be derived as:

$$P_m = \frac{1}{2Hk} (E_b + E_m) \dots\dots\dots 3.18$$

Therefore, to calculate the mean crushing force for each developed conceptual design structure substitute the value of Bending dissipated energy and membrane deformation dissipated energy.

**3.7.1. The mean crushing force of P-1, Single-cell original hexagonal tube (SC-OHT)**

To get the mean crushing force, substitute Eqn. (3.9) and (3.11) into Eqn. (3.18), and the mean crushing force of the SC-OHTs can be obtained as:

$$P_m^{SC-OHT} \cdot 2H \cdot k = 2\pi M_0 \cdot L_c + 6 \frac{4.328 M_0 H^2}{T} \dots\dots\dots 3.19$$

where  $P_m^{SC-OHT}$  represents the mean crushing force of SC-OHT Pattern structure under axial quasi-static compression. It is assumed that the folding unit is deformed in the most ideal crushing manner during the folding and crushing process, that is, with a minimum average crushing [61]. So:

$$\frac{\partial P_m^{SC-OHT}}{\partial H} = 0 \dots\dots\dots 3.20$$

Thus,  $H$  can be derived and calculated as:

$$H = \sqrt{\frac{L_c \cdot T \cdot \pi}{12.984}} = \sqrt{\frac{\pi \cdot T \cdot B}{2.164}} \dots\dots\dots 3.21$$

Where  $L_c$  is the total length of the all-wall flange and  $B$  is the width of the wall. Substituting the value of  $H$  into Eq. (3.27) can be obtained:

$$P_m^{SC-OHT} = \frac{1}{8K} \sqrt{\pi B (311.161 \sigma_0^2 T^3 + 48K^2)} \dots\dots\dots 3.22$$

In a similar fashion for all structures, the mean crushing force will be calculated given in the following Table 3.9.

Table 3.9 The formulated formula of mean crushing force for all structure

Structure	Mean crushing force
SC-OHT	$P_m^{SC-OHT} = \frac{1}{8K} \sqrt{\pi B (311.161\sigma_0^2 T^3 + 48K^2)}$
MC-FTHT	$P_m^{MC-FTHT} = \frac{\delta_0}{k} \sqrt{20.207625\pi B T^3}$
MC-ICHT	$P_m^{C.M-ICHT} = \frac{\delta_0 T^2}{4K} \sqrt{800.1 \frac{\pi B}{T}}$
MC-DFHT	$P_m^{C.M-DFHT} = \frac{\delta_0 T^2}{4K} \sqrt{722.952 \frac{\pi B}{T}}$
MC-FQCHT C2C	$P_m^{C.M-FQCHT(c2c)} = \frac{\delta_0 T^2}{4K} \sqrt{201.15\pi \frac{(2b + \pi D)}{T}}$
MC-FQCHT W2W	$P_m^{C.M-FQCHT(w2w)} = \frac{\delta_0 T^2}{4K} \sqrt{268.72\pi \frac{(6b + \pi D)}{T}}$
MC-FQCHT (c2c&w2w)	$P_m^{C.M-FQCHT(c2c\&w2w)} = \frac{\delta_0 T^2}{4K} \sqrt{445.12\pi \frac{(6b + \pi D)}{T}}$
MC-FQCHT C2W	$P_m^{C.M-FQCHT(c2w)} = \frac{\delta_0 T^2}{4K} \sqrt{445.12\pi \frac{(6b + \pi D)}{T}}$

Both MC-FQCHT (C2C and W2W) and MC-FQCHT (C2W) have the same energy absorb element and number, hence they have also the same mean crush force. Only the difference between these two structures is the configuration of the internal cell cross-section. In analytical it hasn't affected, but in numerical simulation results, it has its factor.

The influence of structural dynamic effects on the dynamic load for P-5 w2w connection is:

$$P_{m-w2w}^d = EC \cdot P_{m-w2w} = 1.11 \cdot P_{m-W2W} \dots\dots\dots 3.23$$

### 3.8. Crashworthiness performance indicators

To evaluate the quality of the energy absorber more comprehensively, besides  $P_m$ , there are also some criteria to demonstrate the crashworthiness performance of energy absorbers, to evaluate the other typical indexes, to evaluate the crashworthiness of metallic thin-walled structures. For instance, total energy absorption (TEA), Specific Energy Absorption (SEA), Mean crush force ( $F_{mean}$ ), Peak crushing force ( $F_{Peak}$ ), Energy Absorption, Efficiency (EAE), and Crush Force Efficiency (CFE) are depicted underneath with numerical methods.

#### 3.8.1. Total energy absorption

Total energy absorption (TEA) portrays the vitality retention capacity of examples. It can be decided by the integration of the axial crushing force versus displacement.

$$TEA = \int_0^{Sef} Fdl \dots\dots\dots 3.24$$

where F is the instantaneous crushing force with a work of the crushing distanced. From numerical demonstrations, the instantaneous crushing force can be obtained.

**3.8.2. Specific energy absorption**

Specific energy absorption (SEA) is characterized as retained energy per unit mass of the thin-walled tube. It is one of the common criteria for comparing the energy absorption capacity of structures with distinctive mass which is given by:

$$SEA = \frac{TEA}{m} \dots\dots\dots 3.25$$

where m is the mass of the structure. A higher SEA indicates a higher energy absorption capability.

**3.8.3. Mean crushing force**

Mean crushing force (Fmean) is the reaction parameter for the energy absorption capability of a structure, which is calculated as

$$F_{mean} = \frac{TEA}{\delta} \dots\dots\dots 3.26$$

where TEA is the energy absorbed during collapse and relocation (d) or crush displacement.

**3.8.4. Peak crushing force**

Peak crushing force (FPeak) shows the arrangement of the first overlay while crushing the thin-walled structure. FPeak is the most extreme load in the load-displacement curve. It ought to be minimized and be close to the normal crushing force as much as conceivable for superior occupant’s survival rate.

**3.8.5. Energy absorption efficiency**

Energy absorption efficiency (EAE) is characterized by the proportion of mean crush force of the multi-cell tube and single-cell tube. EAE proposes the advancement of the normal crush force of the multi-cell tubes.

$$EAE = \frac{F_{mean.multi.cell.tube}}{F_{mean.single.cell.tube}} \dots\dots\dots 3.27$$

**3.8.6. Crush force efficiency**

Crush force efficiency (CFE) is characterized as the proportion between the mean crush force and the peak crush force. The consistency of the load-displacement curve is demonstrated by CFE.

$$CFE = \frac{F_{mean}}{F_{peak}} \dots\dots\dots 3.28$$

**3.8.7. Fluctuation coefficient (ω) in plateau stage**

It is defined as:

$$\omega = \frac{F_{\max} - F_{\min}}{P_m} \dots\dots\dots 3.29$$

By substituting all the responding parameters introduced in sections 3.4 and 3.5 into the Eqs under these sections, the final theoretical results are obtained and will be discussed in chapter 5.

**3.9 Finite Element Method Computational Analysis Procedure**

LS-DYNA is a non-linear transient dynamic finite element program that is planned to solve short-duration dynamic problems. This study used the explicit dynamic analysis system of LS-prepost for modeling and LS-DYNA for solving the axial impact crush analysis. The overall procedures of FEM analysis for this study after selecting explicit dynamics from the rest analysis types are listed as follows.

**a) Importing Geometries**

The CAD of thin-walled tube structure modeled in SOLIDWORK and saved with the format of IGS file is imported into geometry ls-prepost and aligned to with global coordinate system as Figure 3.7 below. After meshing surfaces generated for the compatibility of the shell element type in the analysis of the imported tube structure by autoM, the moving impactor was created by shapeM with the standard size of the shell tube.

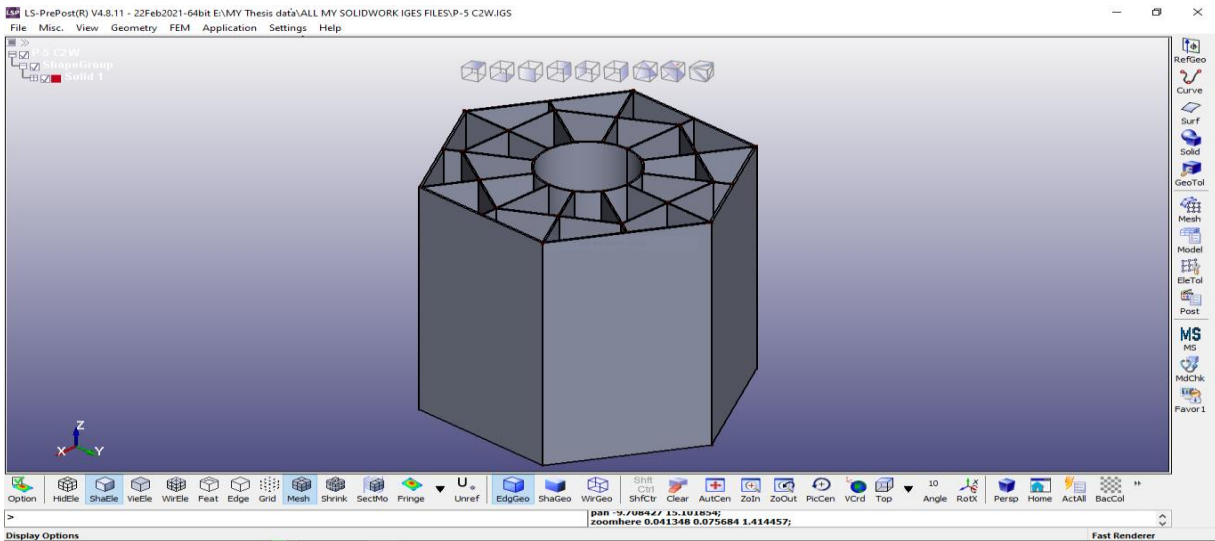


Figure 3.7 Importing IGS file crash box into LS-Prepost

**b) Meshing**

The meshing element size for the ACB is set to be 4 mm initial simulation and comparison and 2mm for the best-designed one as recommended with NHTSA. Since the average thickness of the tube elements is smaller than the other dimension of the part, the best meshing for the element was the shell element with the type of mixed triangular node-quadrilateral element. The four-node Belytschko-Tsay shell elements with five integration points through-thickness were used to discretize the hybrid structure [80]. Under the premise of ensuring that the simulation calculation met the

accuracy, the mesh size of the finite element model in this work was set to  $4\text{ mm} \times 4\text{ mm}$  as shown in Figure 3.8. To save the computational cost, no convergence analyses were carried out to determine the appropriate element size in this study. The meshed model, statics, and material properties or all FE model keyword for the parts of the model are attached in the LS-prepost keyword. K.file APPENDIX A.

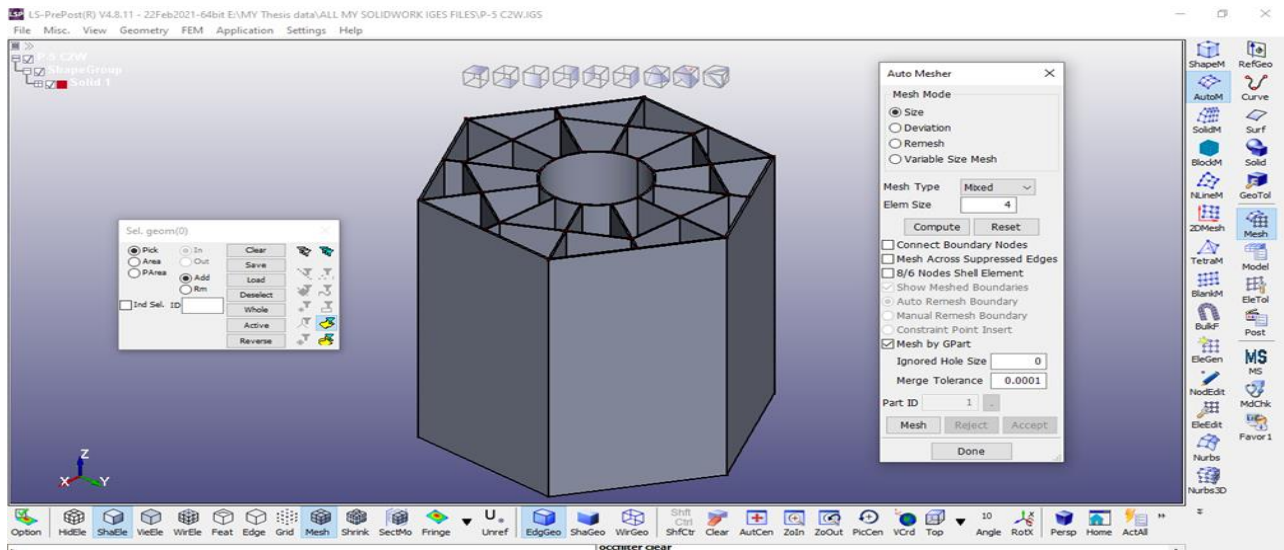


Figure 3.8 The meshing of the crash box in LS-Prepost

The boundary condition setup for this simulation is that the bottom of the tube was fixed in all global directions to ground by segment node as illustrated in Figure 3.9 when other parts are deformed and displaced. The solid impactor was fixed globally in the x and y direction and free in the z-direction with an initial velocity of 15 m/sec to simulate the dynamic crushing process. The bottom end of the tube was supported by a rigid wall, and the top end of the tube was compressed by a 700 kg mass of impactor. When the deformation displacement of the tube reached 168 mm (70% of the tube length), the tube was unloaded and the simulation stopped.

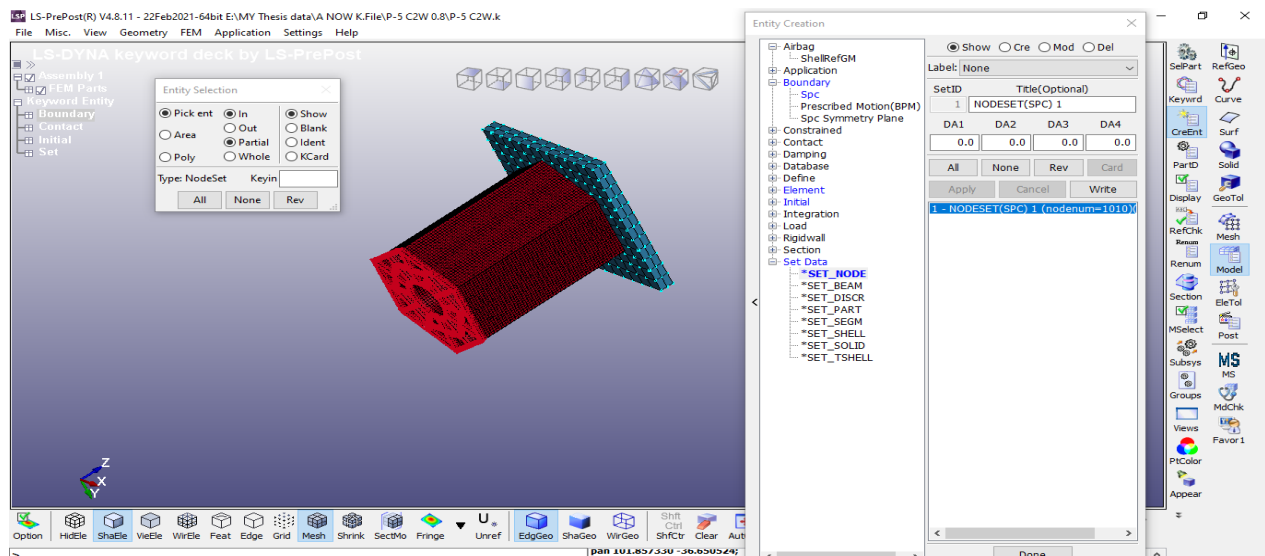


Figure 3.9 Assigning boundary condition for crash box in LS-Prepost



### c) Assigning intended material and its mechanical properties value

The perspective material modeling (MAT) type for each component was assigned from the Model keyword and their mechanical properties values are interred manually in cards listed from some engineering data with consistent units as shown in Figure 3.10. The hybrid tubes of aluminum alloy AL7075-T651 modeled a piecewise linear elastic-plastic strain hardening material (Mat-24 in LS-DYNA). Von Mises plasticity and isotropic hardening were chosen for the material model. The impactor and the rigid wall constraint were modeled using the rigid material (Mat-20) of LS-DYNA to simulate thin-walled tubes and upper-end compression rigid plates, respectively. Properties of each material used for this study are shown in the material property APPENDIX B.

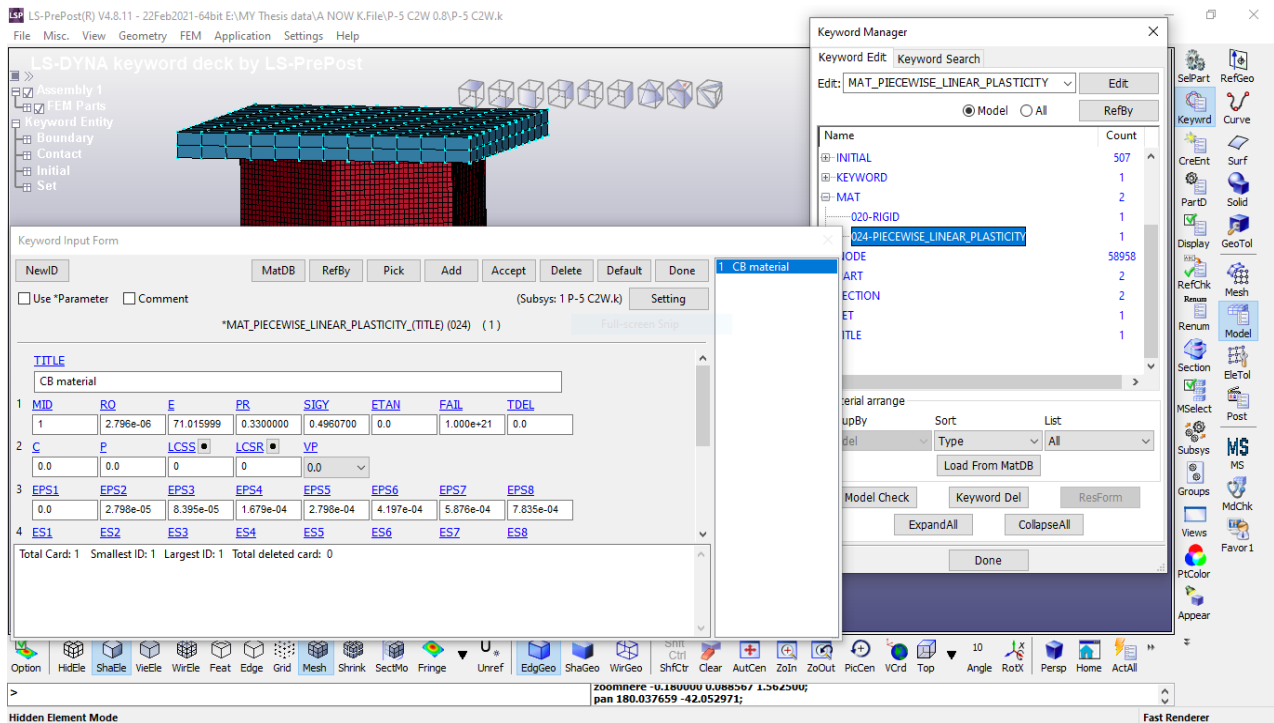


Figure 3.10 Assigning material types and property for crash box in LS-Prepost

### d) Defining the connections and contacts

The contact interaction among the component of tube structure and moving undeformable impactor was defined as Figure 3.11 an automatic surface-to-surface contact was applied at the interface between the impactor and the tubes to simulate their interaction during crush deformation and Automatic single-Surface contact was applied to hybrid tubes to prevent penetrating during the crushing process. The failure of the connection (spot-welded type) between the beam tube and ground or bottom support is taken as negligible and it is supposed that all segment node set of bottom tube parts is constrained to the fixed support in all degree of freedom without modeling the mechanical strength of the coupled part. This also was taken for the connection between the tube and fixed bottom support. Contact surfaces can be defined to have friction. The static friction coefficient and dynamic friction coefficient were set to 0.3 and 0.2 respectively in the numerical model [81]. The effect of strain rate was ignored in the FE models because aluminum was not sensitive to strain rate. [10,28].

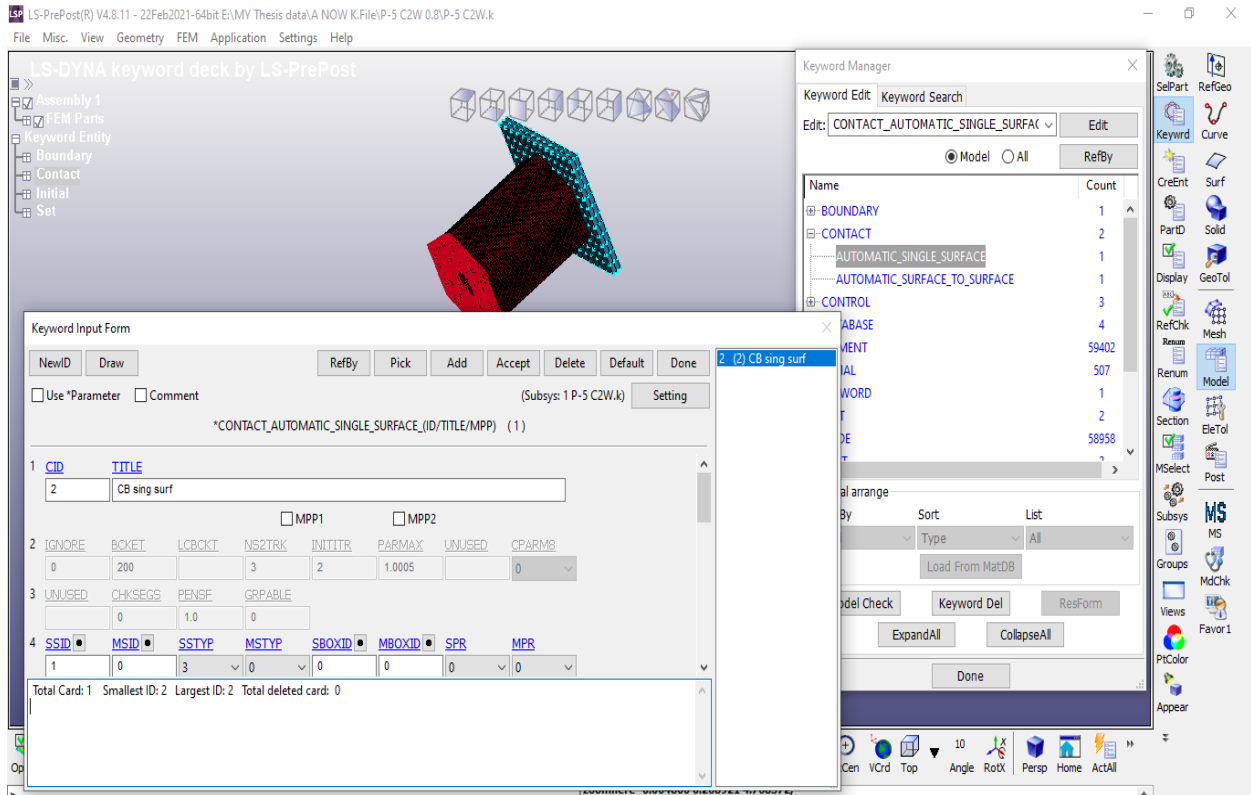


Figure 3.11 Defining connection and contact part for crash box in LS-Prepost

### e) Setting the Analysis

The choice of the simulation speed and time was based on the fact that the ratio of the total kinetic energy to the total internal energy was controlled to be less than 5% [61]. Hence, a loading velocity of 15 m/s is acceptable. The dynamic explicit algorithm was applied in this study, which has been considered an effective method to improve efficiency [20]. Extra care was taken to assign a smooth step time function to minimize inertial effects, thereby mimicking the quasi-static rate of crushing of the experiment. A general contact was created to avoid self-penetration between all potential contacted surfaces in the crash process while Hourglass control was used to capture the mechanical performance of metal tubes undergoing large plastic deformation. To avoid a zero-energy deformation mode and volumetric locking a stiffness-based hourglass control was used [67]. Reduced integration was chosen to obtain an efficient approach.

Under the control keyword, the types of energy to be computed were selected, termination (Maximum number of cycles) and time step for analysis were assigned to be 50 ms and 0.9 ms respectively as Figure 3.12 shown below. Normally, the number of the cycle depends on the time increment/step which by itself depends on the number of element size and material properties. Small numbers of elements end up faster than large amounts of the element size. Most axial impact analyses taken assigned to be 0.9 and less. In this study, the maximum allowable 0.9 ms was enough for the end of deformation.

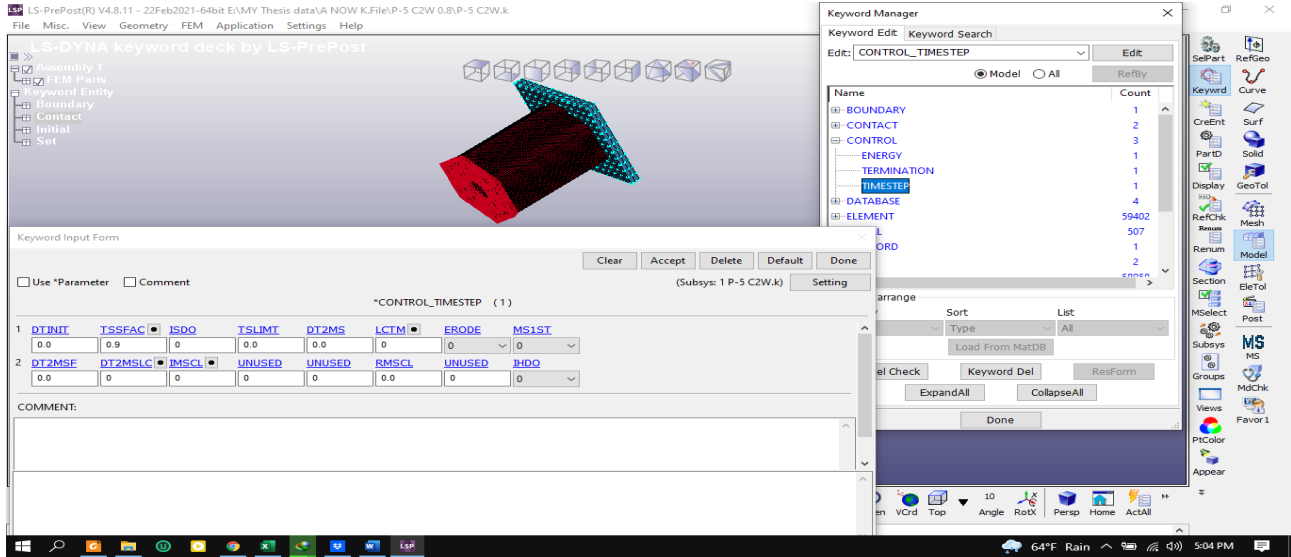


Figure 3.12 Assigning setting analysis for crash box in LS-Prepost

**f) Solve/Run the Analysis**

Once all necessary input parameters are set and the model is checked the analysis was run in LS-DYNA and information related to dynamic crushing is recorded and post-processing was done in LS-prepost and display with figures, charts, curves and also exporting in excel files of all crashworthiness indices. Generally, this study conducted eight explicit dynamics analyses with refined mesh for the best design selected structure part.

The general setup of FE models was developed using the nonlinear explicit finite element code LS-DYNA as shown in Figure 3.13 was used to simulate the crushing process.

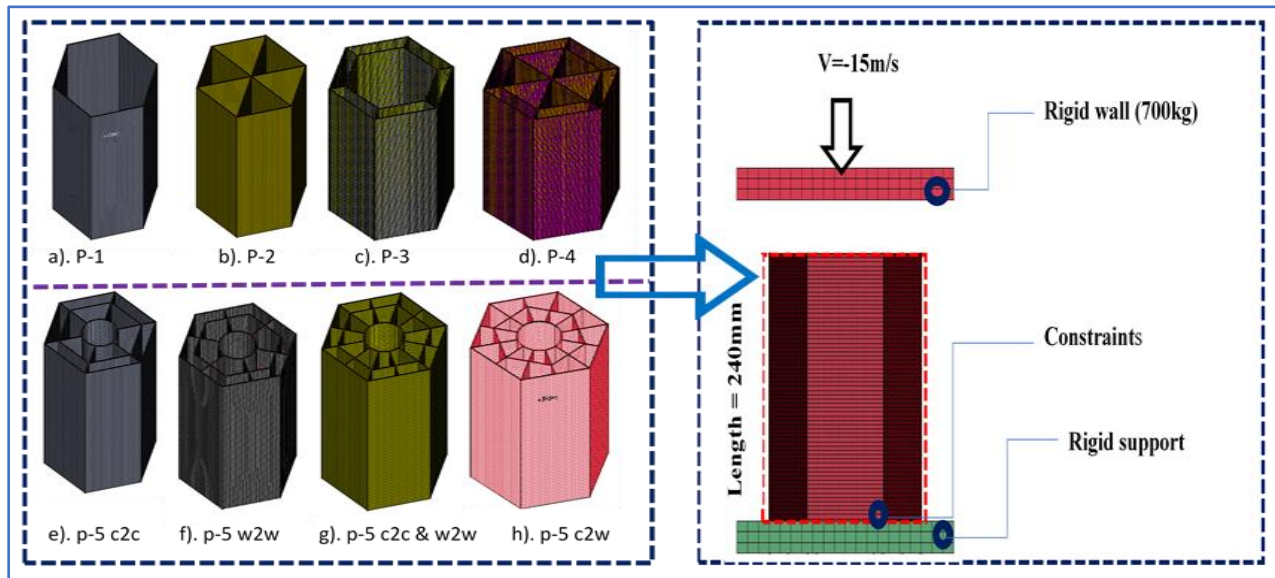


Figure 3.13 Finite element models of integrated bionic structures with the mesh size of 4 mm × 4 mm with its overall setup for modeling and simulation (a) SC-OHT (original hexagonal tube), (b) MC-FTHT (full triangular hexagonal tube); (c) MC-ICHT (internal clone hexagonal tube)

## CHAPTER FOUR

### 4. DESIGNXPLORER ANALYSIS AND PARAMETRIC OPTIMIZATION USING MULTI-OBJECTIVE ALGORITHM IN ANSYS

This chapter deals with the DesignXplorer and sampling design points for the Structural optimization process by the Parameterization approach of the automotive crash box in a general framework for structural optimization. Overview of parameterizing via finite element analysis (FEA) with the geometry CAD software; formulation for geometric parameterization of finite element models, design explorer implementation with the procedure of parametric and finite element analysis. In the end parameterization with FEA implementation response surface modeling in optimization using a multi-objective algorithm, which power to the mathematical model will be developed.

#### 4.1. Optimization and ANSYS

FE-based design optimization is currently a well-recognized and influential practice for engineering design. The application of this technique involves several stages such as geometric modeling, mesh generation, k2finite element method implementation, numerical optimization techniques, and some post-processing stages [82]. Software enhancements have made the overall design process more versatile and reliable. Ansys 2020 R1 as the selected finite element software for this study, is one of the leading multi-objective optimization software in engineering. Its improved user interface offers effective user-machine communication where the engineering intent, data relationships, and the state of the analysis can be effortlessly understood.

#### 4.2. Parameterization with Finite Element Analysis

Finite Element Analysis (FEA) is a numerical method for solving problems of engineering and mathematical physics. Typical problem areas of interest include structural analysis, heat transfer, fluid flow, mass transport, and electromagnetic potential. The analytical solutions of these problems generally require the solution to boundary value problems for partial differential equations.

Then FEA methods divide the structure into small but finite, well-defined, elastic substructures called elements. By using a system of simultaneous algebraic equations polynomial functions, together with matrix operations, the continuous elastic behavior of each element is developed in terms of the element's material and geometric properties. Loads can be applied within the element, on the surface of the element, or at the nodes of the element. The element's nodes are the fundamental governing entities of the element, as it is the node where the element connects to other elements, where elastic properties of the element are eventually.

#### 4.3. Parameter Optimization in ANSYS workbench

A parametric study was undertaken to find the optimum value of different crash box parameters on crashworthiness index. The parameters considered for the analysis were shell thickness, crash box length, outer and inner hexagonal side, and diameter of center circle geometry. The results of the parametric study have been plotted in terms of performance indexes such as total deformation and total elastic strain.

Workbench is a suite of powerful engineering simulation programs based on the finite element method, the workbench is designed as a general-purpose simulation tool, and the workbench can be used to study more than just structural (stress/displacement) problems. Workbench offers a wide range of capabilities for the simulation of linear and nonlinear applications. In a nonlinear analysis workbench automatically chooses appropriate load increments and convergence tolerances and continually adjusts them during the analysis to ensure that an accurate solution is obtained efficiently.

#### 4.4. Parametric optimization procedure

After the analysis with a finite structural element of the crash box has been carried out, for the condition imposed the client, a parametric optimization project is carried out, starting from the optimization input parameters: a) the thickness of the crash box shell (mm) b) Outer and inner hexagonal side width (mm) c) diameter of center circle (mm) d) length of the crash box (mm) then adjust the optimization output parameters: a) total deformation b) equivalent elastic strain c) strain energy. Whose values are determined according to the results of the static structural analysis as well as the limit values as objectives of multi-objective optimization? A standard optimization procedure (Optimization Process) in Ansys is described in Figure 4.1 below.

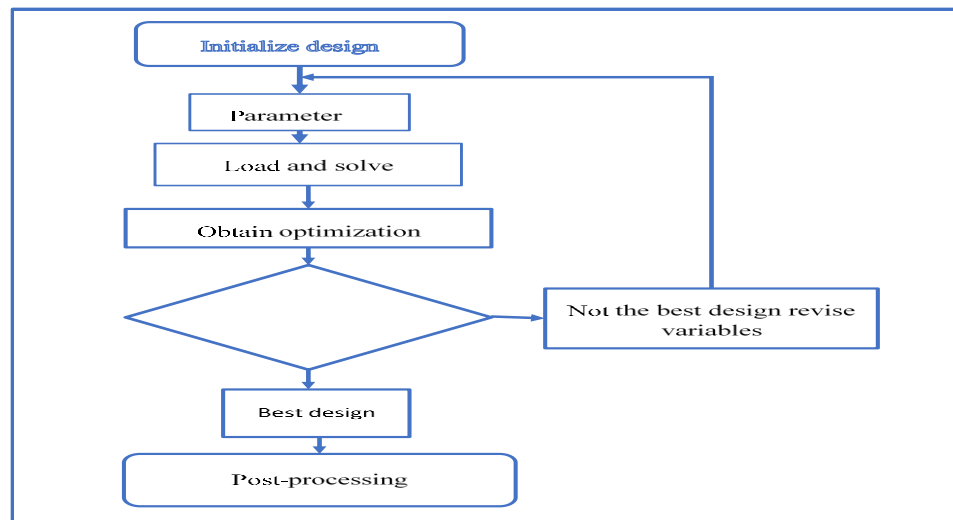


Figure 4.1 The crash box optimization process

##### 4.4.1. Determine the design variables

Design variables are shape parameters of basic geometric features. The number of design variables of this formulation is small whereas various constraints can be considered. The finite element method formulation of the problem results in a system of algebraic equations. The method yields approximate values of the unknowns at a discrete number of points over the domain. The simple equations that model these finite elements are then assembled into a larger system of equations that models the entire problem. A formulation for geometric parameterization of finite element models is derived from efficient shape optimization. The formulation allows us to express the stiffness and the mass matrix for the geometrically parameterized hexagonal element in an explicit form allowing versatile design parameterizations [83].

From the result of CAD and conceptual design modeling analysis, it can be seen that the shell element thickness, side length, and diameter have a significant influence on the performance of the crash box. Therefore, the shell thickness ( $T$ ), the diameter of the core circle ( $D$ ), the Length of the crash box ( $L$ ), and side length  $B_i$  ( $i=1, 2$ ) of the outer and inner side design variables of multi-objective optimization, as shown in Figure 4.2. The variation ranges of  $T$ ,  $D$ ,  $L$ , and  $B_i$  are used as the dimension constraints. Thus, considering the actual design requirements of the thickness in the traditional crash box, and the analysis results.

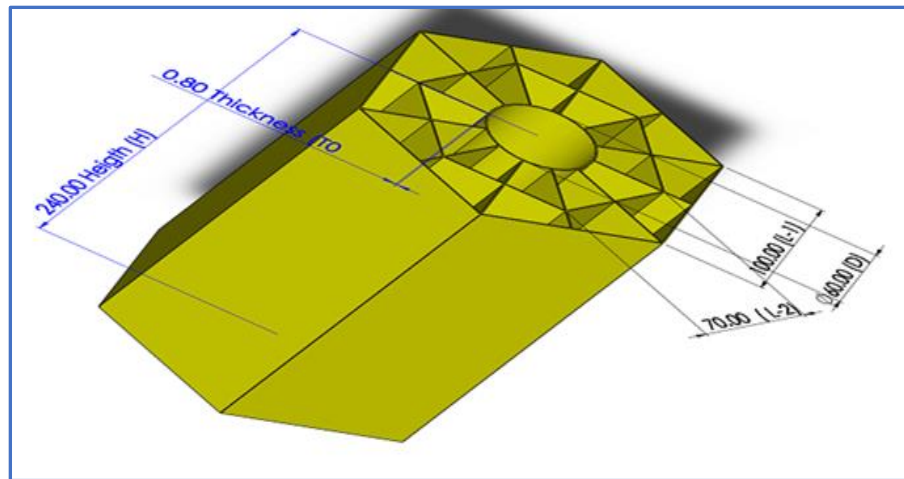


Figure 4.2 Design variables of parameter optimization

Also, the parameter selected for the optimization is given in table 4.1.

Table 4-0-1 design variable of parameter selected for optimization

Parameter	Length of tube	Thickness	Outer Width	Inner width	Diameter of circle
Value	240 mm	0.8 mm	100 mm	70 mm	60 mm

#### 4.4.2. Approximate model of optimization objectives and constraints

It has been pointed out in the previous chapter that the energy-absorbing, cushioning capacity, and compression displacement are three important indexes in evaluating the comprehensive performance of the newly designed crash box. In combination with all content in this chapter,  $ESEA$  is selected as the optimization target to characterize the energy absorption performance. Meanwhile, the average collision force can represent the average buffer performance of the crash box in the whole collision process. Thus,  $F_{av}$  is chosen as the other optimization objective of the multi-objective optimization.

As for the constraints, the cross-section of the new crash box is a thin-walled structure with many edges and corners, and it is prone to deformation in actual use. Therefore, the range of compression displacement  $S$  caused by the deformation should be rationally controlled, whose upper limit is selected as 70% (168 mm) of the total length of the crash box, in another case maximum total deformation. Meanwhile, the impact on the rear part of the crash box should not be too large, so the peak impact force  $F_{max}$  must not exceed the allowable value. Besides, from the view of being lightweight, the mass  $M$  of the crash box should be as small as possible. However, too small quality

means that the thickness of the shell and the inner core is too thin, which is detrimental to the overall performance of the structure. Therefore, this work sets the variation range of  $M$  based on the quality of the original crash box.

#### 4.4.3. *Defining Optimization modules*

The powerful module for parameter optimization in Ansys is DesignXplorer™ Module. DesignXplorer is a component of ANSYS Workbench that can help to make designs more efficient and robust. And also, a powerful tool for designing and understanding uses response surfaces and assemblies. The sensitivity of the response of the system is determined to variations in the input quantities to identify which input variables play a dominant role in the response. These help to develop a surrogate function that enables you to quickly predict the system output for any parameter combination within the design space. By using this surrogate function to determine the optimum input settings for a defined set of goals and constraints [84].

The main purpose of the DesignXplorer™ module is to effectively identify the relationship between the design variables and the desired performance of a model. Based on the output, the analyst can modify and influence the design, so the required outcomes are obtained. DesignXplorer™ provides enough tools to perform parametric optimization cases with a reasonable number of parameters in a single or Multiphysics analysis. In other words, DesignXplorer is a powerful approach to explore, understand, and optimize an engineering challenge. Once run, the DesignXplorer™ module comprises a series of steps to obtain an optimized model. As soon as the model is generated, and the parameters or design variables are set, a what-if study can be carried out. The *What if* study feature of the module automatically runs through a list of specified design points. Then, a sensitivity or parameter correlation analysis identifies input parameters that do not have a major impact on the outcomes of the simulation and can be implemented where a large number of parameters would hinder the successful continuation of a study.

A Design of Experiments (DoE) phase specifies the type and range of each parameter and design points are automatically chosen to effectively explore the parametric design space. Subsequently, a response surface model can be implemented to rapidly provide approximated values for the output parameters without having to perform a complete simulation. After this step, the optimization phase takes place where objectives, constraints, and input parameters are defined. If a response surface was implemented, thousands of configurations are then explored in a few seconds depending on the type of study. If a direct solver is preferred without a response surface, convergence algorithms are followed. Finally, a design robustness analysis can be carried out after the optimization phase to understand the system's performance and trade-off variables involved. The DesignXplorer™ module is one of the most advanced optimization tools available and is widely used in the engineering industry as well as in a variety of research fields.

### 4.5. Optimization Methods implemented

#### 4.5.1. *DesignXplorer Implementation with Optimization*

In module ANSYS the DesignXplorer provides a much more efficient approach by providing a response surface that is based on a finite element solves combined with the use of mesh morphing

[85]. The ever-increasing demand to lower production costs due to increased competition has prompted engineers to look for rigorous methods of decision making such as optimization. Optimization in its broad sense can be applied to solve any engineering problem. And methods coupled with modern tools of computer-aided design are also being used to enhance the creative process of the conceptual and detailed design of engineering systems.

Ansys 2020 R1 implements a variety of optimization techniques involving complex numerical optimization methods as well as modern optimization algorithms. There is no single method or technique for solving all optimization problems efficiently. Hence many optimization methods have been developed for solving different types of optimization problems. It is at the entire discretion of the engineer to choose a method that is computationally efficient, accurate, and appropriate for design problems [86]. Input parameters can either come from design modeler or various CAD systems these parameters can be in terms of thickness, length, and depth, etc. they can also come from mechanical in terms of force, materials properties, etc. the output parameters are calculating in mechanical and can, for example, be in terms of total mass stress or response. After setting up an analysis with several input parameters and out parameters there are the steps that can be run within design explorer.

The optimization method applied depends on the type of problem and defined parameters. Additionally, the desired optimization technique can be specified, or external optimization tools can be integrated which is a field with ongoing research and advances. Parametric optimization solvers in Ansys 2020 R1 use a variety of techniques and specific algorithms depending on the model and output requirements.

#### *4.5.2. Parametric Optimization Techniques*

Once the model constraints and requirements are defined and the simulation's responses are characterized, DesignXplorer™ provides the following types of optimization algorithms:

- **Shifted Hammersley Sampling:** An optimization method used for sampling generation in the analysis. The Shifted Hammersley algorithm is a quasi-random number creator generally used for Quasi-Monte Carlo analyses (numerical integration simulations) where the algorithm provides low-discrepancy sequences (samples).
- **Multi-Objective Genetic Algorithm (MOGA):** The MOGA is a development of the NSGAI (Non-dominated Sorted Genetic Algorithm) which is a type of Evolutionary algorithm. The the main purpose of the algorithm is to augment the adaptive fit of a population of potential solutions to a Pareto front constrained by a set of specified objective functions.

The technique implements an evolutionary procedure with selection, genetic crossover, and mutation operators [87]. The typical steps involved in a MOGA analysis include the incorporation of an initial population from the defined parameters. Then, MOGA creates a new population via Crossover and Mutation, and the design points in the new population are updated. Consequently, a convergence validation is carried out, if the optimization converged, the analysis is ended, and the results are generated. However, if the study did not converge, a stopping criteria validation is conducted. Depending on whether the maximum number of iterations set was reached, the analysis can be



finished without iteration of the algorithm is run again generating a new population if the maximum number of iterations set was not reached. Figure 4.3 illustrates the workflow of the MOGA optimization method in this study.

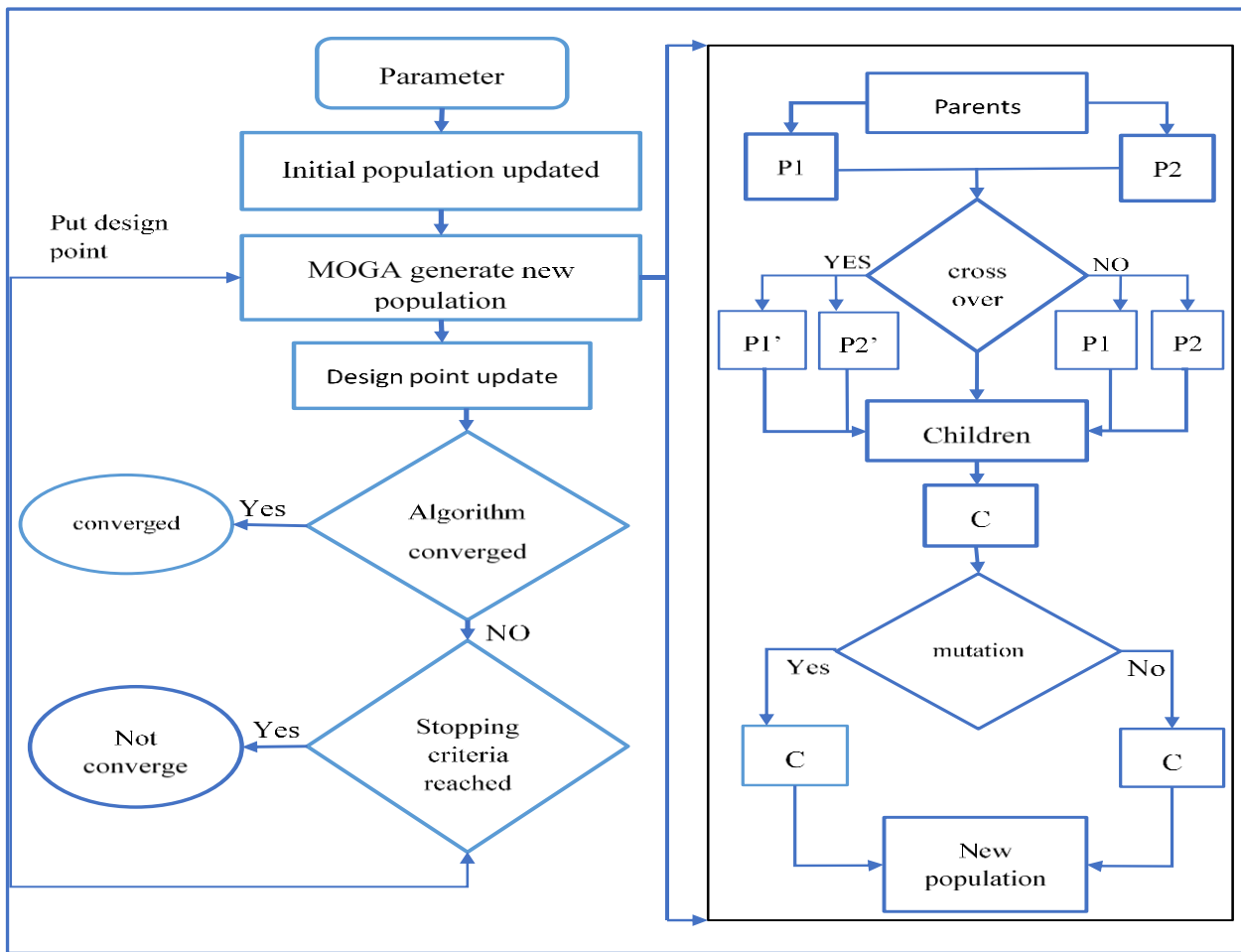


Figure 4.3 MOGA method workflow

- Nonlinear Programming by Quadratic Lagrangian: The NLPQL method is a numerical optimization algorithm. This technique is specially developed to solve constrained non-linear programming models. In principle, the method generates a sequence of subproblems obtained from a quadratic approximation of the Lagrangian function and linearization of constraints. Consequently, the information is updated by an iterative Newton's method and finally stabilized by a line search. The method assumes the problem size is relatively small-scale and the accuracy largely depends on numerical gradients obtained.
- Adaptive Single and Multi-Objective Optimization: ASO is a mathematical optimization a technique that implements the MOGA optimization algorithm supporting single or multiple objectives, multiple constraints, and limited to continuous parameters. In addition to the optimization algorithms embedded on DesignXplorer™, the implementation of external optimizers within the DesignXplorer™ module is also possible. Available optimization

extensions can be installed, integrating the features of the external optimizer into the design workflow.

#### 4.6. Design of experiments and response surface modeling in optimization

Optimization methods known as mathematical programming techniques are generally studied as a part of Operations Research. Mathematics scientific methods and techniques to decision-making problems to establish the best or optimal solutions. The design of the experiment is one such well-defined area of operation research. This method enables one to analyze the experimental data and build empirical models to obtain an accurate representation of the physical situation. Design of experiment (DOE) and response surface modeling (RSM) is made to minimize the computational expense incurred in solving such a problem.

##### 4.6.1. Set up generate for the response surface and response surface optimization.

During set up and generate the input and output parameters are known in which the geometry of the parameter of shell thickness and length of the crash box is the input parameter, and the safety factory minimum and mass are the output parameters for the response surface. Figure 4.2, shows the ANSYS 2020 R1 workbench for designXplorer set up for analysis. The purpose of the response surface to interpolate value the multiple dimensions.

To define the design of experiments (DOE) is used to affect a design space parameter for crash box so that a statistical model can be built to predict responses like the maximum stress, safety factory minimum, total deformation, and solid mass of a given design. DOE is useful when one can only sample a limited number of points (i.e., run a limited number of simulations). The key the idea of DOE is to “spread out” the samples so that the resultant statistical model has low uncertainty in its model estimation and thus high prediction accuracy. Define parameters and response; To conduct DOE for a given model first define the list of design variables and objectives that we care about (In Ansys, these are called input and output parameters). To do so, open the “Project Schematic” window, which shall look like Figure 4.4.

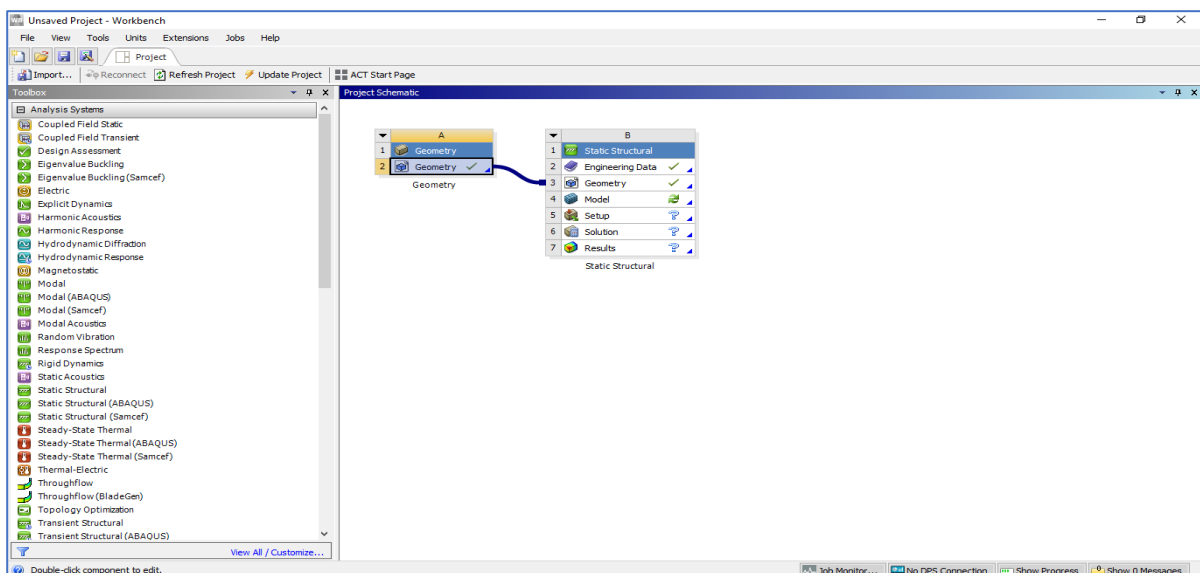


Figure 4.4 The outline of the project schematic window

Choose a Design Exploration method, in the design exploration window, find the response surface. This will allow us to perform DOE to create a predictive model, called a response surface. Drag the “Response Surface” tab from the Toolbox on anyone dashed box near “Parameter Set” this is shown in Figure 4.5. The Design of Experiments (DOE); is the procedure to collect a representative set of data relating to a process, technology, or an engineering project, adequate, data to calculate a response surface, and then executing an optimization (for optimization of a Response Surface too). The Response Surface accuracy will depend plenteously on the DOE scheme adopted, and in particular, the number of Design Points that have been computed.

	A	B
1		Enabled
2	✓ Design of Experiments	
3	Input Parameters	
4	Geometry (A1)	
5	P1 - P3@DS_Thickness_of_shell@Extrude_Thin1@Crash_box_Model.Part	✓
6	P2 - P3@DS_Length_of_shell@Extrude_Thin1@Crash_box_Model.Part	✓
7	P3 - P3@DS_Diameter_of_cirde@Sketch1@Crash_box_Model.Part	✓
8	P4 - P3@DS_Inner_hex_side@Sketch1@Crash_box_Model.Part	✓
9	P5 - P3@DS_Outer_hex_side@Sketch1@Crash_box_Model.Part	✓
10	Output Parameters	
11	Static Structural (B1)	
12	P6 - Total Deformation Maximum	
13	P7 - Equivalent Elastic Strain Maximum	
14	P8 - Strain Energy Maximum	
15	Charts	
16	✓ Parameters Parallel	
17	✓ Design Points vs Parameter	

Figure 4.5 The outline of the parameter set in the design of the experiment module

The Parametric correlation; uses the responses that can be easily obtained as the study offers an excellent graphical approach through the Parameters Correlation and the parametric correlation study allows two very important things: which input parameters have the greatest impact on design and identifies how the input-output relationship becomes linear or quadratic. The finite element analysis has been performed, and the influence and impact of the input parameters on the output parameters are described.

Defining the parametric simulation model with ANSYS workbench.

- Start ANSYS workbench 2020 R1
- Insert a static structural (ANSYS) system in the schematics

- Right-click on the geometry then browse and select the crash box file
- Select the model and double-click the crash box item.
- The select model then edit or double click
- Note that the project page now contains a parametric set bar that holds the DM parameters.

In this geometric parametric are defined from ANSYS Design Modeler and are automatically collected in the parameter set regardless of their name. Geometric parameters can also be defined directly from the CAD system using a prefix to flag the ones that are relevant for the simulation. And also mix parameter sources could be imported from the CAD model and additional ones defined in ANSYS Design Modeler.

Under mesh, insert a sizing, pick the crash box body and set the size of 5mm and insert a mapped face meshing and select all faces. Under static structural insert cylindrical support and free the tangential degree of freedom (radial and axial should be fixed). Insert a pressure load 3.256 MPa in the direction (set the pressure definition to the component). The pressure is applied on the small surface of a thin-walled cross-section of the crash box. Under solution insert total deformation, equivalent elastic strain, and strain energy, then solve the model optional.

Output parameters are quantities maximum total deformation, maximum equivalent elastic strain, and maximum strain energy for safety factor minimum. To set these as parameters, go to the solution under the properties of the bodies check the maximum total deformation, equivalent elastic strain, and strain energy. Parametric variation for the crash box, going to perform the deterministic analysis of the crash box for the following parameter ranges.

- Ds- width of the outer hexagonal 90 mm to 110 mm
- Ds -width of the inner hexagonal 63 mm to 77 mm
- Ds-thickness of shell tube 0.9 mm to 1.1 mm
- Ds-length of the tube 216 mm to 264 mm
- Ds-diameter of core circle 54 mm to 66 mm. do not need to specify how many points are to be taken for each parameter the DOE method will give us necessary points.

Setup up the response surface, go back to the schematic page and insert a ‘response surface’ as Figure 4.6 a cell from the design exploration toolbox. Select the design of experiments then set the upper and lower bounds of each input parameter or make its automatic setting. Once the simulation has been performed select the ‘response surface’ then ‘update’

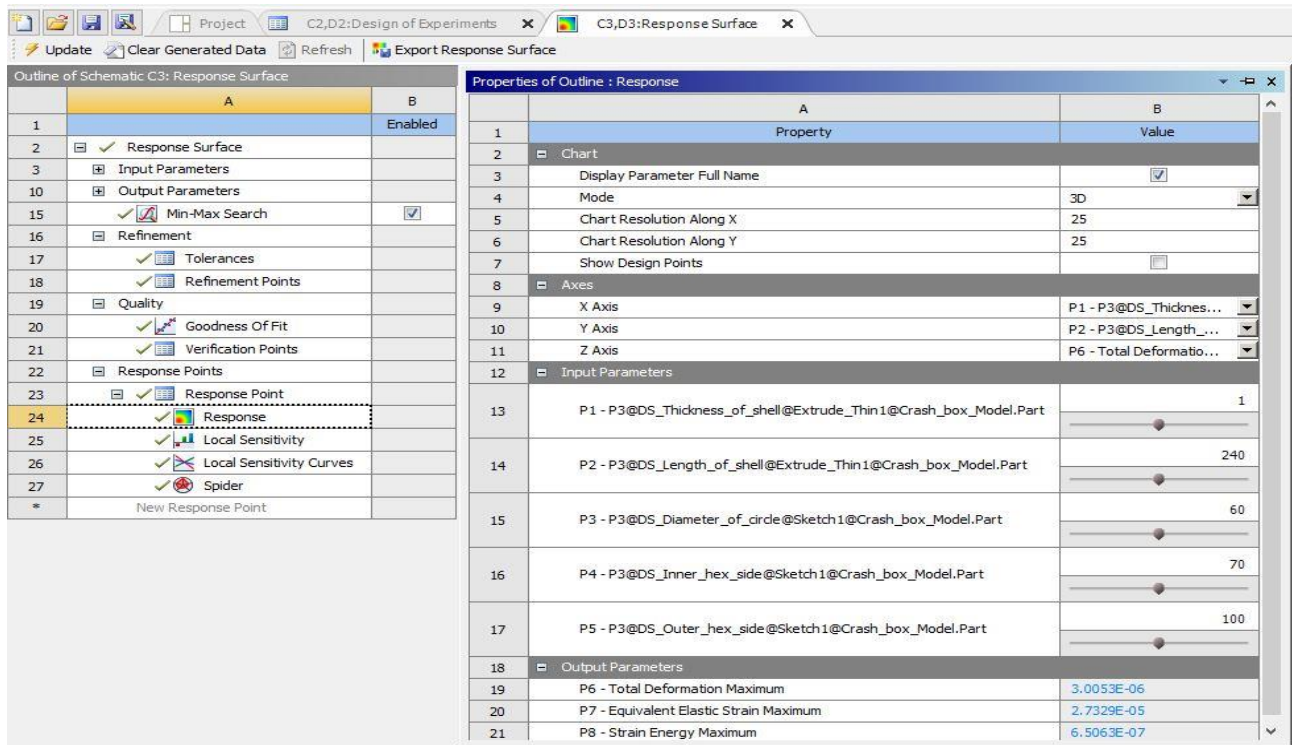


Figure 4.6 Outline schematic of the response surface set-up

#### 4.6.2. A MOGA optimization Setup

After response surface optimization as Figure 4.7, the next step has to do with setting the optimization method and other parameters to be taken into consideration by the optimization module. The selected optimization method is a Multi-Objective Genetic Algorithm (MOGA) A MOGA optimization supports multiple objectives/constraints and aims to find a global optimum.

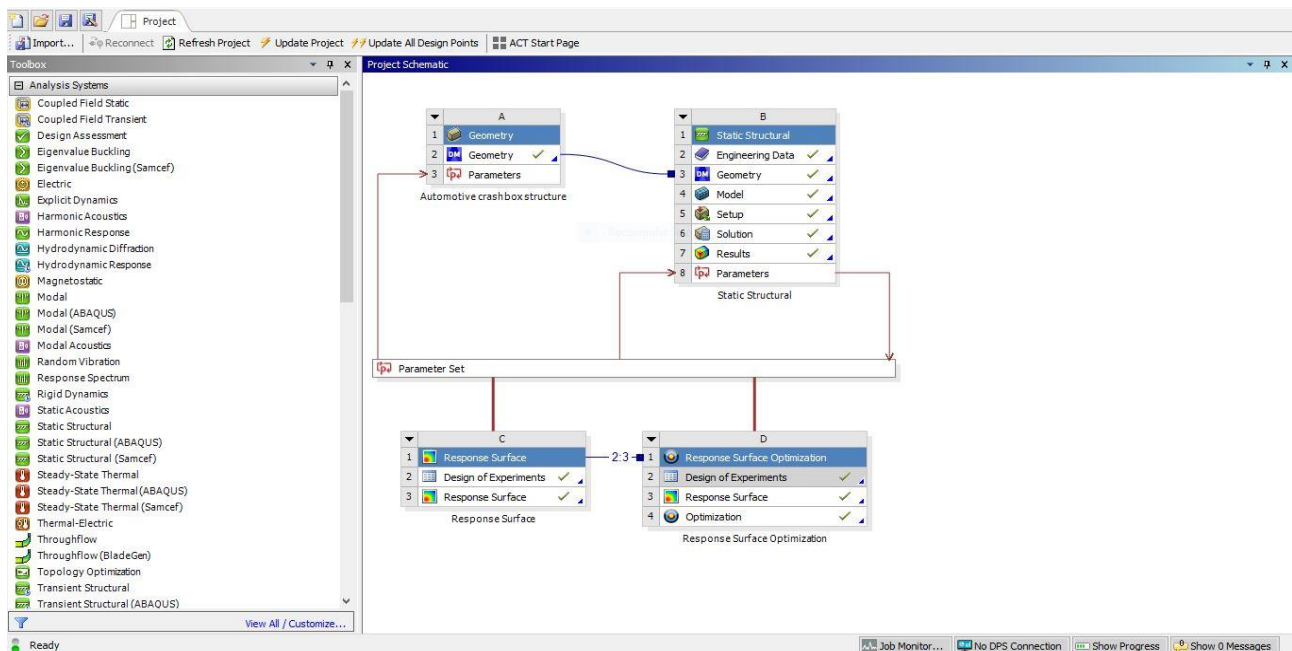


Figure 4.7 Set-up demonstration for surface response optimization

Once the optimization method is selected as Figure 4.8, the number of sample points is defined. The default value of 500 initial sample points is kept as well as iteration parameters and allowable Pareto percentage. A solution is said to be Pareto efficient if the objective functions can no longer be improved without degrading other objective values.

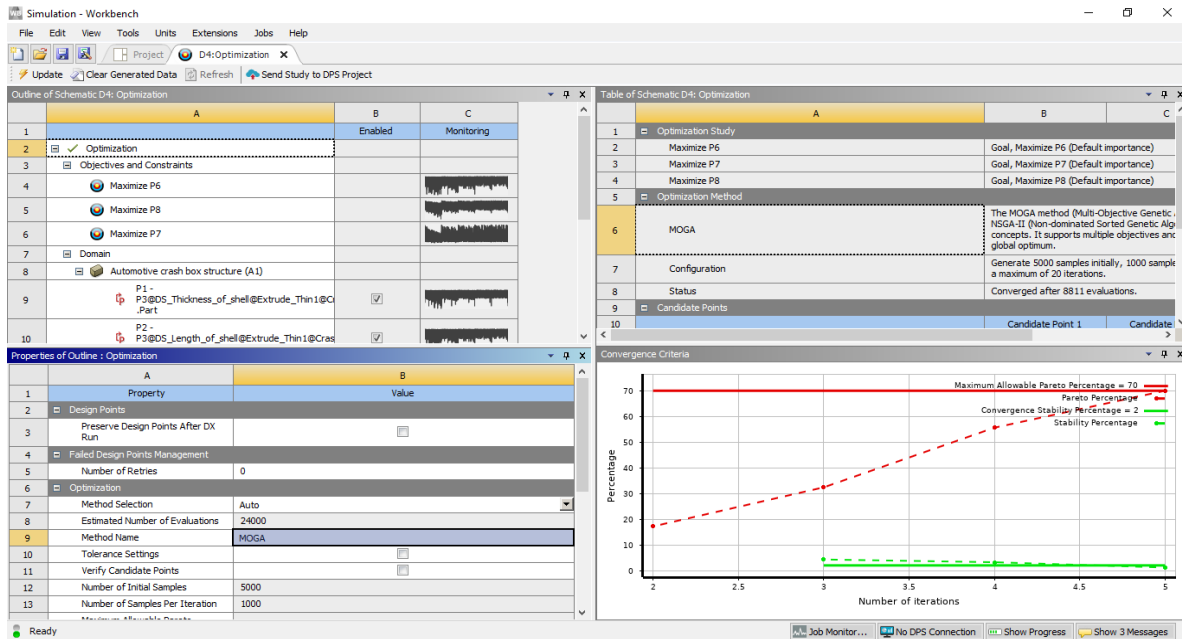


Figure 4.8 Optimization Methods selection setup

After the optimization settings have been defined, the optimization process can be run. When the optimization process is run, the initial samples are created and individually solved by the respective module (Fluent, Mechanical, etc.) After all the initial samples are solved, the specified optimization algorithm (MOGA) is automatically run and 3 candidates that meet the requirements are suggested by the optimization module when the process is completed. Some samples may have issues while being solved and output values would not be updated by the optimization module.

The specified number of design candidates (3) are suggested by DesignXplorer once the optimization process is completed and using the optimized values for the input parameters, a new FEM in LS-Prepost and experimental simulation is run in LS-DYNA, then compared the result with original design one.

#### 4.7. Sensitivity analysis of parameters

The sensitivity analysis method is carried out to analyze the influence of each parameter on the energy absorption performance. The newly designed crash box contains five main input parameters, to be analyzed in this section. In general aspects, the parameters that have significant impacts on the performance will be identified, and the parameters with smaller sensitivity will be treated as constants, and based on this, the high-sensitive parameters are selected to be optimized. This type of analysis is used to minimize the number of parameters or variables. But in this study, there are only five input parameters and need to sensitive analysis for this purpose.

## CHAPTER FIVE

### 5. RESULTS AND DISCUSSION

This chapter deals with the discussion of the results obtained from biomimetics structure conceptual modeling, analytical analysis, experimental simulation analysis, and parameter optimization by using multi-objective optimization algorithm in ANSYS of automotive crash box depend on the listed methodology and approach. The CAD structure and geometry of the new crash box conceptual modeled by using biomimetics approach and tools are developed in SOLIDWORK. The performance of the new crash box is tested by an experimental simulation modeling in LS-PREPOST and solved in LS-DYNA. After making the comparison between those results the best model is chosen for validation and Parameter optimization in ANSYS. Hence, the results obtained from all those works are explained briefly in this chapter.

#### 5.1. Results and discussion of Biomimetic structure modeling of crash box.

Eight new automotive crash box concept designs were developed by using a hybrid method of TRIZ, morphological charts, and biomimetics generated (results) as shown in Figure 5.1. The 3D model was developed on a 1:1 scale for better visualization of product design features. The first concept idea labeled by P-1 was the single hexagonal honeycomb structure for the outermost profile and cross-section. This type of structure is also known as a single-cell original hexagonal tube (SC-OHT). In the second concept idea labeled by P-2, the model still used a hexagonal honeycomb structure for the outermost profile and each parallel edge of the hexagonal tube is reinforced by ribs connection for better strength. These ribs divide the first single hexagonal tube into the different multicell, full triangular hexagonal tubes (MC-FTHT). These types of partition were increasing the numbers of shell side connections, in which the deformable membrane energy depends on it. Concept design labeled by P-3 was like self-hierarchy, the other small width hexagonal tube is inserted into the first hexagonal and their parallel edge was connecting by ribs shell, which increases the strength and energy-absorbing capability of the structure. The concept for the P-4 model was almost similar to P-3, but in P-4 the ribs connection reinforced are extended to the center of the tube which makes the structure stronger.

Finally, the P-5 concept design had a hexagonal outer profile similar to others reinforced by a spider web structure inside the part and with a core circle of fiber foam acting like a sponge in a woodpecker's skull to protect its brain during a collision. However, for this concept, only a single layer of spider web structure was to be used as a part-reinforcement supported by circle profile at the center to optimize the energy absorption capability. Only used a single structure to absorb energy by removing the fiber foam at the center to reduce the mass of the product design. Next, the concept design, P-6, P-7, and P-8 are all similar but the ribs connection orientations are different since it affects impact load energy absorption capability. Their ribs connection is also oriented as, for P-5 corner to corner connection, P-6 wall to wall connection, P-7 corner to corner and wall to wall connection, and P-8 corner to wall connection.

These ribs connection has played a great role in creating energy absorption unit numbers and types of membrane element which are important in the calculation of deformable membrane energy as it is shown in analytical analysis for each type.

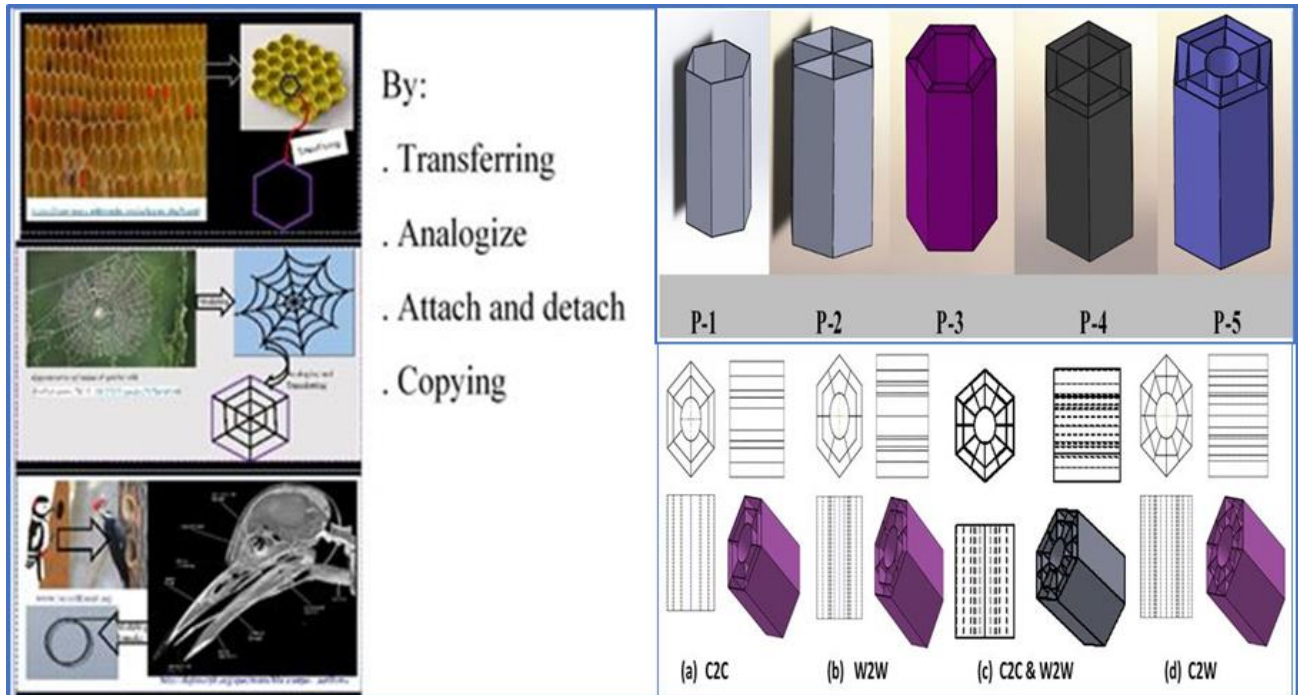


Figure 5.1 Conceptual design CAD model based on the biomimetic structure

Where the model and 2-d Auxiliary view of the newly designed crash box (a) Corner to Corner, (b) Web to Web (c) Combination of (a) and (b) and (d) Web to Corner ribs connection.

### 5.2. Analytical analysis result discussion

As shown in the following Table 5.1 mean crash force ( $P_m$ ) and other indexes have been calculated for all eight conceptual models. The energy absorption unit such as type MC-FQCHT (C2C & W2W and C2W) provides a significant contribution to actual energy absorption. All these analyses reveal the huge improvement of each criterion found in simulations by mechanical theory. Therefore, as we can observe from the result as the number of reinforced ribs increase the total energy absorbed by the structure is also increase with its mass, and the orientation of ribs connection is very important in the design of the crash box. In general, from the result of analytical analysis result, we can say that as the cell numbers of the structure increase or as the structure reinforced more the crashworthiness index, mean crushing force, total energy and specific energy are increase continuously. But there were to some extent constrained the mass of the structure because as the numbers of ribs connection reinforced increase the mass of the crash box also increase. Hence during the process of such design, we have constrained the mass of the crash box to the fixed optimized point.

These results indicate that the number and types of energy absorber units, like Circular element, 2-panel element, Concave T-shape, 3-panel element-I, 3-panel element-II, 4-panel element, 3-panel crisscross, 2-panel crisscross, and T-shape element had played a great role in the energy absorption capability of the structure. This means that thin-walled structure has many numbers of those energy absorber units as much as important can absorb high axial impact load energy. Also, the result of this crashworthiness indicator for all design models agrees with the numerical result, which will be discussed in the next section.



Table 5.1 The summary result of mean crush force, total and specific energy from analytical analysis

Specimen code	Mean crush force (kN)	Total energy (kJ)	Weight (kg)	Specific energy (kJ)
SC-OHT	21.468	3.349	1.124	2.979
MC-FTHT	43.766	6.828	1.602	4.262
MC-ICHT	57.6025	8.986	1.600	5.616
MC-DFHT	54.7549	8.542	2.147	3.978
MC-FQCHT (C2C)	85.1485	13.283	1.733	7.665
MC-FQCHT (W2W)	98.4158	15.353	1.648	9.316
MC-FQCHT (C2C & W2W)	126.664	19.7596	2.046	9.657
MC-FQCHT (C2W)	126.664	19.7596	2.046	9.657

Also, the mean crushing force and specific energy result from the analytical analysis are compared in the following Figure 5.2 and 5.3 respectively.

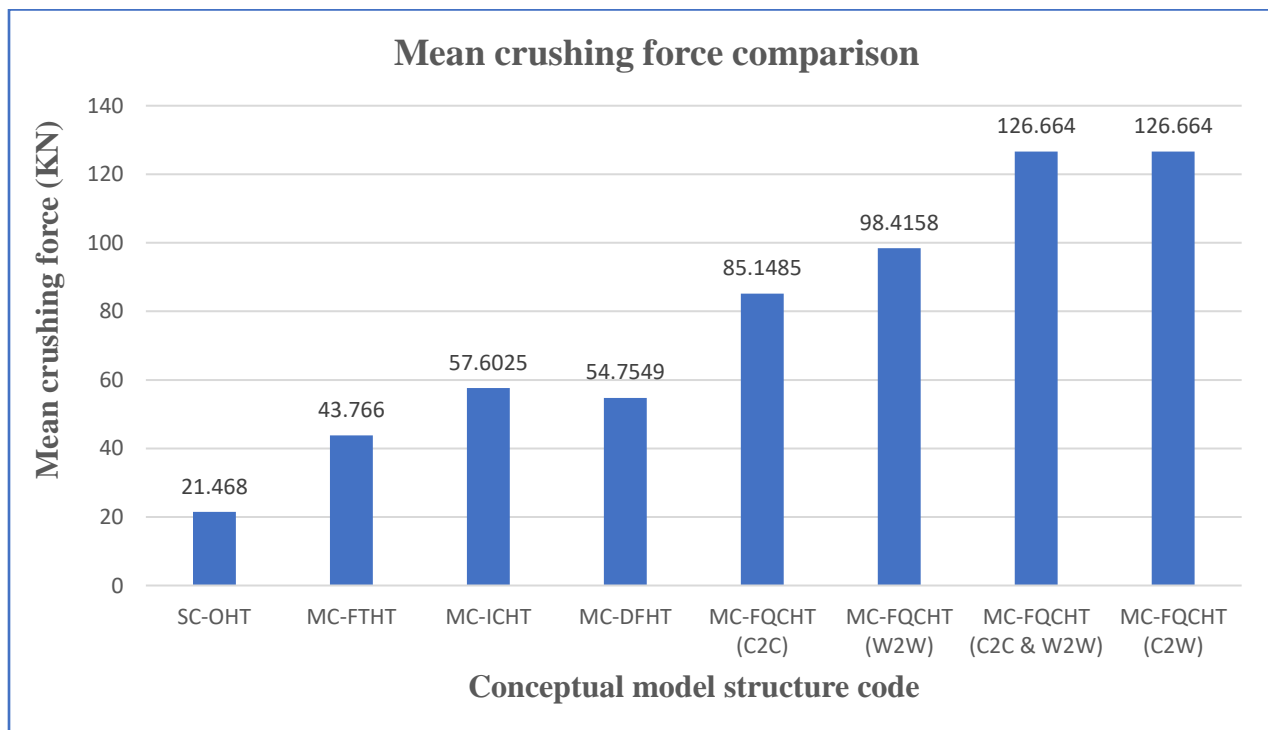


Figure 5.2 Mean crushing force comparison of theoretical result for all mode

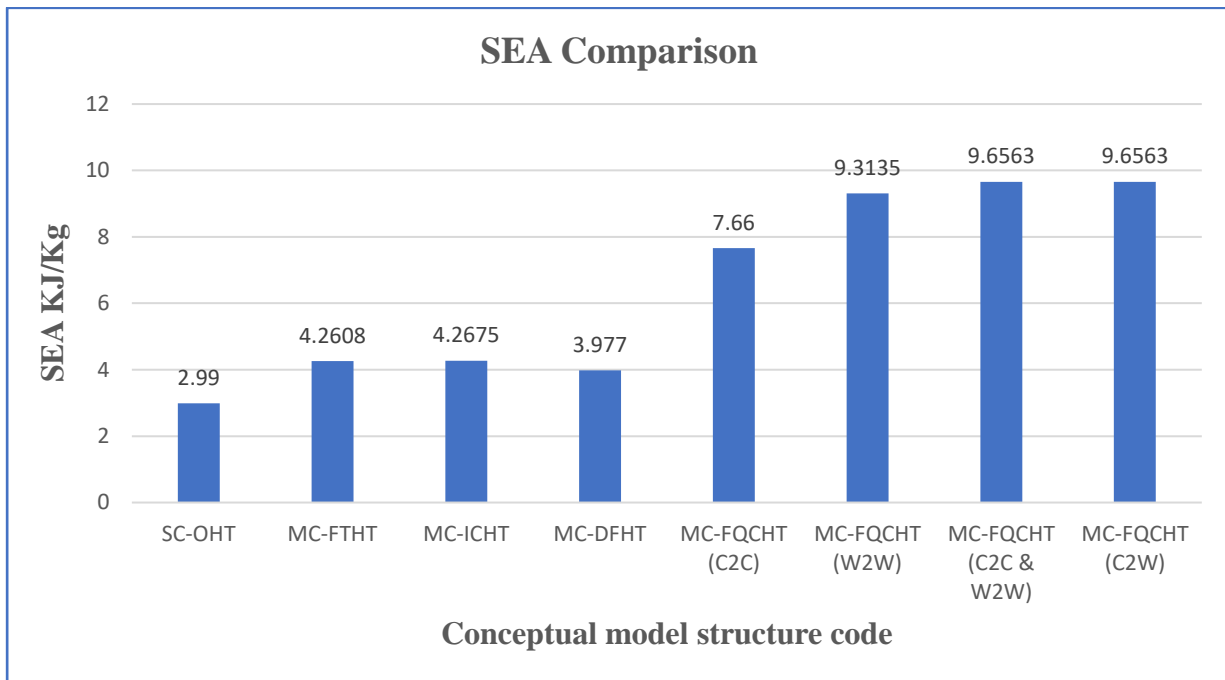


Figure 5.3 Specific energy absorption comparison of theoretical result for all model

### 5.3. Experimental simulation result of the crash box

The statistics property of mesh for both parts, impactor, and shell tubes are shown in the following Table 5.2, which is important to control the mass and simulation cost of the structure. The mass, volume, and number of elements for the impactor are constant for all models through all simulation models. Because the impactor is simply used as a load to deform the tube structure, and no change is applied to it. In case the shell tube is more reinforced the number of elements, nodes, mass, and volume increase comparatively and these need to control at some maximum energy comparative with that quantity especially mass.

Table 5.2 Meshed statistics for the parts model

Structure Code	Components	Number of Element	Number of Nodes	Mass	Volume
SC-OHT	Shell tube	3,2124	32,472	0.403	75,979,2
	Solid impactor	288	507	700.595	2.56e+06
MC-FTHT	Shell tube	37,360	37,332	0.805	57,320,6
	Solid imKpactor	288	507	700.595	2.56e+06
MC-ICHT	Shell tube	36,972	36,912	0.805	57,233,5

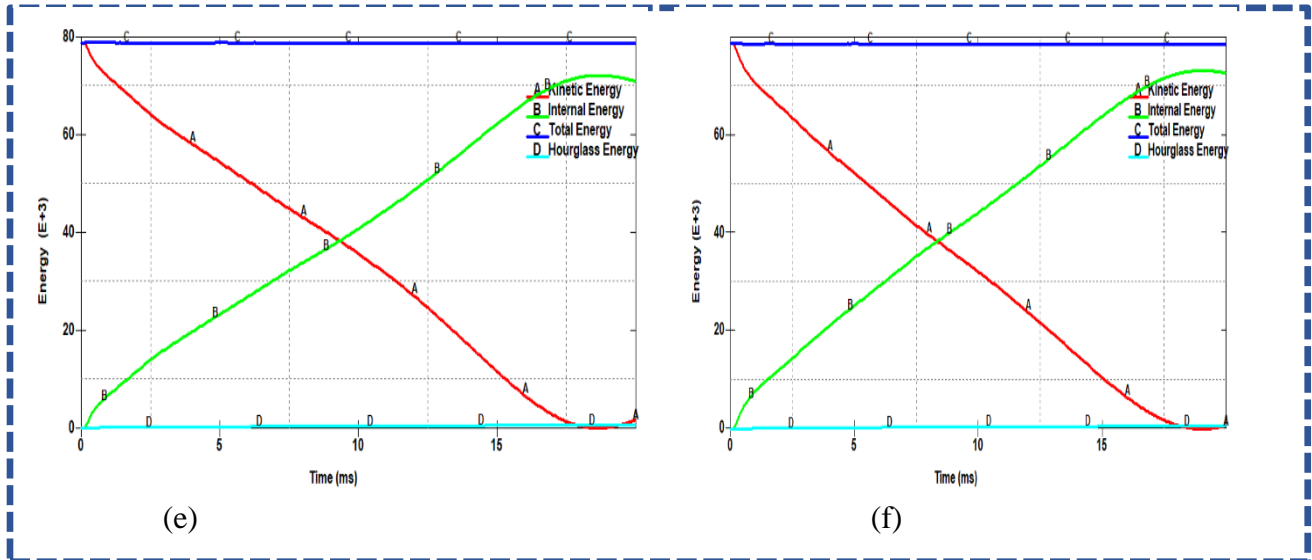
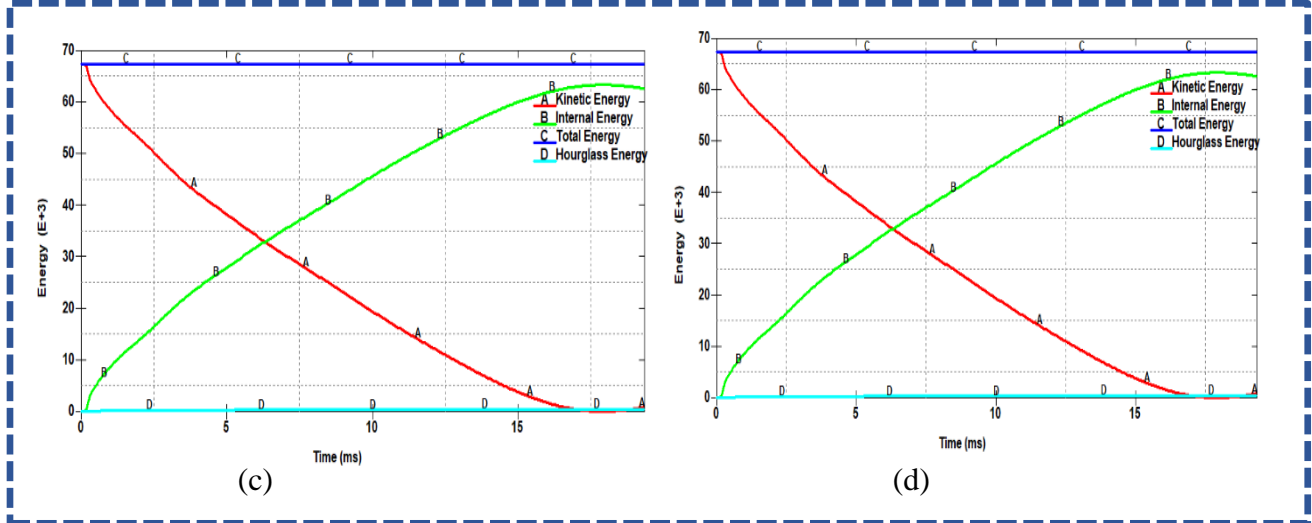
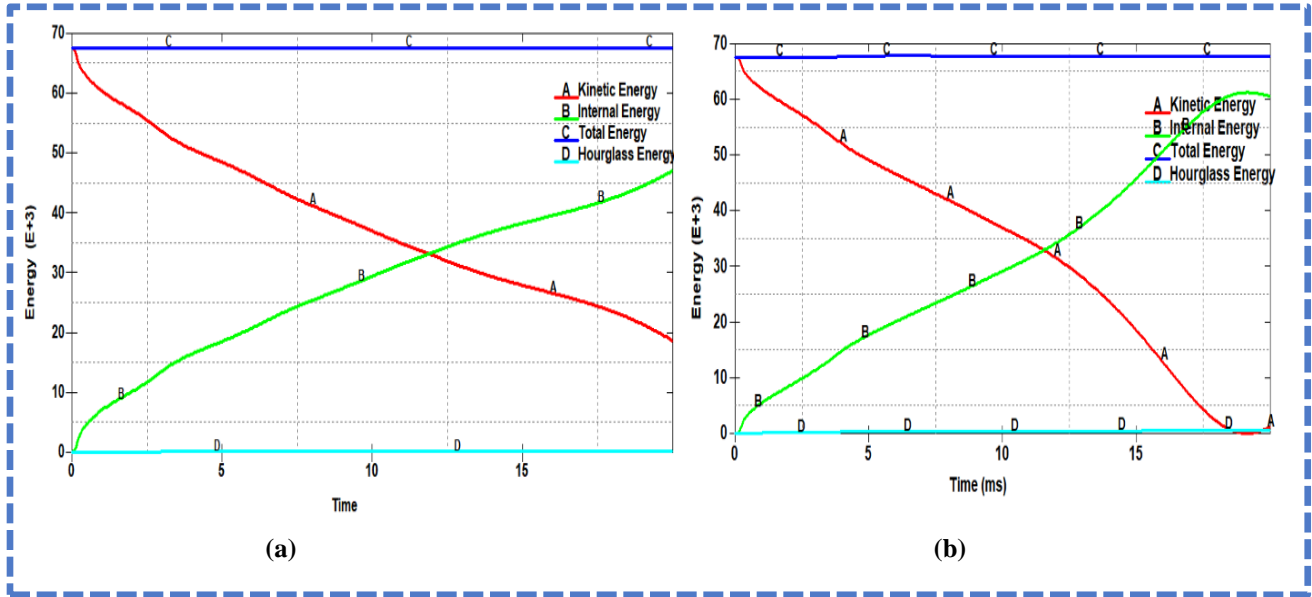
	Solid impactor	288	507	700.595	2.56e+06
MC-DFHT	Shell tube	49,311	49,247	1.087	768117
	Solid impactor	288	507	700.595	2.56e+06
MC-FQCHT (C2C)	Shell tube	49666	49514	1.092	620168
	Solid impactor	288	507	700.595	2.56e+06
MC-FQCHT (W2W)	Shell tube	47107	47,025	1.039	589640
	Solid impactor	288	507	700.595	2.56e+06
MC-FQCHT (c2c&w2w)	Shell tube	58089	57,909	1.320	731855
	Solid impactor	288	507	700.595	2.56e+06
MC-FQCHT (C2W)	Shell tube	58,607	58,451	1.320	732008
	Solid impactor	288	507	700.595	2.56e+06

#### 5.4. Model verification

In this section, energy conservation is conducted to verify the established model. From the Energy change curve, comparing the hourglass energy to the total energy according to RCAR legislation for all new crash box models.

##### 5.4.1. Energy conservation

Energy conservation is a criterion to judge whether a finite element model is reliable. The reduction of integral points in display analysis causes the unit zero-energy mode, and energy dissipation of the contact surface will lead to the hourglass energy, which should generally be no more than 5% of the total energy [52]. The reliability and accuracy of the established models are verified according to RCAR legislation. Energy conservation is a criterion to judge whether a collision model is reliable and the collision process, the reduced integration method often produces the hourglass energy loss, which will affect the energy balance and simulation accuracy of the system. It can be seen from Figure 5.10 shows the energy change curves of all crash boxes under the high-speed impact (a) to (h) that the system energy compositions of all crash boxes are reasonable, and the total energy is conserved. The hourglass energy can be controlled within a small positive range and no more than 5% of the total system energy. Accordingly, it is necessary to take the hourglass control and ensure the hourglass energy is less than 5% of the total energy which satisfies the permissive range of the legislation. Therefore, the finite element models of all crash boxes are all effective and it is acceptable to continue further analysis.



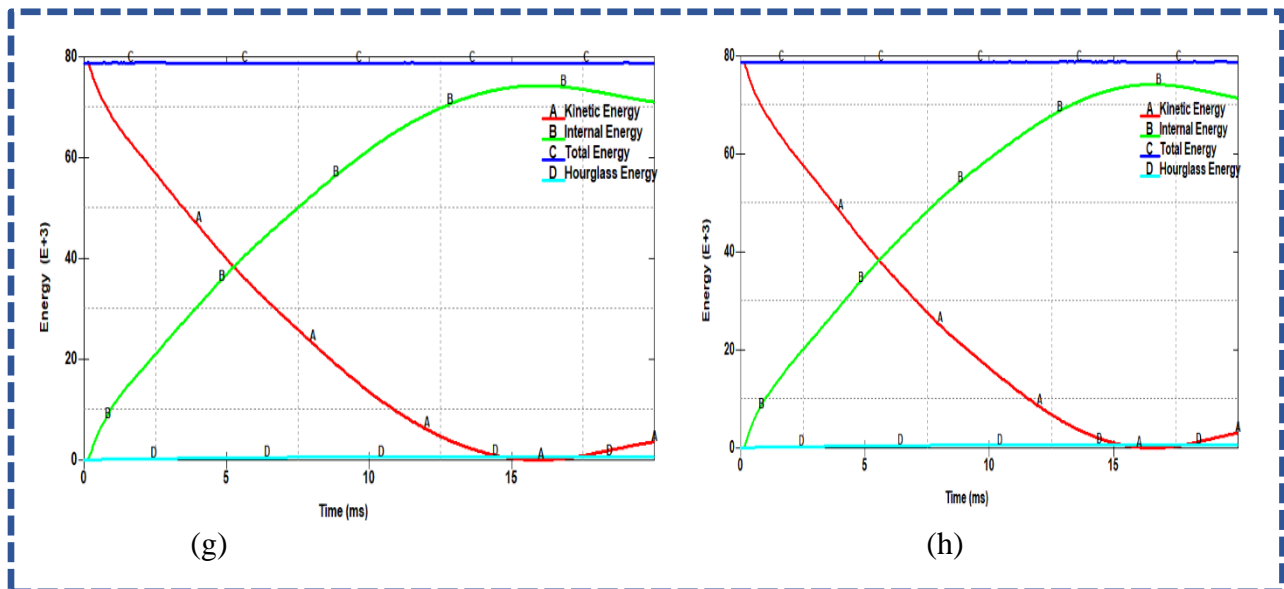


Figure 5.4 Energy change curve of all new crash box models, (a) SC-OHT, (b) MC-FTHT, (c) MC-ICHT, (d) MC-DFHT, (e) MC-FQCHT (C2C), (f) MC-FQCHT (W2W), (g) MC-FQCHT (C2C & W2W) and (h) MC-FQCHT (C2W).

### 5.5. Crashworthiness Evaluation

To evaluate the crashworthiness performance of the newly designed Crash Box thin-wall structures, several crashworthiness indicators are used, these indicators are energy absorption, Mean Crashing Force (MCF), Pick Crash Force (PCF), and total deformation or deformation length that occurred during impact. The front impact or crash analysis takes place with an initial vehicle velocity of 15 m/sec, the time range of impact is 0 to 0.05 sec (5 milliseconds). The gap between the Crash Box and the front rigid wall is 1mm for all eight Crash Box models to keep consistency and see their results within the given time intervals. When the crash scenario takes place, it is more complex to predict the best result, therefore, the Johnson-Cook strength and failure model considered for the material modeling of automotive Crash Box, which states that the material is loaded with impact environment in the form of the plastic range including large strains, large strain rates, high pressures, and high temperatures for Aluminum 7075-T651 plate for Crash Boxes.

#### 5.5.1. Deformation mode

To compare the crashworthiness of biomimetic multi-cell tubes and traditional multi-cell tubes, FE simulations of different conceptual design models of crash boxes are carried out under axial impact loading. The structure that has a good and stable deformation mode is excellent in impact energy absorption. Some deformation mode types are, diamond mode and square, pentagon and hexagon specimens are folded like a concertina and few hexagonal multi-cell tubes are folded like diamond mode. As discussed former and the deformation mode is one criterion of crashworthiness evaluation, and hence the deformation modes of all specimen are displayed in Figure 5.13 following from the LS-prepost window.

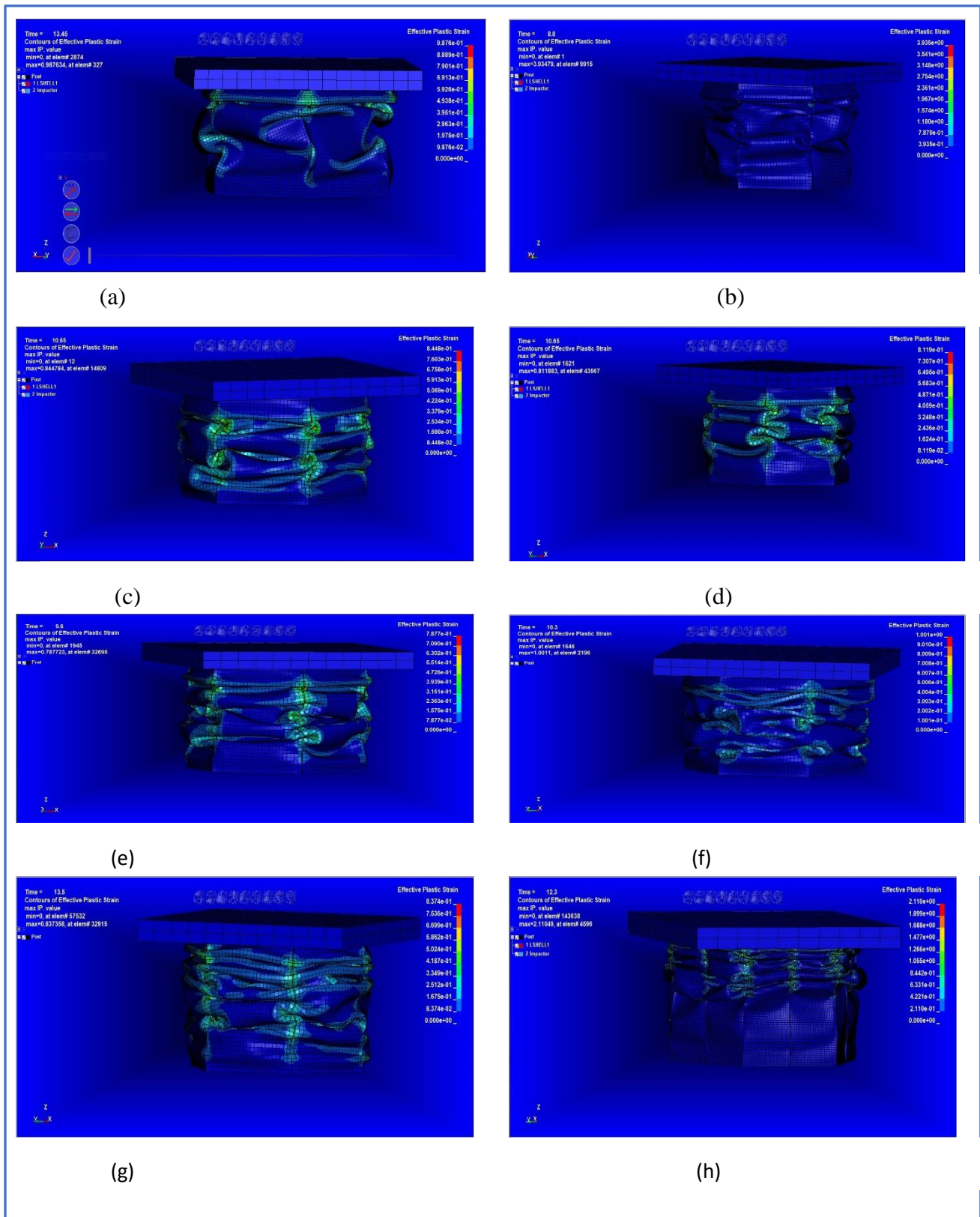


Figure 5.5 deformation modes of representative lobes folding (a) SC-OHT, (b) MC-FTHT, (c) MC-ICHT and (d) MC-DFHT (e) MC-FQCHT (C2C) (f) MC-FQCHT (W2W) (g) MC-FQCHT (C2C & W2W) (h) MC-FQCHT (C2W).

### 5.5.2. Performance indicators

The evaluation of crashworthiness from experimental simulation results for all samples, in terms of all indexes, is given as shown in Table 5.3 below. As the result of mean crush force and energy absorption capability, the design model MC-FQCHT (C2W) (P-5 C2W) has a stable deformation mode and good performance than other samples. Therefore, this one is also selected for the next parameter optimization using a multi-objective Algorithm in ANSYS and further investigation.

Table 5.3 Simulation Results of a different conceptual design model of the crash box

Specimen code	Peak Force (kN)	Mean crush force (kN)	Total energy (kJ)	Mass (kg)	Specific energy (kJ/kg)	CFE	$\omega$
SC-OHT	56.612	14.15	1.082	0.403	2.684	0.249	3.532
MC-FTHT	45.560	14.28	2.842	0.805	3.530	0.313	3.213
MC-ICHT	59.158	22.34	4.296	0.805	5.336	0.377	4.151
MC-DFHT	50.217	17.18	3.270	1.087	3.008	0.342	3.173
MC-FQCHT (C2C)	52.910	22.17	6.428	1.092	5.886	0.419	2.982
MC-FQCHT (W2W)	59.340	24.92	6.627	1.039	6.079	0.419	1.951
MC-FQCHT (C2C & W2W)	55.375	25.27	9.045	1.320	6.852	0.456	1.523
MC-FQCHT (C2W)	69.319	25.99	9.060	1.320	6.864	0.375	1.447

## 5.6. Result and discussion in terms of performance indicator

### 5.6.1. Concept design p-1 (SC-OHT)

From the experiment simulation of the SC-OHT model, the values recorded were the lowest as compared to any other geometry probably because it is a single-celled thin-walled member while the other specimens were multi-walled. Due to their multi-walled nature, they have shown appreciable results in terms of the testing parameters. The peak force was recorded at short displacement, which is not recommended for about 2 mm deformation with a value of 56.612 KN. The average crush force was found to be at 14.15 KN and the total energy absorbed was about 1.082 KJ, which is the least among all the geometries. The force displacement curve is given as Figure 5.14.

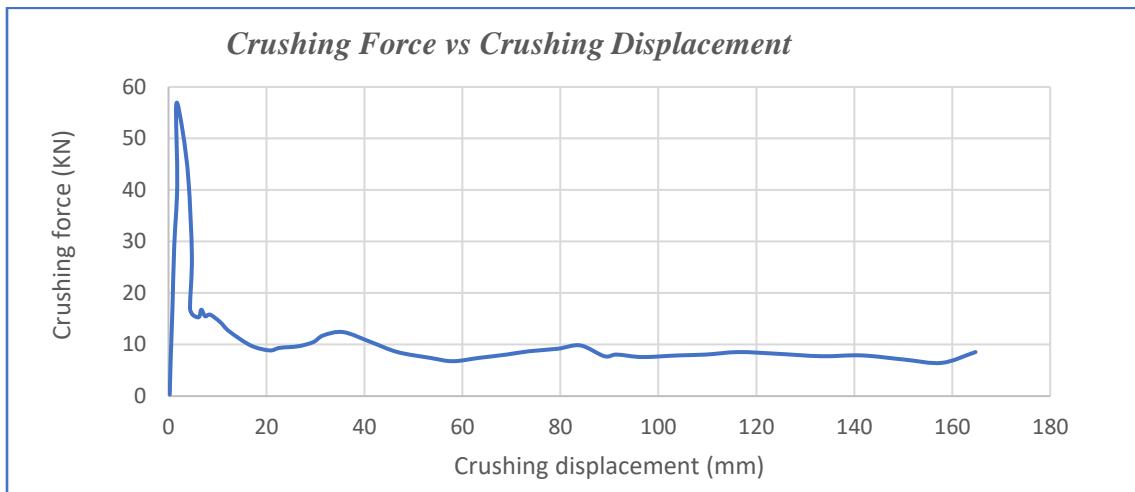


Figure 5.6. Force vs. displacement curve for model p-1

### 5.6.2. Concept design P-2 (MC-FTHT)

The results of the P-2 and P-1 models were quite similar and comparable but for other models, there was a remarkable difference. Both models gave almost similar results for the average crush values and energy absorbed values while the value of peak force decline was negligibly when compared to the P-1 section as it seen Figure 5.15. Only a few rising trends were found in the case of the values of average crushing force and energy absorbed values which were found to be 14.28 kN and 2.842 kJ respectively. The energy absorption capacity increased by about 1.76 when compared to the *p-1* (SC-OHT) model.

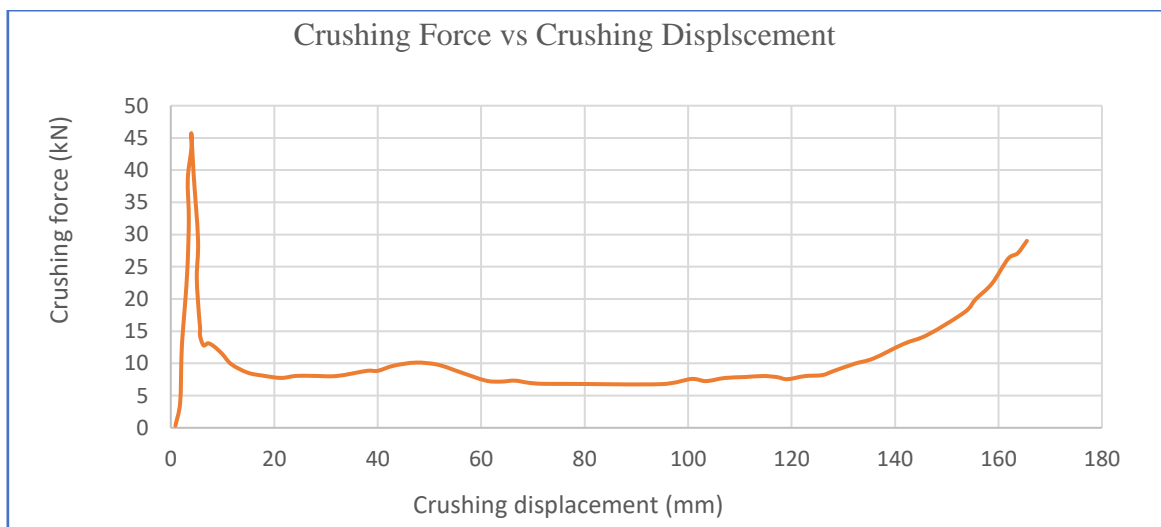


Figure 5.7 Force vs. displacement curve for model P-2

### 5.6.3. Concept design P-3 (MC-ICHT)

The P-3 model performed much better than the simple hexagonal tube model and showed a few increases in the value of Peak force which was found around 5mm of deformation as it shown Figure 5.16. The value of peak force was recorded to be about 59.158 kN the most rising trend was found in



the case of the values of average crushing force and energy absorbed values than both model P-1 and P-2 which were found to be 22.34 kN and 4.296 kJ respectively.

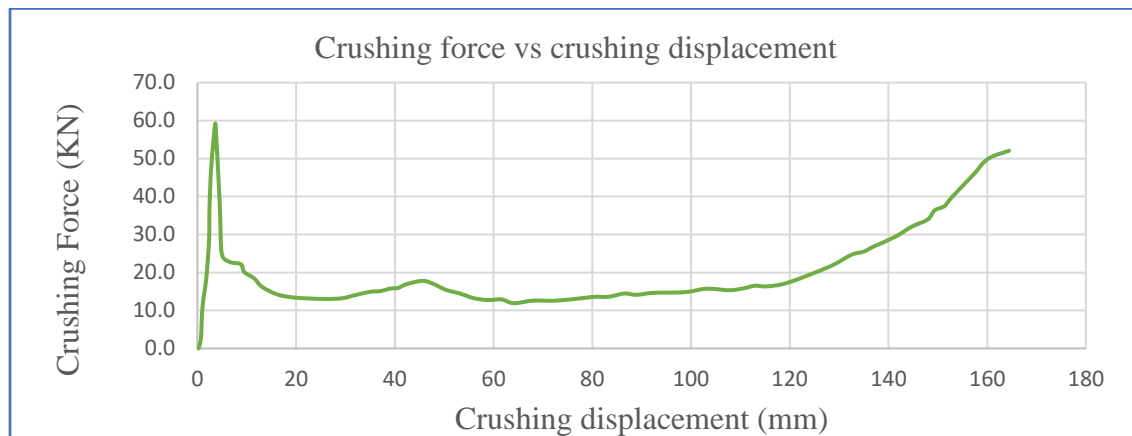


Figure 5.8 Force vs. displacement curve for model P-3

#### 5.6.4. Concept design P-4 (MC-DFHT)

The p-4 model was quite contemporary in its performances the values of the Peak force, average crush force, and energy absorbed of the above mention model were having hardly a difference. Thus, it can be said that the results obtained by the variation of the inner wall as reinforce together at the center revealed different results. But Following the P-4 models, the peak force decreased by about having a value of 50.217 kN the values of average crush force and the energy absorbed also got decreased in similar proportion having the value of 17.18 kN and 3.270 kJ respectively.

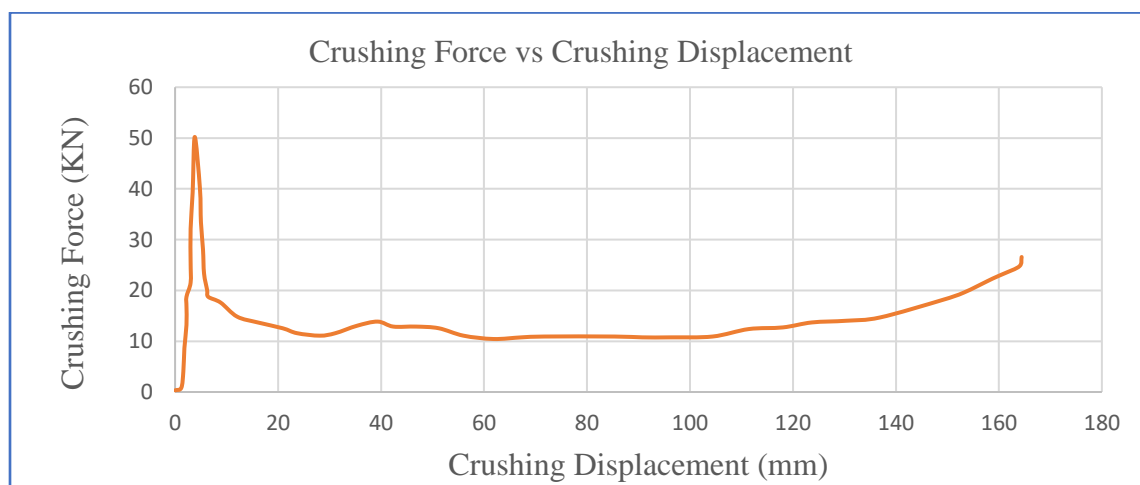


Figure 5.9 Force vs. displacement curve for model P-4

#### 5.6.5. Concept design P-5 (MC-FQCHT (C2C, W2W, C2C & W2W and C2W))

Among all the above numerical simulation specimens the best results were obtained in the P-5 (MC-FQCHT) geometry the values of peak force, average crush force, and the energy absorbed was recorded in this specimen the values of crush force and the energy absorbed increased by 11.84 kN and 7.978 kJ respectively than simple hexagonal honeycomb outer profile and cross-section tube. This is because that all P-5 models have reinforced cross-sections by spiderweb structure and

woodpecker at the core of cross-section. The value of peak force was recorded for instance after the 5mm deformation of the model as shown in Figures 5.18, 19, 20, 21 below. Also depending on the number and orientation of reinforced ribs connection, which increase the membrane deformation energy absorption and hardness of the model P-5(c2c & w2w and c2w) model have better performance in terms of all crashworthiness indicators, with the value of mean crushing force and total energy absorption 25.27 kN, 9.045 kJ, and 25.99 kN, 9.060 kJ respectively. Therefore, because that p-5 c2w has slightly better performance in terms of mean crushing force and total energy absorption it would be selected for optimization.

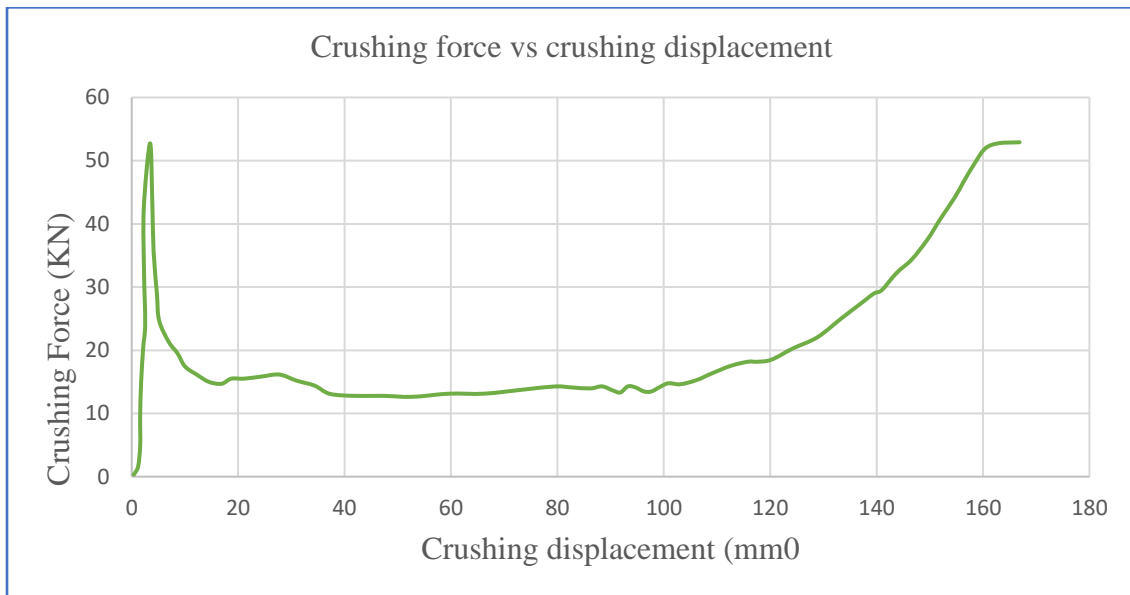


Figure 5.10 Force vs. displacement curve for model P-5(c2c)

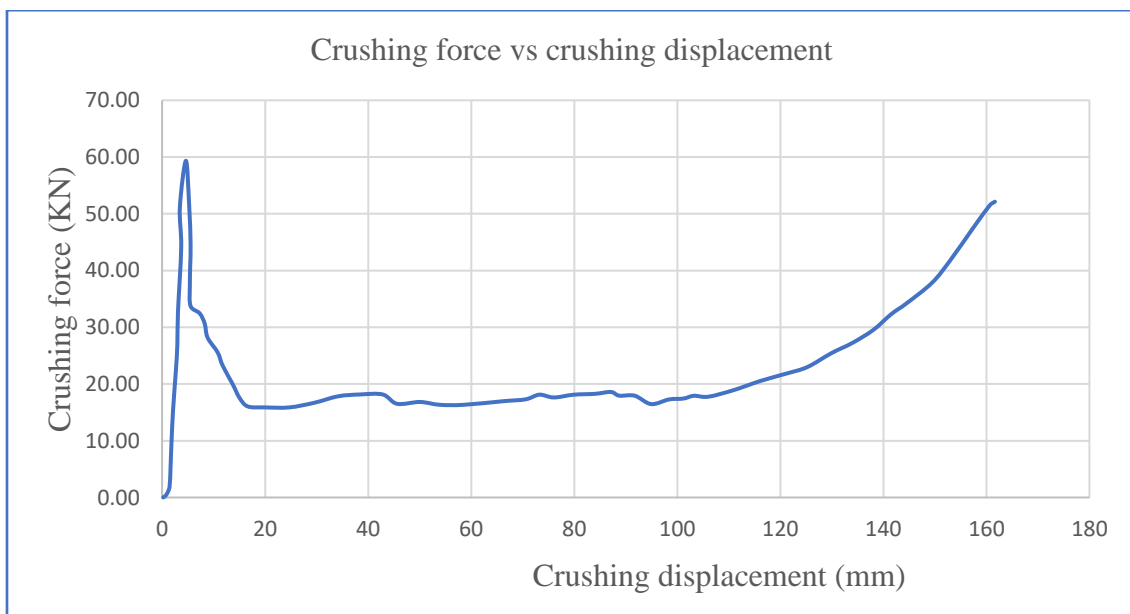


Figure 5.11 Force vs. displacement curve for model P-5(w2w)

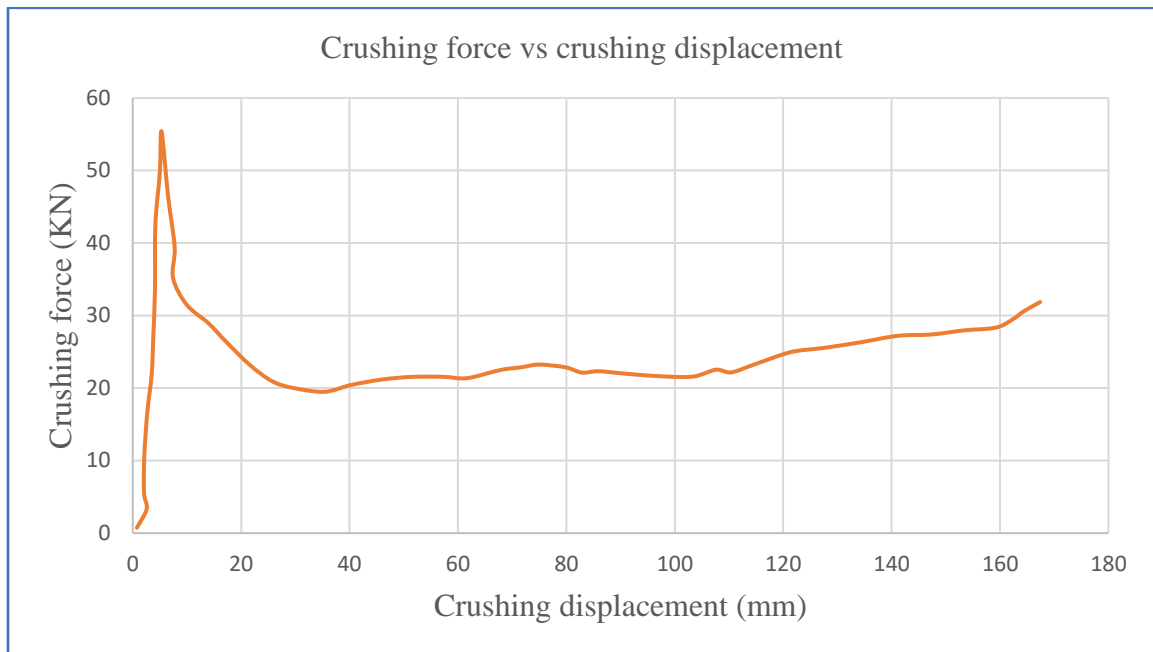


Figure 5.12 Force vs. displacement curve for model P-5(w2w and c2c)

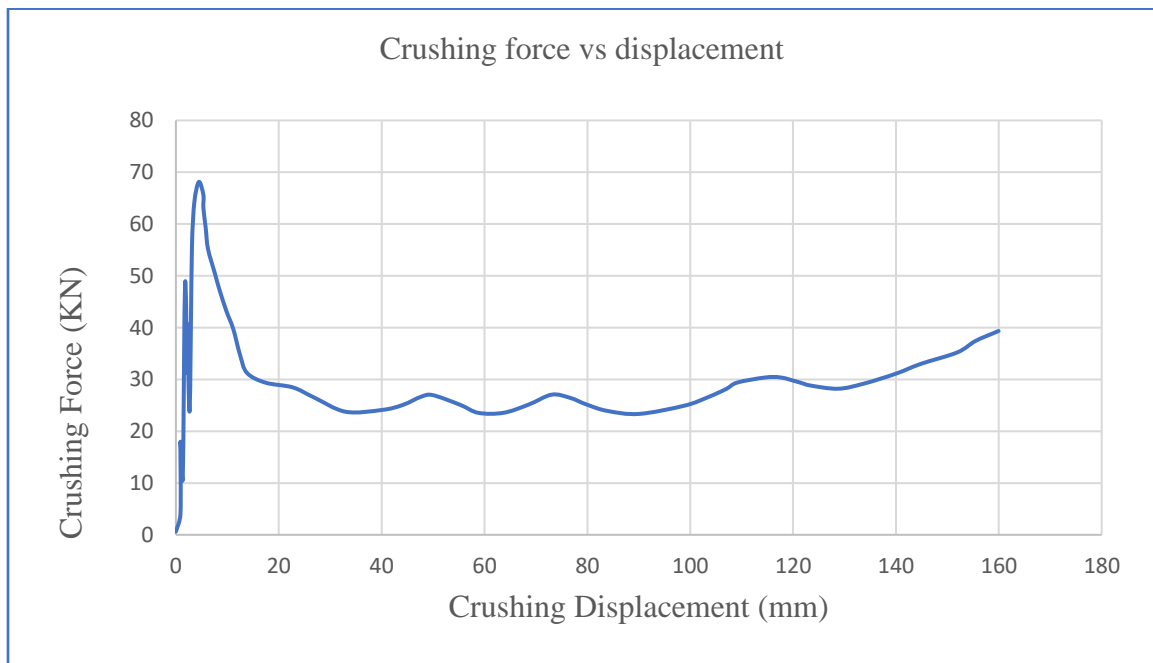


Figure 5.13 Force vs. displacement curve for model P-5(c2w)

### 5.7. Summary of results and comparison discussion all model in one

A comparison of crushing force vs displacement curve values for all specimens is presented in Figure 5.22 and the specific energy absorption of each conceptual model is given in Figure 5.23 below as a bar chart and to see the difference.

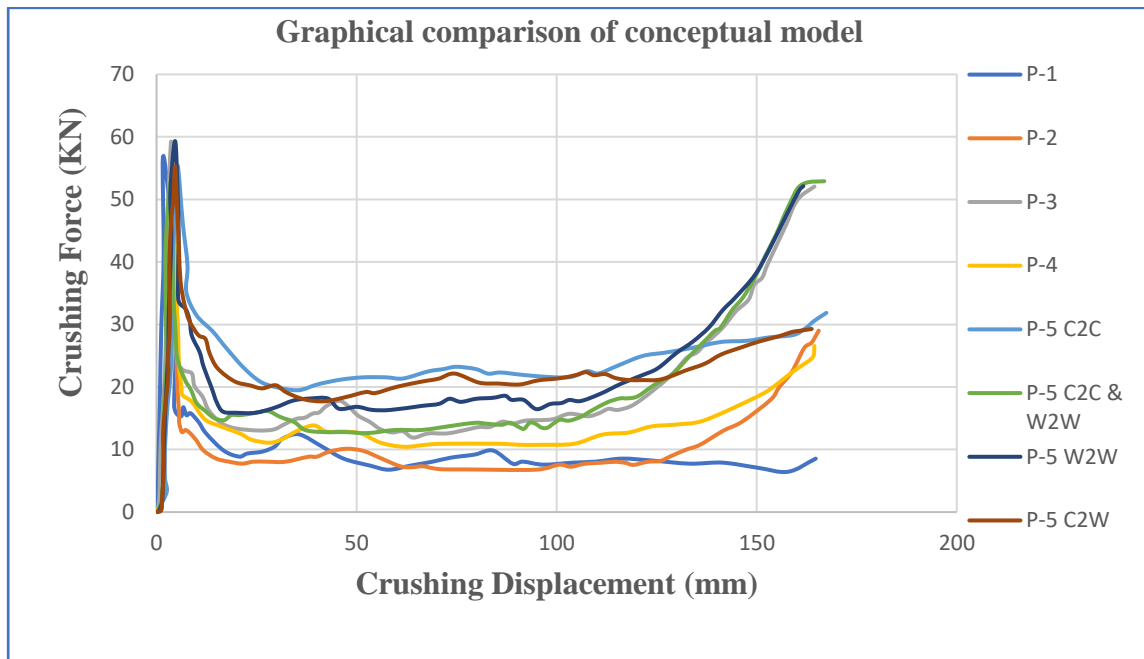


Figure 5.14 Force vs displacement curve for all model specimens

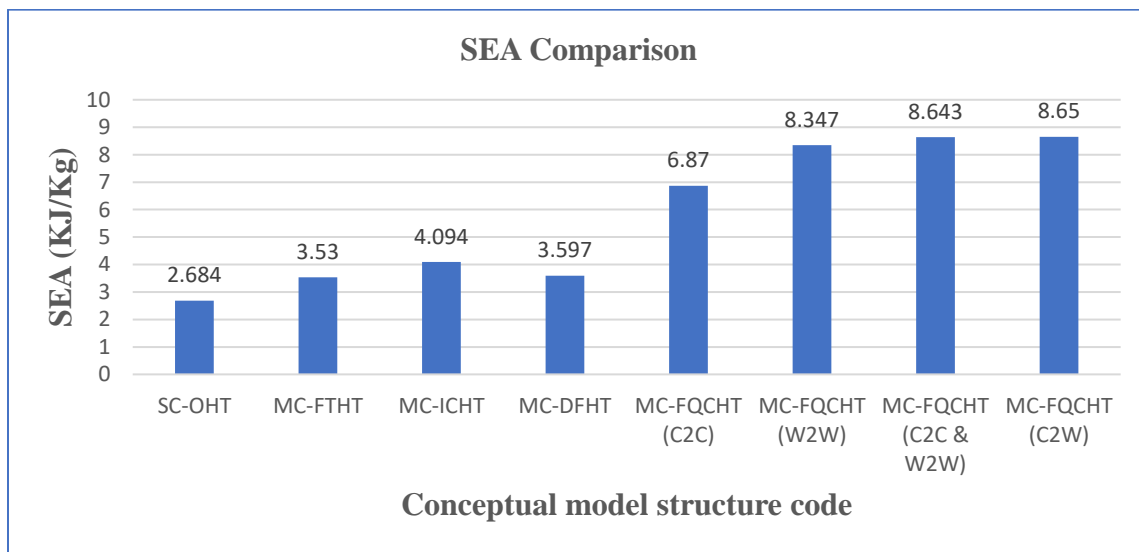


Figure 5.4 SEA comparison between all model structure

### 5.8. Consistency of the numerical results with analytical solutions

It is necessary to compare with numerical results to validate the accuracy of the theoretical model. SEA correlation is illustrated to validate the theoretical analyses. It should be noted that the most analytical solution of SEA was based on quasi-static loading while the numerical results SEA was obtained under dynamic loading. In this study, the comparison is conducted with increasing ratios of SEA of, MC-FTHT, MC-ICHT, MC-DFHT, MC-FQCHT (C2C), MC-FQCHT (W2W), MC-FQCHT (C2C & W2W), and MC-FQCHT (C2W) to that of SC-OHT. With these normalizations, the effect caused by dynamic impact can be eliminated. Theoretical SEA increase ratio  $\eta T$  and numerical SEA increase ratio  $\eta N$  can be calculated as below, respectively:

$$\eta_T = \frac{(SEA_T)MC - XHT}{(SEA_T)SC - OHT} \dots\dots\dots 5.1$$

$$\eta_N = \frac{(SEA_N)MC - XHT}{(SEA_N)SC - OHT} \dots\dots\dots 5.2$$

where  $(SEA_T)MC - XHT$  represents *sm* of MC-XTH, and MC-XHT represents anyone MC-FTHT, MC-ICHT, MC-DFHT, MC-FQCHT (C2C), MC-FQCHT (W2W), MC-FQCHT (C2C & W2W) and MC-FQCHT(C2W). Similarly,  $(SEA_N)MC - XHT$  represents SEA of MC-XTH, and MC-XHT represents any one of MC-FTHT, MC-ICHT, MC-DFHT, MC-FQCHT (C2C), MC-FQCHT (W2W), MC-FQCHT (C2C & W2W), and MC-FQCHT(C2W).

The final result is shown in Figure 5.27, It can be seen that a good consistency has been achieved. The largest error of SEA between numerical results and that of theoretical results of MC-FTHT is only 6.8%. This minor deviation is reasonable and acceptable. Thus, the theoretical model proposed in this study and corresponding conclusions were reliable.

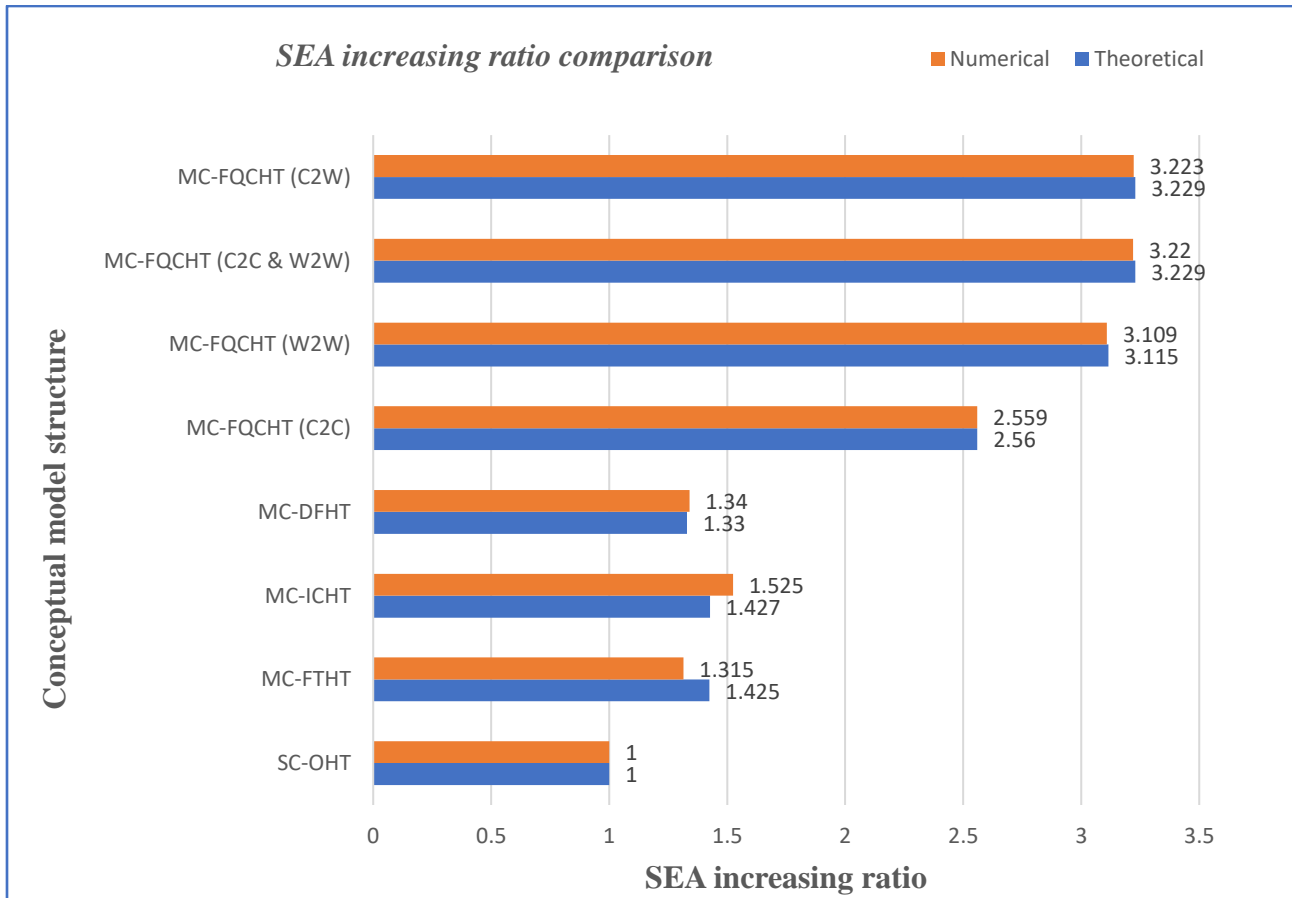


Figure 5.19 SEA increasing ratio comparison (validation) between a theoretical and numerical result

### 5.9. Finite element model validation


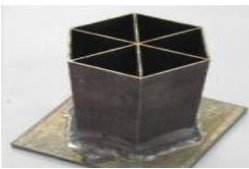

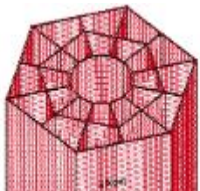



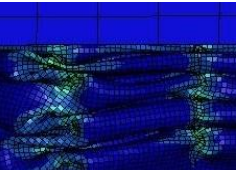
The accuracy of the finite element analysis (FEA) was directly affected by a numerical model. To ensure the reliability of FE models, the numerical model was validated by experimental test data from

the literature carried out by the author. The validation was performed by comparing the load-displacement response, energy-displacement response, crush load, specific energy absorbing capacity, and the collapse modes. It should be noted the validation process is conducted by comparing the energy absorption parameters only. This was because a simple material model was used to develop the FE model for predicting the behavior of thin-walled tubes under lateral loading, but which is very complex in real life. The finite element model and the numerical results used in the study of MC-FQCHT (C2W) or (P-5 C2W) under axial loading were compared and validated with the experimental results as shown in Figure 5.24, 25, 26 respectively.

The resultant force versus displacement curves of MC-FQCHT was obtained by numerical simulation had validated with three experimental results, J. Wang, Y. Zhang, N. He, and C. H. Wang, Zhang's and X. Xu, Y. Zhang, J. Wang, F. Jiang, and C. H. Wang [81, 88, 89]. In all of the analyses of tubes under axial crushing, mostly the average crushing force was concerned because this is one of the most important parameters in evaluating the energy-absorption capacity of these tubes under such loading [43]. In this study, the error between the crushing force of the experiments and simulation were all about less than 7 %. Besides, any tiny defect or other manufacturing factors would lead to a different mechanical response in peak force, which is difficult to be considered precisely in FE modeling [35]. The actual welding area in the experiment is larger than that of the FE model and the effect on the local stiffness spreads to an area above the bottom edge of the tube fixed to the ground. Hence, the difference between the simulation and experimental results is inevitable.

The general information of the experiments are given in Table 5.4.

Table 5.4 Information of the experiments for validation

Factors considered	Experiments			
	[81]	[88]	[89]	Present simulation
Material types	Aluminum alloy 6061-O	Aluminum alloy 6061-O	Aluminum alloy 6061-O	Aluminum alloy 6061-O
Initial velocity	15 m/s	10 m/s	10 m/s	15 m/s
Cross section				
Deformation mode				

Moreover, it can be seen from Figure 5.24 (b) below, that the present dynamic simulation deformation mode of MC-FQCHT (C2W) (P-5 C2W) matched well with that in Zhang's experiment [88]. Whether

in numerical simulation or experiment, the lobes experienced alternating inward folding and outward stretching in one wall. And their final quantity along each exterior wall was all three or above. For instance, the FE model has been sufficiently validated as a reliable tool here, and the overall FE model for the optimized structure will be validated precisely.

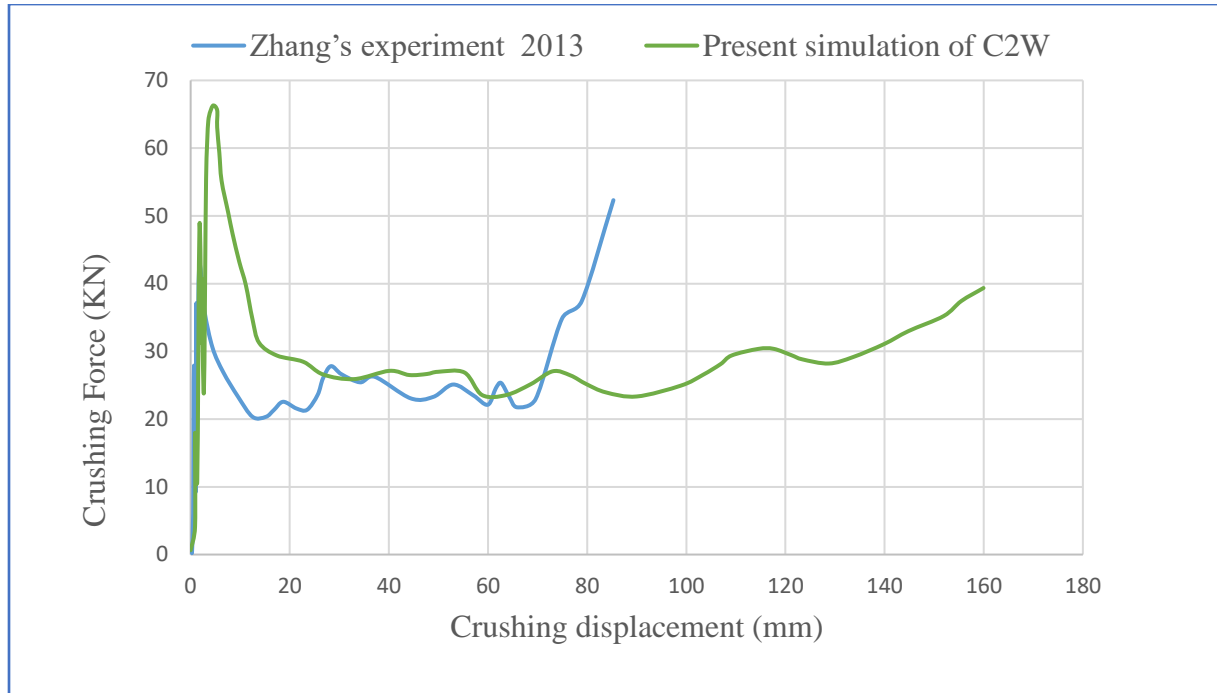


Figure 5.16 (a) Agreement of mean force between experiment and simulation, only 4.53% error in representative MC-FQCHT (C2W) (P-5 C2W); (b) deformation modes also agree to some extent.

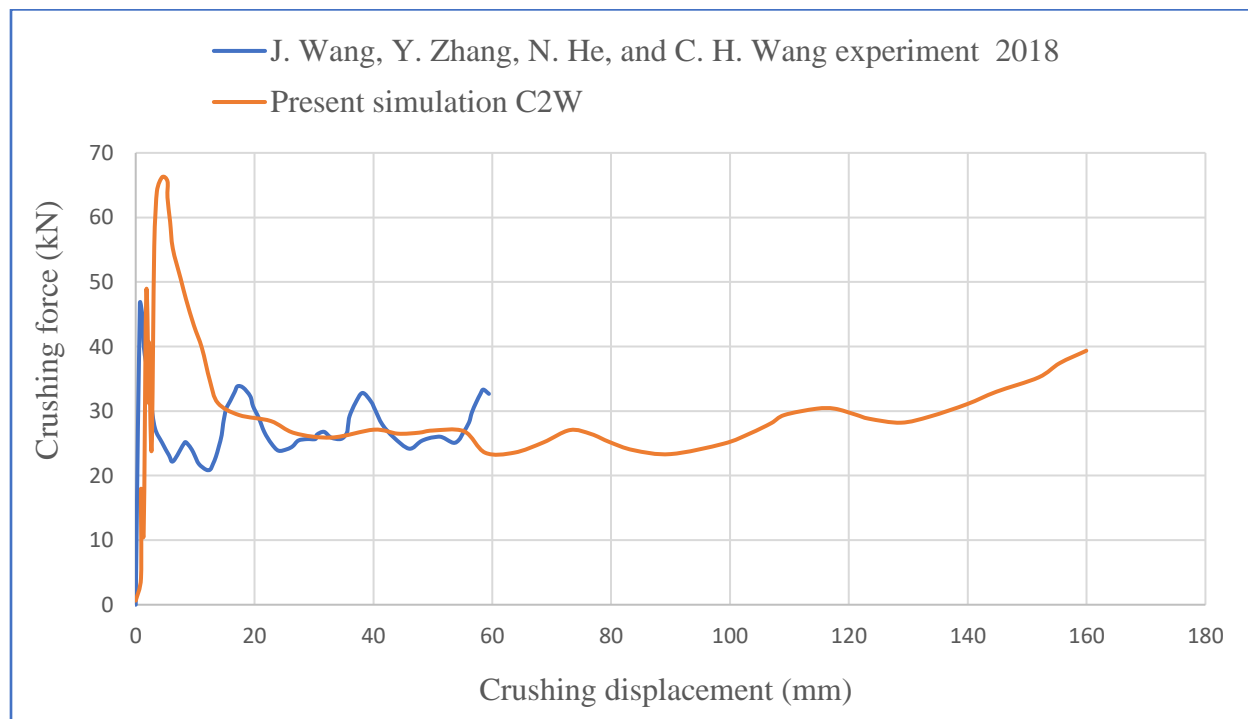


Figure 5.17 Validation comparison of J. Wang, Y. Zhang, N. He, and C. H. Wang experiment result with a present experimental simulation of model P-5 MC-FQCHT (C2W)

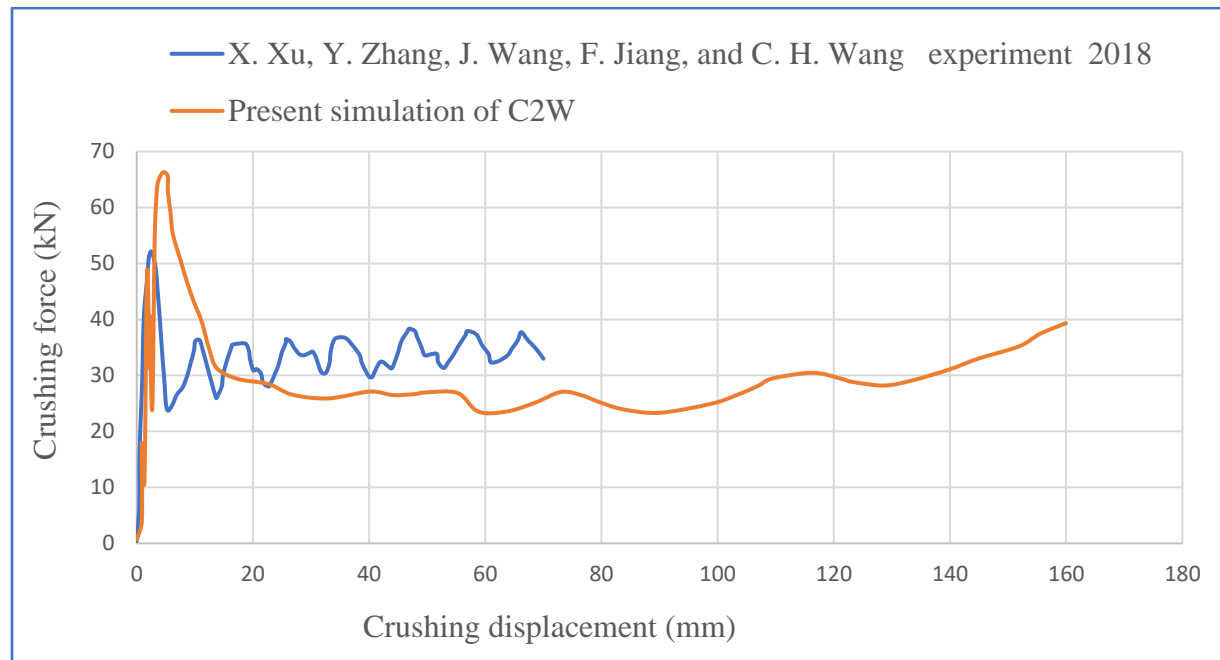


Figure 5.18 Validation comparison of X. Xu, Y. Zhang, J. Wang, F. Jiang, and C. H. Wang experiment result with a present experimental simulation of model P-5 MC-FQCHT (C2W)

## 5.10. Optimization results

### 5.10.1. DesignXplorer analysis results.

DesignXplorer is a simulation tool or module in the ANSYS workbench that is implemented using surface response sensitivity and design of the experiment to define the input and output relationship. In the design of crash box analysis, the total deformation, the elastic strain, elastic stress, and strain energy analysis as output parameters are related to the width of the outer surface, the width of the inner surface, and depth of the cross-section and thickness of shell tube wall of the crash box which is the input parameters. These input parameters decide the total deformation and other output listed above, which decides the total energy absorption of the crash box. In this thesis work, the main objective is to improve the crashworthiness of automotive crash boxes. So, the maximum equivalent plastic strain and strain energy concerning the design optimization of the crash box is determined.

### 5.10.2. Response surface modeling and optimization.

Based on the number of input parameters (ANSYS workbench-simulation), a given number of solutions (design points) are required to build a response surface. A design of an experiment determines how many and which design points should be solved. Once the required solution is complete, a response surface is fitted through the results allowing the design to be queried where no hard solution exists. In the outline of the response surface, then it is possible to see a response points folder defaults response points under it (usually the center of the design space) Each response point can be affected by different charts.



- Spider chart to examine the value and variation of all output parameters on a single graph
- Local sensitivity to examine the weight of each parameter around the response point.
- Response 2D or 3D graph represents the variations of one output with the response to one or two input parameters as shown in Figure 5.29.

Design points in X-axis and maximum total deformation in Y-axis, for the checking value for each design point at which values of the maximum total deformation value are achieved. Design points and output parameters are shown in Figure 5.28, this output is maximum total deformation. At this point 3.2 to 3.3 the total deformation shows at the design points at point 5. Also, at design points, 14 to 15, 18 to 19, 22 to 23, and 26 to 27 are the point where the mean total deformation of the crash box had occurred.

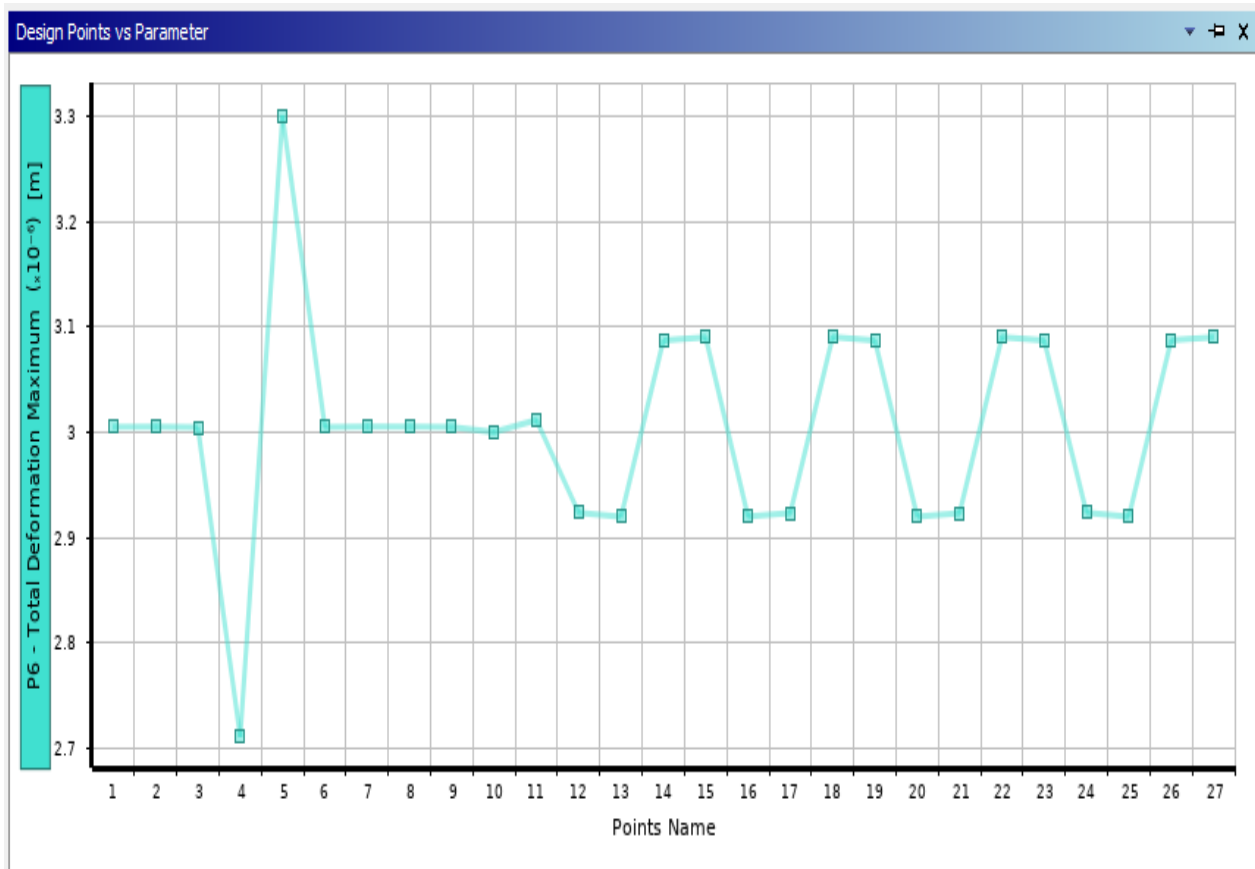


Figure 5.20 Plot of minimum safety factor vs design point

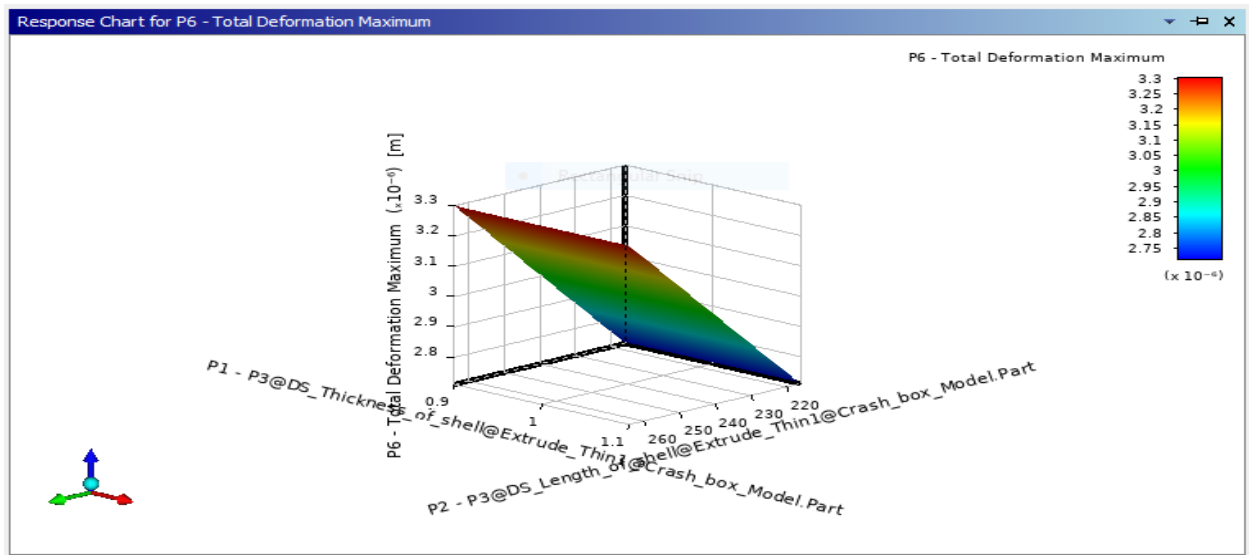


Figure 5.21 The 3D response chart maximum total deformation

### 5.10.3. Sensitivity of all maximum output parameter

Figure 5.30 shows the Sensitivity of maximum total deformation, equivalent elastic strain, and strain energy. This point implies all maximum output parameters with the impact of the input parameters of the thickness, width of the inner and outer hexagonal, diameter core circle, and length of crash box.

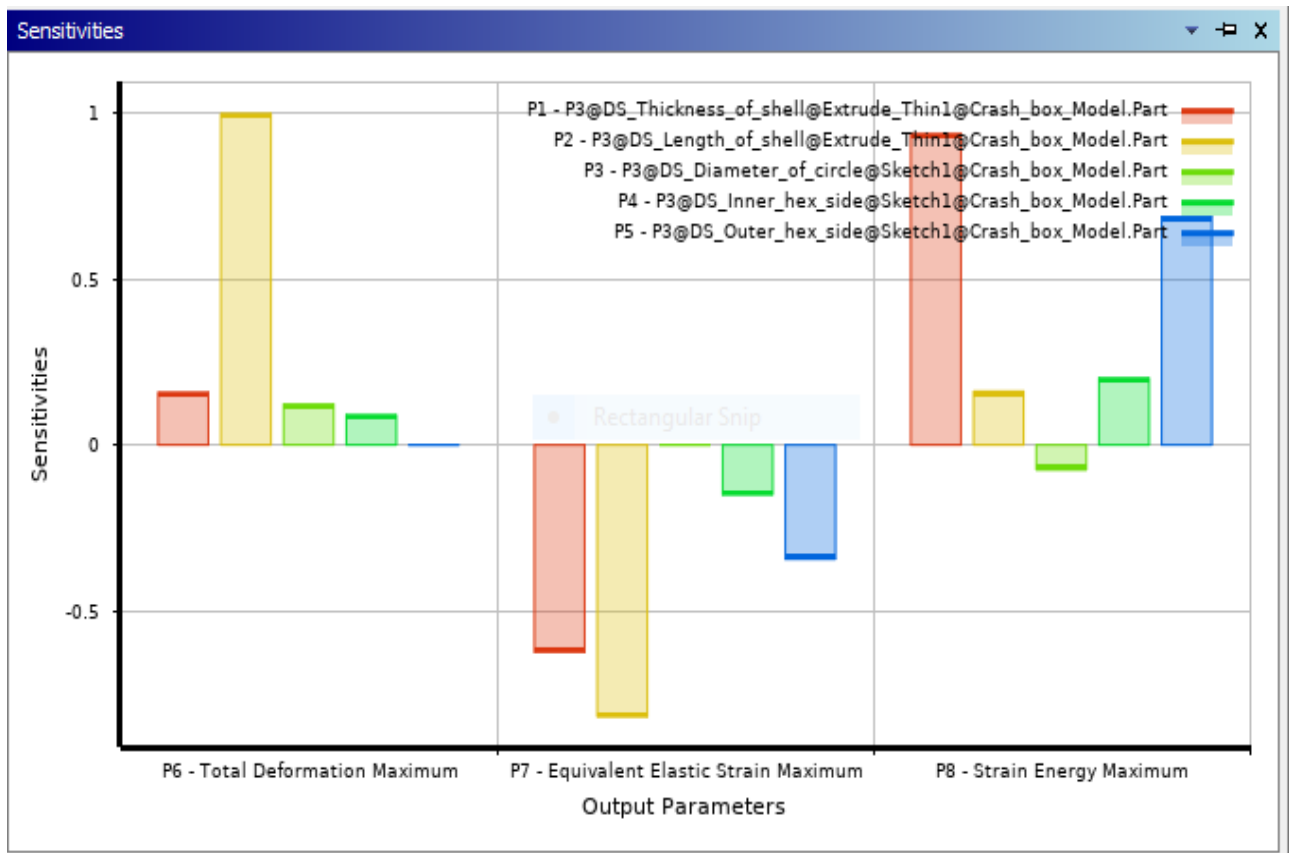


Figure 5.22 Sensitivity of input parameter vs. output parameter

**5.10.4. Response surface local sensitivity curve of maximum total deformation**

There are two types of Sensitivity in response surface sensitivity (1) local sensitivity and (2) local sensitivity curve. In Figure 5.31, the ‘‘X’’ axis represents the design points and the ‘‘Y’’ axis stands for p-6- maximum total deformation and represents the local sensitivity curve, while the black squares are the response points. As shown in figure 5.20, the P2-length of the crash box or excluded length shows the highest sensitivity, while both thicknesses of shell and diameter of core circle have neutral sensitivity and the rest have no local sensitivity to the output parameter.

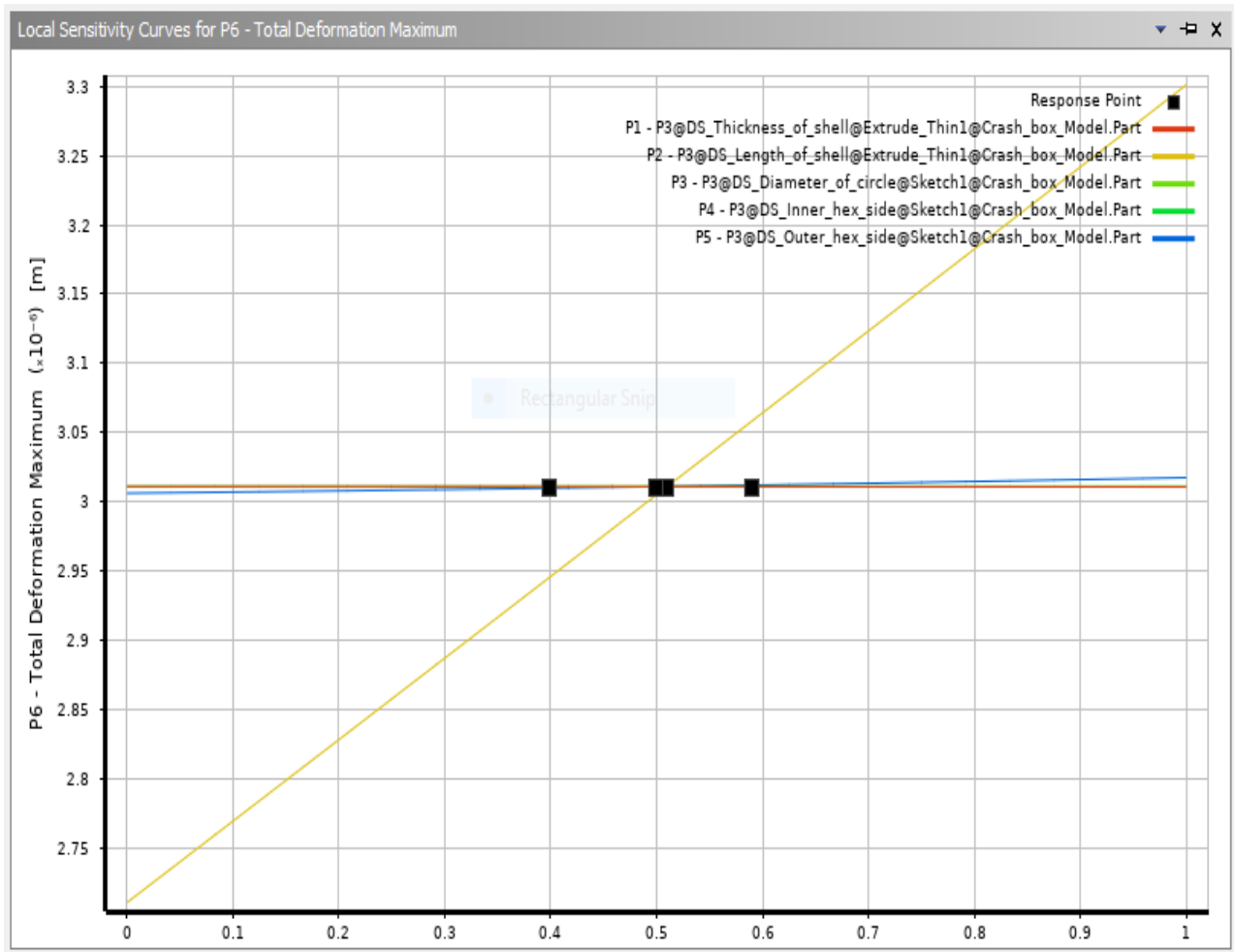


Figure 5.23 Local sensitivity curve for the maximum total deformation

**5.10.5. Comparison of local sensitivity of all output parameter**

Figure 5.32 represents the response local sensitivity chart, the impact of both input and output. This shows the sensitivity range across the chart that the output correlated with the input that shows the bar heights with sensitivity. The negative correlated influence the inversely, neutral points have the little impact, and all the positive shows the proportional impact on the optimization of the crash box. For this reason, a P-4 length of the crash and outer hexagonal side have high positive sensitivity with all output parameters. Other is little impact and neutral on the output parameter.

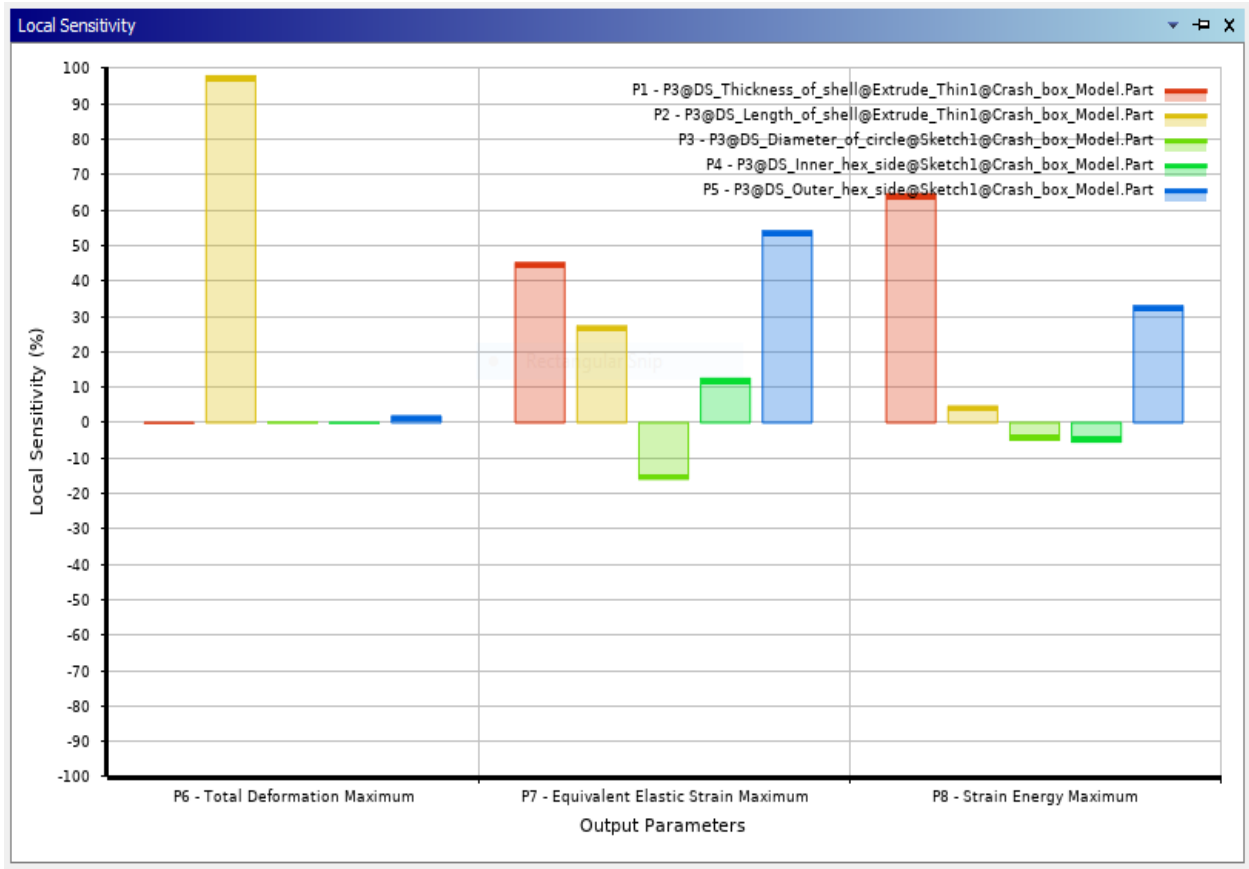


Figure 5.24 Local sensitivity of input parameter vs. output parameter

Spider chart

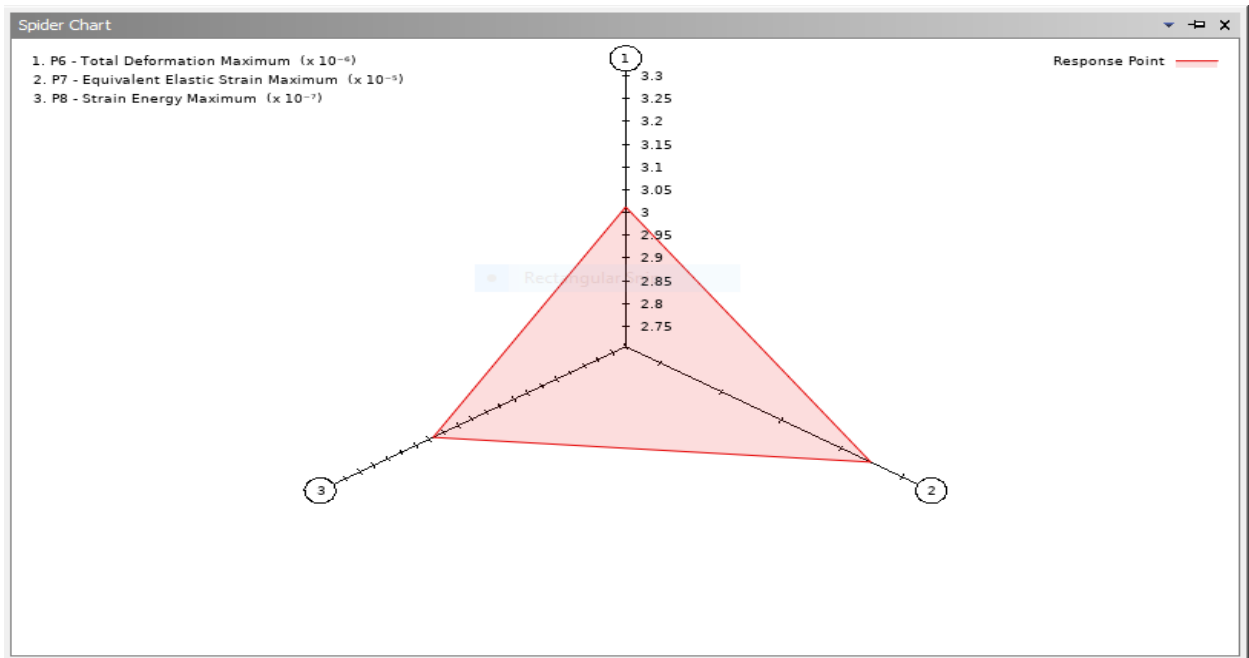


Figure 5.25 The spider chart of the maximum all output parameter

**5.10.6. The candidate parameter design point suggested by DesignXplorer**

The specified number of design candidates (3) as shown in Figure 5.34 are suggested by DesignXplorer and the result is listed in Table 5.4 once the optimization process is completed. The candidates are displayed along with a performance identifier (stars, crosses, dashes). A candidate with three stars has met all the specified objectives, one or two stars suggest the candidate meets some objectives or constraints, three crosses mean that the optimization analysis failed, and a grey dash means that the design cannot be more efficient than it currently is. In this case, all 3 candidates meet the specified objectives. Candidate number 1 is selected as the optimized design point and the simulation is now run with the suggested input parameters in the LS-Prepost model and solve in LS-DYNA.

Table of Schematic D4: Optimization , Candidate Points													
	A	B	C	D	E	F	G	H	I	J	K	L	M
1	Reference	Name	P1 - P3@DS_... .Part	P2 - P3@DS_Le... .Part	P3 - P3@DS_... .Part	P4 - P3@DS_In... .Part	P5 - P3@DS_O... .Part	P6 - Total Deformation Maximum (m)		P7 - Equivalent Elastic Strain Maximum (m m^-1)		P8 - Strain Energy Maximum (J)	
2								Parameter Value	Variation from Reference	Parameter Value	Variation from Reference	Parameter Value	Variation from Reference
3	☉	Candidate Point 1	1.0997	263.99	57.412	73.207	109.92	★★★ 3.3056E-06	0.00%	★ 2.7275E-05	0.00%	★★★ 7.4911E-07	0.00%
4	☉	Candidate Point 2	1.099	263.81	62.59	66.441	109.72	★★★ 3.3035E-06	-0.06%	★ 2.7275E-05	0.00%	★★★ 7.484E-07	-0.09%
5	☉	Candidate Point 3	1.0994	263.82	60.619	71.714	109.77	★★★ 3.3035E-06	-0.06%	★ 2.7281E-05	0.03%	★★★ 7.4726E-07	-0.25%

Figure 5.26 Optimum parameter candidates suggested by design explorer

Table 5.5 The three-option candidate value of optimized crash box parameters

No	Name	P-1, shell thickness	P-2, CB Length,	Core circle diameter, p3	Internal hex-side, p-4	Outer hex-side, p-5
1	Candidate 1	1.0997 mm	263.99 mm	57.412 mm	73.207 mm	109.92 mm
2	Candidate 2	1.099 mm	263.81 mm	62.59 mm	66.441 mm	109.72 mm
3	Candidate 3	1.0994 mm	263.82 mm	60.619 mm	71.714 mm	109.77 mm

**5.11. Simulation Results of the crash box with optimized parameter**

From candidate optimized parameters in ANSYS, we can develop CAD modeling and experimental simulation and further investigation of crash box crashworthiness. By choosing a candidate point, the cad modeling in SOLIDWORK and experimental simulation are carried in LS-Prepost and LS-DYNA respectively as before.

### 5.11.1. Deformation mode

Lobes that appeared in the compression process represent wavelength which is hugely significant for energy absorption devices. More lobes mean a favorable collapse mode. Therefore, the optimized model had the good and more lobes collapse mode as shown in Figure 5.35.

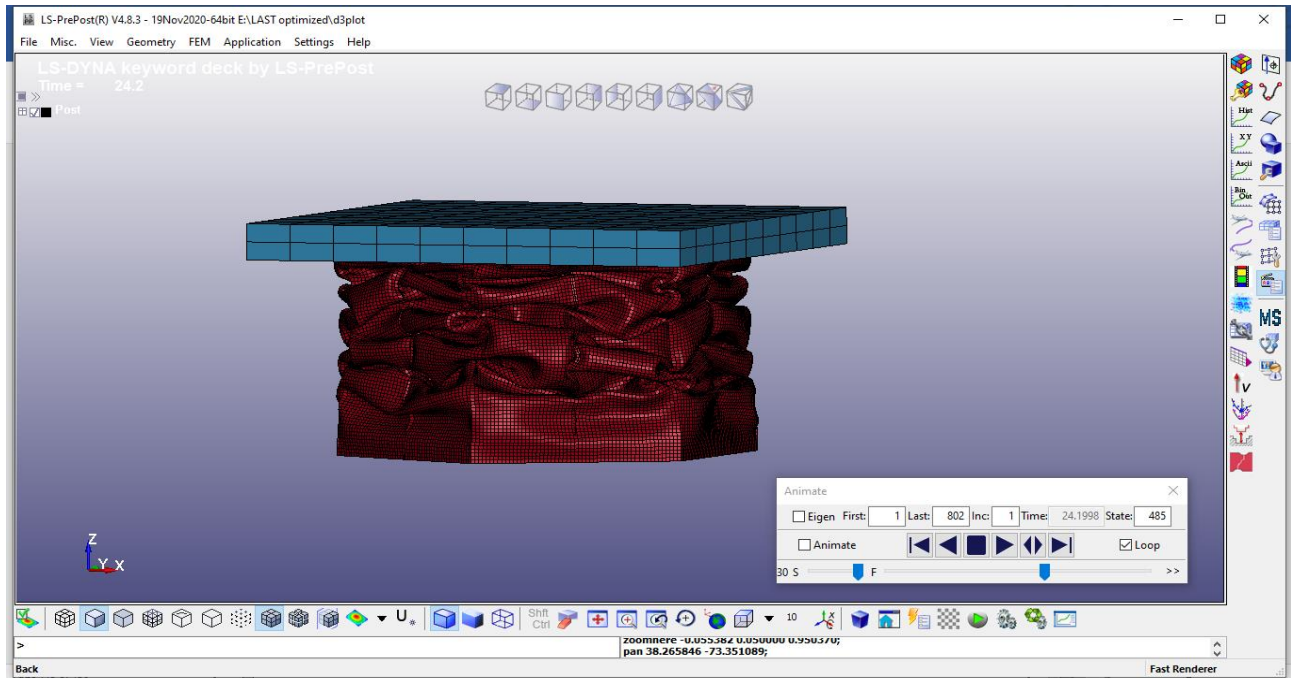


Figure 5.27 Deformation mode of optimized model after simulation.

### 5.11.2. Performance indicator result

Among all the above numerical simulation specimens the best results were obtained in the optimized parameter geometry with the best values of peak force, average crush force and the energy absorbed was recorded from the simulation result of the model. Also, the results are given in Table 5.5 as the following.

Table 5.6 Simulation Results of the parametrically optimized crash box

Specimen code	Peak Force (kN)	Mean crush force (kN)	Total energy (kJ)	Mass (kg)	Specific energy (kJ/Kg)	CFA	$\omega$
Optimized structure	69.13	30.25	12.342	1.320	9.35	0.569	1.647

## CHAPTER SIX

### 6. CONCLUSION AND RECCOMENDATION

#### 6.1. Conclusion

The ideas behind the biomimetics (bio-inspired) structures are mainly from natural honeycomb and spider web hierarchical structures with woodpecker cores. Compared with the original hexagonal tubes and other common geometry structures, the new bio-inspired structures proposed in this study show improved crashworthiness. Based on the investigations mentioned above, some important conclusions can be drawn as below.

(1) The new biomimetic hexagonal structures proposed in this study perform better than the original hexagonal tube in terms of energy absorption, crush force efficiency, and stability. From the result of an experimental simulation result, MC-FQCHT (C2C & W2W) and MC-FQCHT (C2W) is an excellent structure, with mean force, crush force efficiency, and fluctuation coefficient at 25.27 kN, 25.99 kN, 0.456, 0.375, and 1.523, 1.447 respectively. These values are about 1.836 times, 1.832 times, and 0.26 times bigger than that of SC-OHT, respectively. The improvement of specific energy absorption of MC-FQCHT(C2W) is the most significant, with the figure of 6.864 kJ/kg, which is 2.557 times bigger than that of SC-OHT (2.684 kJ/kg). Therefore, full quadrilateral and circular hexagonal tubes and C2W ribs connected (MC-FQCHT) was recommended as optimal geometry. After optimized this structure parameter the crashworthiness indicators are increased Peak Force (69.13 KN), Mean crush force (30.25 KN), Total energy (12.342 KJ) Specific energy (9.35KJ/Kg), and crushing force efficiency (CFE) 0.569 respectively.

(2) The proposed self-similar hierarchical and reinforced by a spider web and core circle woodpecker design can greatly increase the stability of the axial collapse process. While the more ribs reinforced by the corner to corner and wall to wall and corner to wall design shows higher SEA compared with other designs, due to the substantial contribution of the number of membrane energy absorption element units.

(3) The details of crushing patterns show that the formation of lobes is accompanied by the strong interaction of walls which is significant to dissipate plastic energy. Hierarchical designs produce more lobes and improve crushing patterns, which can guide the reinforcement design of energy absorption devices.

(4) The explicit dynamics theoretical model presented in this study can predict well the mean force of biomimetic tubes under axial compression. It reveals the huge improvement mechanism of each criterion found in simulations. Moreover, it suggests that the geometric effect strongly affects the tubes' energy absorption ability. The mechanism of improving the energy absorption ability of eight patterns of biomimetic hexagonal tubes has been revealed. However, in the crossings of these biomimetic hexagonal prismatic structure tubes, the current manufacturing will generate thick shells or even solids.

#### 6.2. Recommendation and future work

Future work is to focus on manufacturing and basic properties of materials and make the corresponding adjustment to the numerical and theoretical model to further improve the accuracy.

Experiments are also crucial work for further study. On the other hand, exploring the influence of the hierarchy order and angle of interior ribs connection on the deformation mode and crashworthiness of hierarchical structures still need to be done. Also, specifically, there are some future works recommended depending on the analysis and result of this study. These are listed as the following:

- The Crash Box design needs additional filler materials to increase energy absorption by stabilizing the crushed pattern and bettering the collapse of the tube.
- Types of connection used between the shell of Crash Box.
- Different types of geometrical optimization of the Crash Box by varying the geometrical shape and other mechanical properties.
- Using composite material with appropriate structural geometry and arrangement of layer material that has a better crashworthiness property.
- Reduced the mass of Crash Box MC-FQCHT(C2W) by using the proper optimization method.
- Compare and analyze the energy created on the front part of the Crash box with and without beam bumper.
- Determine optimum simulation cost of a highly reinforced cross-section of crash box.



## Reference

- [1] T. Toroyan, “Global status report on road safety,” *Inj. Prev.*, vol. 15, no. 4, p. 286, 2009.
- [2] K. G. Micheale, “Road traffic accident: Human security perspective,” *Int. J. Peace Dev. Stud.*, vol. 8, no. 2, pp. 15–24, 2017.
- [3] D. Deme, “Road Traffic Accident in Ethiopia from 2007/08-2017/18,” *Am. Int. J. Sci. Eng. Res.*, vol. 2, no. 2, pp. 49–59, 2019.
- [4] D. H. Mariam, “Road traffic accident: A major public health problem in Ethiopia,” *Ethiop. J. Heal. Dev.*, vol. 28, no. 1, pp. 1–2, 2014.
- [5] N. A. Khatri, H. Shaikh, Z. A. Maher, A. Shah, and S. F. Ahmed, “A review on optimization of vehicle frontal crashworthiness for passenger safety,” *Int. J. Eng. Technol.*, vol. 7, no. 2, pp. 1–4, 2018.
- [6] P. R. Andhare, A. M. Badadhe, and R. Shahu, “Case Study on Design Optimisation & Regulation Review of Vehicle Front End Structural Crashworthiness,” pp. 839–843, 2019.
- [7] “2013\_Wiley\_Bookchapter\_Crash.pdf.” .
- [8] B. Bhushan and Y. C. Jung, “Natural and biomimetic artificial surfaces for superhydrophobicity, self-cleaning, low adhesion, and drag reduction,” *Prog. Mater. Sci.*, vol. 56, no. 1, pp. 1–108, 2011.
- [9] H. Mulla Salim, D. Yadv Sanjay, D. Shinde, and G. Deshpande, “Importance of federal motor vehicle safety standards 207/210 in occupant safety - A case study,” *Procedia Eng.*, vol. 64, pp. 1099–1108, 2013.
- [10] N. H. T. S. NHTSA, “2015 Motor Vehicle Crashes: Overview,” *Traffic Saf. facts Res. note*, vol. 2016, pp. 1–9, 2016.
- [11] S. Salehghaffari, M. Tajdari, M. Panahi, and F. Mokhtarnezhad, “Attempts to improve energy absorption characteristics of circular metal tubes subjected to axial loading,” *Thin-Walled Struct.*, vol. 48, no. 6, pp. 379–390, 2010.
- [12] Y. Liu, “Crashworthiness design of multi-corner thin-walled columns,” *Thin-Walled Struct.*, vol. 46, no. 12, pp. 1329–1337, 2008.
- [13] “DYNAMIC PROGRESSIVE BUCKLING OF C I R C U L A R S Q U A R E TUBES w.,” vol. 4, no. 4, pp. 243–270, 1986.
- [14] Z. Ahmad, D. P. Thambiratnam, and A. C. C. Tan, “Dynamic energy absorption characteristics of foam-filled conical tubes under oblique impact loading,” *Int. J. Impact Eng.*, vol. 37, no. 5, pp. 475–488, 2010.
- [15] G. M. Nagel and D. P. Thambiratnam, “A numerical study on the impact response and energy absorption of tapered thin-walled tubes,” *Int. J. Mech. Sci.*, vol. 46, no. 2, pp. 201–216, 2004.
- [16] S. Hou *et al.*, “Multiobjective optimization for tapered circular tubes,” *Thin-Walled Struct.*, vol. 49, no. 7, pp. 855–863, 2011.
- [17] C. Kiliçaslan, “Numerical crushing analysis of aluminum foam-filled corrugated single- and double-circular tubes subjected to axial impact loading,” *Thin-Walled Struct.*, vol. 96, pp. 82–94, 2015.
- [18] G. Sun, S. Li, Q. Liu, G. Li, and Q. Li, “Experimental study on crashworthiness of empty/aluminum foam/honeycomb-filled CFRP tubes,” *Compos. Struct.*, vol. 152, pp. 969–993, 2016.
- [19] G. R. Srinivas, A. Deb, R. Sanketh, and N. K. Gupta, “An Enhanced Methodology for Lightweighting a Vehicle Design Considering Front Crashworthiness and Pedestrian Impact Safety Requirements,” *Procedia Eng.*, vol. 173, pp. 623–630, 2017.

- [20] A. Alavi Nia and M. Parsapour, "Comparative analysis of energy absorption capacity of simple and multi-cell thin-walled tubes with triangular, square, hexagonal and octagonal sections," *Thin-Walled Struct.*, vol. 74, pp. 155–165, 2014.
- [21] H. Wan, H. Ohtaki, S. Kotosaka, and G. Hu, "A study of negative Poisson's ratios in auxetic honeycombs based on a large deflection model," *Eur. J. Mech. A/Solids*, vol. 23, no. 1, pp. 95–106, 2004.
- [22] S. Boria and G. Forasassi, "Honeycomb sandwich material modelling for dynamic simulations of a crash-box for a racing car," *WIT Trans. Built Environ.*, vol. 98, pp. 167–176, 2008.
- [23] N. S. B. Yusof, S. M. Sapuan, M. T. H. Sultan, and M. Jawaid, "Conceptual design of oil palm fibre reinforced polymer hybrid composite automotive crash box using integrated approach," *J. Cent. South Univ.*, vol. 27, no. 1, pp. 64–75, 2020.
- [24] F. K. Ko and J. Jovicic, "Modeling of mechanical properties and structural design of spider web," *Biomacromolecules*, vol. 5, no. 3, pp. 780–785, 2004.
- [25] T. Wierzbicki and W. Abramowicz, "on the Crushing Mechanics of Thin-Walled Structures.," *Am. Soc. Mech. Eng.*, no. 83, 1983.
- [26] D. Wang, S. Zhang, C. Wang, and C. Zhang, "Structure-material-performance integration lightweight optimisation design for frontal bumper system," *Int. J. Crashworthiness*, vol. 23, no. 3, pp. 311–327, 2018.
- [27] F. Tarlochan, F. Samer, A. M. S. Hamouda, S. Ramesh, and K. Khalid, "Design of thin wall structures for energy absorption applications: Enhancement of crashworthiness due to axial and oblique impact forces," *Thin-Walled Struct.*, vol. 71, pp. 7–17, 2013.
- [28] J. Marzbanrad, M. Alijanpour, and M. S. Kiasat, "Design and analysis of an automotive bumper beam in low-speed frontal crashes," *Thin-Walled Struct.*, vol. 47, no. 8–9, pp. 902–911, 2009.
- [29] J. Marzbanrad, M. Mehdikhanlo, and A. Saeedi Pour, "An energy absorption comparison of square, circular, and elliptic steel and aluminum tubes under impact loading," *Turkish J. Eng. Environ. Sci.*, vol. 33, no. 3, pp. 159–166, 2009.
- [30] E. Demirci and A. R. Yildiz, "An investigation of the crash performance of magnesium, aluminum and advanced high strength steels and different cross-sections for vehicle thin-walled energy absorbers," *Mater. Test.*, vol. 60, no. 7–8, pp. 661–668, 2018.
- [31] M. Beusink, "Measurements and simulations on the ( dynamic ) properties of aluminium alloy," 2011.
- [32] A. Hamouda, "Energy absorption capacities of square tubular structures," *J. Achiev. ...*, vol. 24, no. 1, pp. 36–42, 2007.
- [33] S. Yang and C. Qi, "Multiobjective optimization for empty and foam-filled square columns under oblique impact loading," *Int. J. Impact Eng.*, vol. 54, pp. 177–191, 2013.
- [34] X. W. Zhang, H. Su, and T. X. Yu, "Energy absorption of an axially crushed square tube with a buckling initiator," *Int. J. Impact Eng.*, vol. 36, no. 3, pp. 402–417, 2009.
- [35] Z. Wang, J. Liu, and S. Yao, "On folding mechanics of multi-cell thin-walled square tubes," *Compos. Part B Eng.*, vol. 132, pp. 17–27, 2018.
- [36] J. Ma and Z. You, "Energy absorption of thin-walled square tubes with a prefolded origami pattern - Part I: Geometry and numerical simulation," *J. Appl. Mech. Trans. ASME*, vol. 81, no. 1, pp. 1–11, 2014.
- [37] W. Abramowicz and N. Jones, "Dynamic axial crushing of circular tubes," *Int. J. Impact Eng.*, vol. 2, no. 3, pp. 263–281, 1984.
- [38] X. W. Zhang, Q. D. Tian, and T. X. Yu, "Axial crushing of circular tubes with buckling initiators,"

- Thin-Walled Struct.*, vol. 47, no. 6–7, pp. 788–797, 2009.
- [39] K. El Nady, F. Dos Reis, and J. F. Ganghoffer, “Computation of the homogenized nonlinear elastic response of 2D and 3D auxetic structures based on micropolar continuum models,” *Compos. Struct.*, vol. 170, pp. 271–290, 2017.
- [40] G. Nagel, “(TEZ) Impact and Energy Absorption of Straight and Tapered Rectangular Tubes,” no. February, p. 324, 2005.
- [41] S. J. Hosseinipour and G. H. Daneshi, “Energy absorption and mean crushing load of thin-walled grooved tubes under axial compression,” *Thin-Walled Struct.*, vol. 41, no. 1, pp. 31–46, 2003.
- [42] N. Tanlak and F. O. Sonmez, “Optimal shape design of thin-walled tubes under high-velocity axial impact loads,” *Thin-Walled Struct.*, vol. 84, pp. 302–312, 2014.
- [43] G. Lu and T. Yu, *Energy Absorption of Structures and Materials*. 2003.
- [44] H. Yin, Y. Xiao, G. Wen, Q. Qing, and X. Wu, “Crushing analysis and multi-objective optimization design for bionic thin-walled structure,” *Mater. Des.*, vol. 87, pp. 825–834, 2015.
- [45] Y. Zhu, L. Li, and J. Yang, “Frontal structure improvement on car based on RCAR impact test,” *Proc. - 2012 3rd Int. Conf. Digit. Manuf. Autom. ICDMA 2012*, pp. 434–438, 2012.
- [46] Y. Chen and M. H. Fu, “A novel three-dimensional auxetic lattice meta-material with enhanced stiffness,” *Smart Mater. Struct.*, vol. 26, no. 10, 2017.
- [47] J. Knippers and T. Speck, “Design and construction principles in,” vol. 015002, 2012.
- [48] “Vattam, S. S., Helms, M. E., and Goel, A. K. (2009). Nature of creative analogies in biologically inspired innovative design. In,” pp. 255–264, 2009.
- [49] Y. H. Cohen, Y. Reich, and S. Greenberg, “Biomimetics: Structure-function patterns approach,” *J. Mech. Des. Trans. ASME*, vol. 136, no. 11, 2014.
- [50] S. S. Narsale and J. J. Shah, “An Improved Framework for Design Concept Generation Based On Experiential and Intuitive Methods,” vol. 1570504, no. October, p. 280, 2014.
- [51] N. S. Ha and G. Lu, “A review of recent research on bio-inspired structures and materials for energy absorption applications,” *Compos. Part B Eng.*, vol. 181, no. September 2019, p. 107496, 2020.
- [52] C. Y. Wang, Y. Li, W. Z. Zhao, S. C. Zou, G. Zhou, and Y. L. Wang, “Structure design and multi-objective optimization of a novel crash box based on biomimetic structure,” *Int. J. Mech. Sci.*, vol. 138–139, pp. 489–501, 2018.
- [53] E. Wu and W. S. Jiang, “Axial crush of metallic honeycombs,” *Int. J. Impact Eng.*, vol. 19, no. 5–6, pp. 439–456, 1997.
- [54] A. Najafi and M. Rais-Rohani, “Mechanics of axial plastic collapse in multi-cell, multi-corner crush tubes,” *Thin-Walled Struct.*, vol. 49, no. 1, pp. 1–12, 2011.
- [55] A. Najafi *et al.*, “On the crashworthiness of bio-inspired hexagonal prismatic tubes under axial compression,” *Thin-Walled Struct.*, vol. 186, no. Iccsnt, pp. 295–299, 2016.
- [56] N. Du, Z. Yang, X. Y. Liu, Y. Li, and H. Y. Xu, “Structural origin of the strain-hardening of spider silk,” *Adv. Funct. Mater.*, vol. 21, no. 4, pp. 772–778, 2011.
- [57] J. M. Gosline, M. E. DeMont, and M. W. Denny, “The structure and properties of spider silk,” *Endeavour*, vol. 10, no. 1, pp. 37–43, 1986.
- [58] J. Oda, J. Sakamoto, and K. Sakano, “Mechanical evaluation of the skeletal structure and tissue of the woodpecker and its shock absorbing system,” *JSME Int. Journal, Ser. A Solid Mech. Mater. Eng.*, vol. 49, no. 3, pp. 390–396, 2006.

- [59] L. Z. Wang *et al.*, “Biomechanism of impact resistance in the woodpecker’s head and its application,” *Sci. China Life Sci.*, vol. 56, no. 8, pp. 715–719, 2013.
- [60] X. Tag, “A study of woodpecker ’ s pecking process and the impact response of its brain,” vol. 000, pp. 1–9, 2017.
- [61] W. Chen and T. Wierzbicki, “Relative merits of single-cell, multi-cell and foam-filled thin-walled structures in energy absorption,” *Thin-Walled Struct.*, vol. 39, no. 4, pp. 287–306, 2001.
- [62] X. Zhang and H. Zhang, “Energy absorption of multi-cell stub columns under axial compression,” *Thin-Walled Struct.*, vol. 68, pp. 156–163, 2013.
- [63] S. Tabacu, “Axial crushing of circular structures with rectangular multi-cell insert,” *Thin-Walled Struct.*, vol. 95, pp. 297–309, 2015.
- [64] N. Qiu, Y. Gao, J. Fang, Z. Feng, G. Sun, and Q. Li, “Theoretical prediction and optimization of multi-cell hexagonal tubes under axial crashing,” *Thin-Walled Struct.*, vol. 102, pp. 111–121, 2016.
- [65] L. Zhang, Z. Bai, and F. Bai, “Crashworthiness design for bio-inspired multi-cell tubes with quadrilateral, hexagonal and octagonal sections,” *Thin-Walled Struct.*, vol. 122, no. June 2017, pp. 42–51, 2018.
- [66] X. Zhang and H. Zhang, “Axial crushing of circular multi-cell columns,” *Int. J. Impact Eng.*, vol. 65, pp. 110–125, 2014.
- [67] Z. Wang, J. Zhang, Z. Li, and C. Shi, “On the crashworthiness of bio-inspired hexagonal prismatic tubes under axial compression,” *Int. J. Mech. Sci.*, vol. 186, p. 105893, 2020.
- [68] T. N. Tran, S. Hou, X. Han, and M. Q. Chau, “Crushing analysis and numerical optimization of angle element structures under axial impact loading,” *Compos. Struct.*, vol. 119, pp. 422–435, 2014.
- [69] Y. Liu and L. Ding, “A study of using different crash box types in automobile frontal collision,” *Int. J. Simul. Syst. Sci. Technol.*, vol. 17, no. 38, pp. 21.1-21.5, 2016.
- [70] D. B. Kahane and K. V Chandratre, “Experimental and Analytical Investigation for Impact Behavior of Different Shapes of Crash Box,” no. June, 2017.
- [71] M. A. K. Desai, Dhananjay D, “Analysis and Development of Energy Absorbing Crash Box,” *Int. J. Adv. Res. Innov. Ideas Educ.*, vol. Vol-2 Issu, no. 3, pp. 3776–3782, 2016.
- [72] J. C. Brown, J. Robertson, and S. T. Serpento, “Motor Vehicle Structures: Concepts and Fundamentals,” p. 302, 2002.
- [73] E. Corona and G. E. Orient, “An evaluation of the Johnson-Cook model to simulate puncture of 7075 aluminum plates,” 2014.
- [74] J. R. Kissell and R. L. Ferry, *ALUMINIUM STRUCTURES A Guide to Their Specifications*. 2002.
- [75] E. A. Association, “Applications – car body – crash management systems,” *Eur. Alum. Assoc.*, pp. 1–26, 2013.
- [76] J. Besson, *Continuum models of ductile fracture : A review To cite this version : Continuum Models of Ductile*. 2011.
- [77] J. F. V Vincent, O. A. Bogatyreva, N. R. Bogatyrev, A. Bowyer, and A. Pahl, “Biomimetics : its practice and theory,” no. April, pp. 471–482, 2006.
- [78] A. Werritty, “D ’ Arcy Thompson ’ s ‘ On Growth and Form ’ and the Rediscovery of Geometry within the Geographic Tradition D ’ Arcy Thompson ’ s ‘ On Growth and Form ’ and the Rediscovery of Geometry within the Geographic Tradition,” no. November 2014, pp. 37–41, 2011.
- [79] M. Milwich, T. Speck, O. Speck, T. Stegmaier, and H. Planck, “Biomimetics and technical textiles: Solving engineering problems with the help of nature’s wisdom,” *Am. J. Bot.*, vol. 93, no. 10, pp.

- 1455–1465, 2006.
- [80] X. Zhang and H. Zhang, “Numerical and theoretical studies on energy absorption of three-panel angle elements,” *Int. J. Impact Eng.*, vol. 46, pp. 23–40, 2012.
- [81] J. Wang, Y. Zhang, N. He, and C. H. Wang, “Crashworthiness behavior of Koch fractal structures,” *Mater. Des.*, vol. 144, pp. 229–244, 2018.
- [82] A. Vaidya, S. H. Yu, J. S. Ville, and D. T. Nguyen, “Mechanics Based Design of Structures and Machines : An Multiphysics CAD-Based Design Optimization,” no. October 2014, pp. 37–41, 2006.
- [83] B. Fröhlich, J. Gade, F. Geiger, M. Bischoff, and P. Eberhard, “Geometric element parameterization and parametric model order reduction in finite element based shape optimization,” *Comput. Mech.*, 2018.
- [84] G. Nagar, “Design and Optimization of Trapezium in Curved Beam,” vol. 7, no. 11, pp. 263–267, 2018.
- [85] J. D. Jovanovi, “FINITE ELEMENT EVALUATION AND OPTIMIZATION OF GEOMETRY WITH DOE,” vol. 4, no. 4, pp. 39–45, 2011.
- [86] K. Fiedler, B. F. Rolfe, A. Asgari, and T. De Souza, “A systems approach to shape and topology optimisation of mechanical structures,” vol. 125, pp. 145–154.
- [87] J. Brownlee, *Clever Algorithms* .
- [88] X. Zhang and H. Zhang, “International Journal of Impact Engineering Energy absorption limit of plates in thin-walled structures under compression,” *Int. J. Impact Eng.*, vol. 57, pp. 81–98, 2013.
- [89] X. Xu, Y. Zhang, J. Wang, F. Jiang, and C. H. Wang, “Crashworthiness design of novel hierarchical hexagonal columns,” *Compos. Struct.*, vol. 194, no. June 2017, pp. 36–48, 2018.

**Appendix- A**

\$# LS-DYNA Keyword file created by LS-Prepost (R) V4.8.11 - 22Feb2021

\$# Created on Jul-19-2021 (21:07:13)

\*KEYWORD

\*CONTROL\_ENERGY

\$#	hgen	rwen	slnten	rylen	irgen
	2	2	2	1	2

\*CONTROL\_TERMINATION

\$#	endtim	endcyc	endeng	endmas	nosol
	40.0	0	0.0	0.01.000000E8	0

\*CONTROL\_TIMESTEP

\$#	dtinit	tssfac	isdo	tslimt	dt2ms	lctm	erode	ms1st
	0.0	0.9	0	0.0	0.0	0	0	0

\*DATABASE\_GLSTAT

\$#	dt	binary	lcur	ioopt
	0.05	0	0	1

\*DATABASE\_RBDOUT

\$#	dt	binary	lcur	ioopt
	0.05	0	0	1

\*DATABASE\_RCFORC

\$#	dt	binary	lcur	ioopt
	0.05	0	0	1

\*DATABASE\_BINARY\_D3PLOT

\$#	dt	lcdt	beam	npltc	psetid
	0.05	0	0	0	0

\*CONTACT\_AUTOMATIC\_SURFACE\_TO\_SURFACE\_ID

\$#	cid	title
	1	shell tube vs impactor

\$#	ssid	msid	sstyp	mstyp	sboxid	mboxid	spr	mpr
	1	2	3	3	0	0	0	0

\$#	fs	fd	dc	vc	vdc	penchk	bt	dt
	0.3	0.2	0.0	0.0	0.0	0	0.01.00000E20	

```

$# sfs sfm sst mst sfst sfmt fsf vsf
    1.0 1.0 0.0 0.0 1.0 1.0 1.0 1.0
*CONTACT_AUTOMATIC_SINGLE_SURFACE_ID
$# cid title
    2 shell tube self-contact
$# ssid msid sstyp mstyp sboxid mboxid spr mpr
    1 0 3 0 0 0 0 0
$# fs fd dc vc vdc penchk bt dt
    0.3 0.2 0.0 0.0 0.0 0 0.01.00000E20
*ELEMENT_SOLID
$# eid pid n1 n2 n3 n4 n5 n6 n7 n8
*NODE
$# nid x y z tc rc
    1 14.353 -24.86012 263.99 0 0
*PART
$# title
LSHELL1
$# pid secid mid eosid hgid grav adpopt tmid
    1 1 1 0 0 0 0 0
*SECTION_SHELL_TITLE
shell tube
$# secid elform shrf nip propt qr/irid icomp setyp
    1 2 1.0 2 1.0 0 0 1
$# t1 t2 t3 t4 nloc marea idof edgset
    1.0997 1.0997 1.0997 1.0997 0.0 0.0 0.0 0
24*MAT_PIECEWISE_LINEAR_PLASTICITY_TITLE
shell tube material
$# mid ro e pr sigy etan fail tdel
    12.79570E-6 71.016 0.33 0.49607 0.01.00000E21 0.0
$# eps1 eps2 eps3 eps4 eps5 eps6 eps7 eps8
    0.02.79829E-5 8.39488E-5 1.67898E-4 2.79829E-4 4.19744E-4 5.87642E-4 7.83522E-4
$# es1 es2 es3 es4 es5 es6 es7 es8

```

0.4960662, 0.4962469, 0.4966064, 0.4971409, 0.4978446, 0.4987107, 0.4997305, 0.5008945

\*PART title Impactor

\$#	pid	secid	mid	eosid	hgid	grav	adpopt	tmid
2	2	2	0	0	0	0	0	

\*SECTION\_SOLID\_TITLE

impactor

\$#	secid	elform	aet	unused	unused	unused	cohoff	unused
2	1	0				0		

\*MAT\_RIGID\_TITLE

Impactor material

\$#	mid	ro	e	pr	n	couple	m	alias
2	0.5008945	200.0	0.3	0.0	0.0	0.0		

\$#	cmo	con1	con2
1.0	4	7	

\*END



**APPENDIX-B****MATERIAL PROPERTY**

Aluminum alloy AL7075-T651 &gt; 24\*MAT\_PIECEWISE\_LINEAR\_PLASTICITY

Density Kg/mm <sup>3</sup>	Young's Modulus GPa	Poisson's Ratio	Yield stress GPa
2810	71.7	0.33	0.49607

Strain hardening data for aluminum alloy AL7075-T651.

Plastic strain	Plastic stress (GPa)
0.000000000E+00	4.96066158E-01
1.007386037E-03	5.02192754E-01
2.798294546E-05	4.96246893E-01
8.394883638E-05	4.96606405E-01
1.678976728E-04	4.97140851E-01
2.798294546E-04	4.97844647E-01
4.197441819E-04	4.98710662E-01
5.876418547E-04	4.99730461E-01

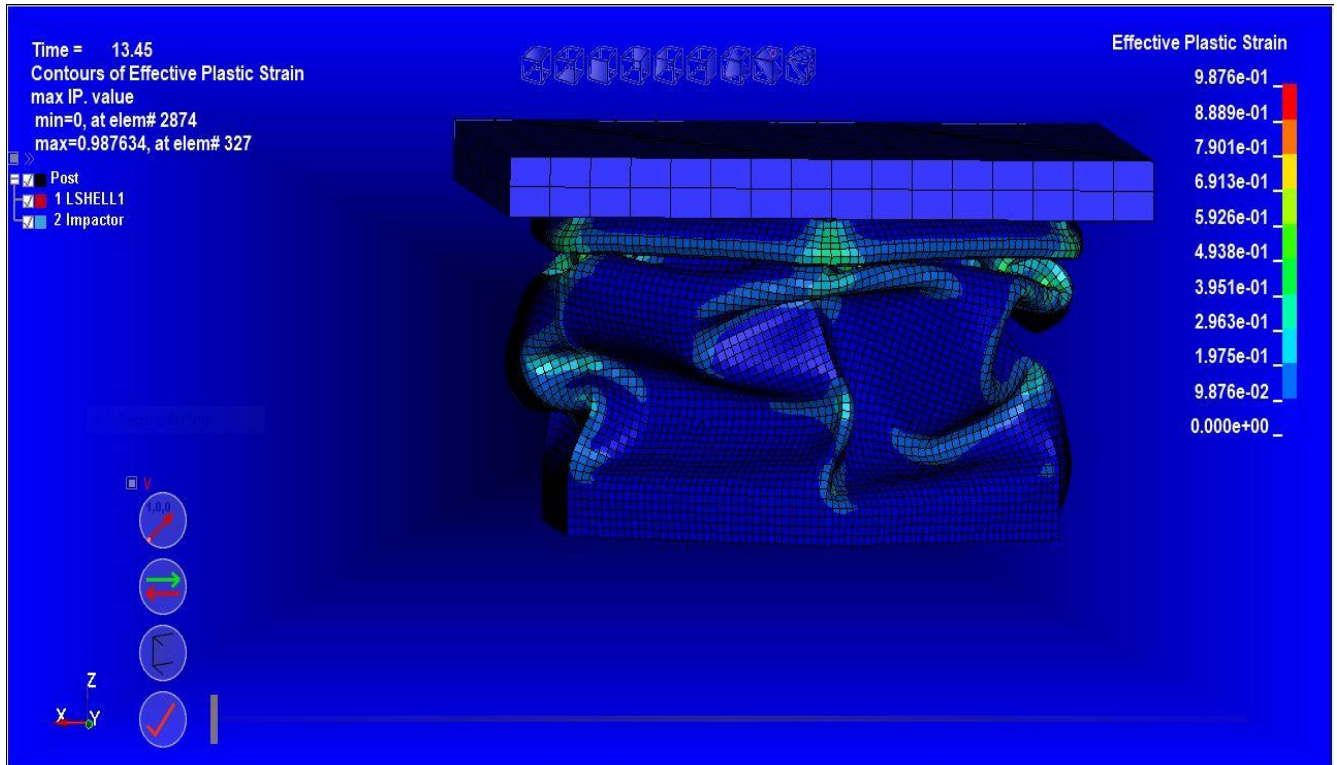
Structural Steel &gt; Isotropic Elasticity

Young's Modulus (GPa)	Poisson's Ratio	Density Kg/mm <sup>3</sup>	Ultimate yield stress ( GPa)
200	0.3	7.85e-6	0.4460

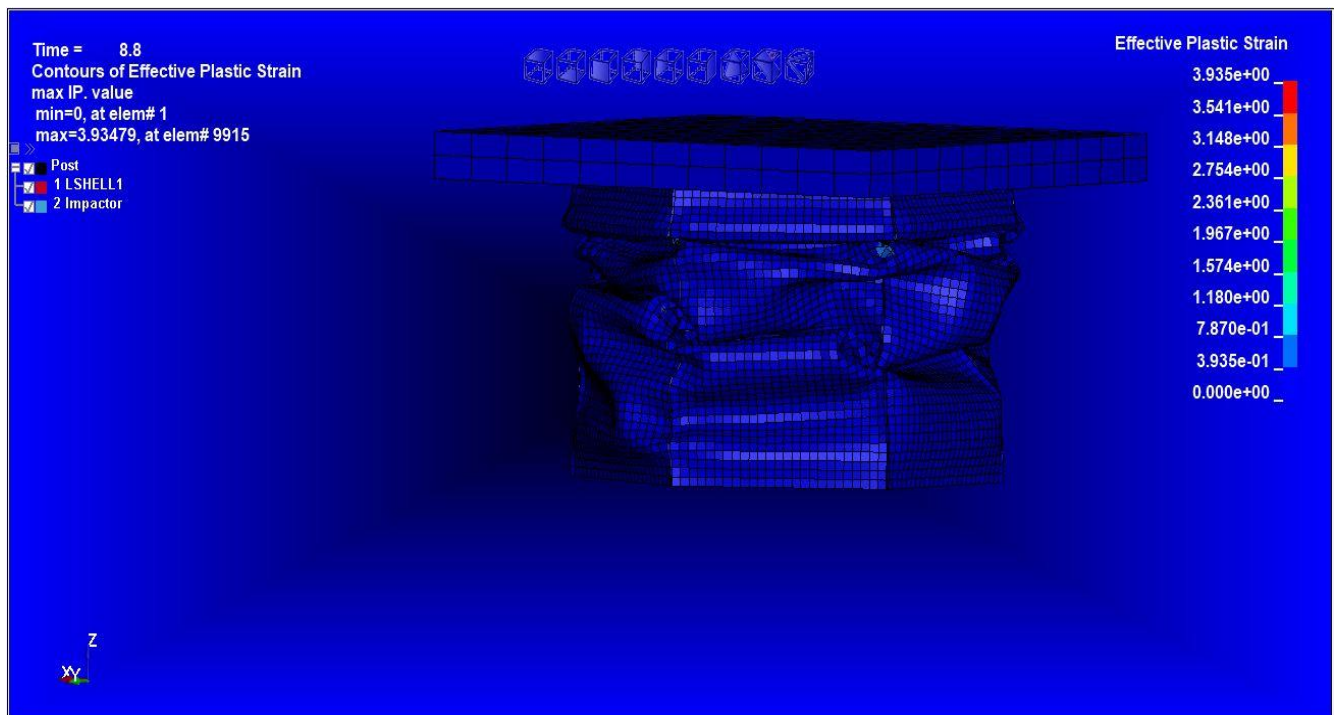
## APPENDIX-C

### Deformation mode of all conceptual model

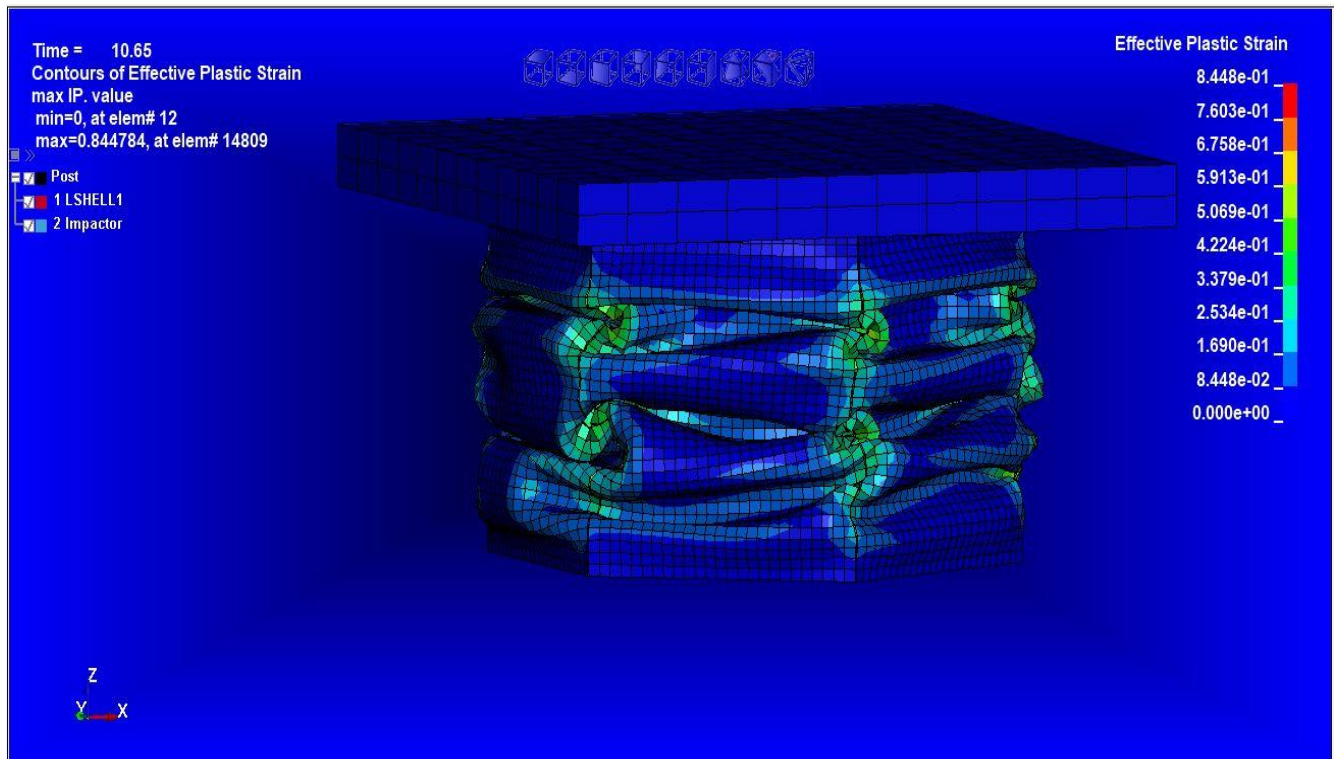
#### 1. Deformation mode for design concept p-1 (SC-OHT)



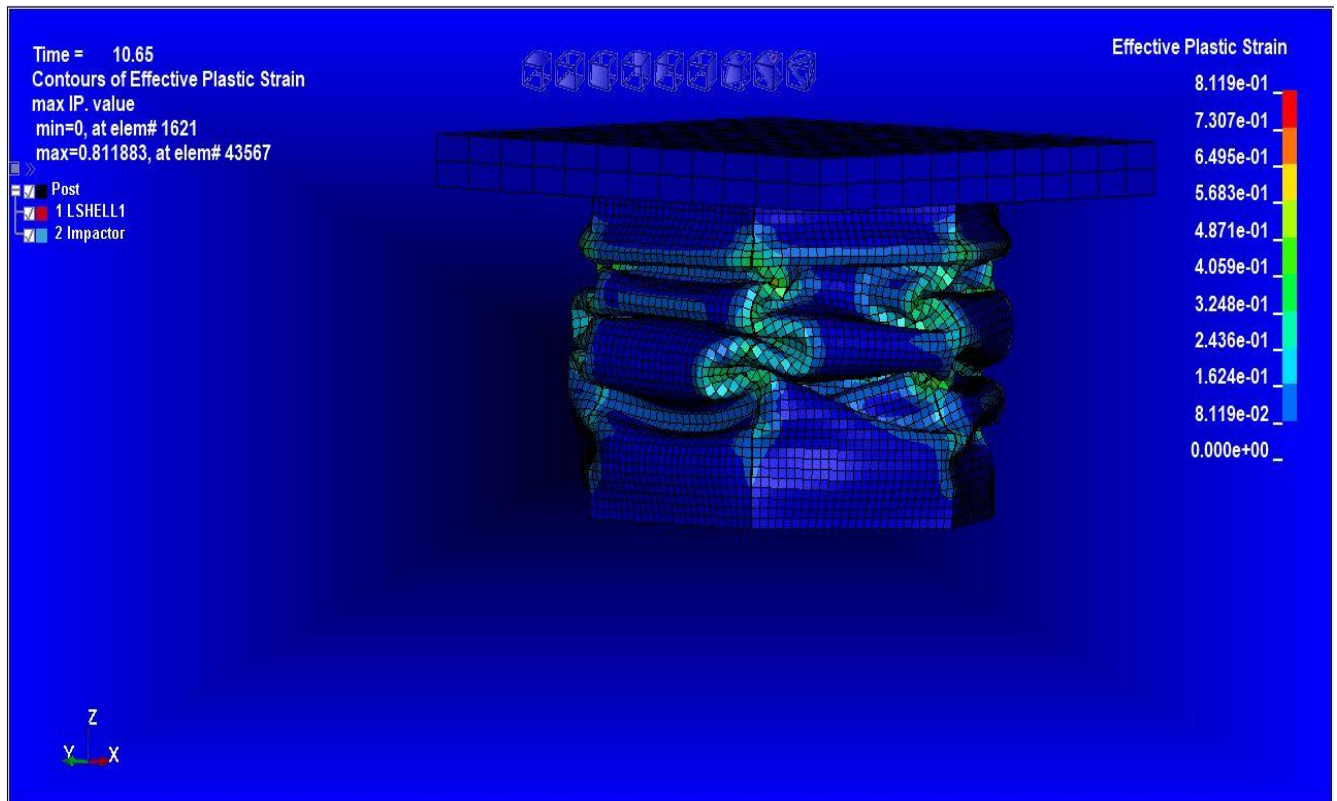
#### 2. Deformation mode for design concept p-1 (SC-OHT)



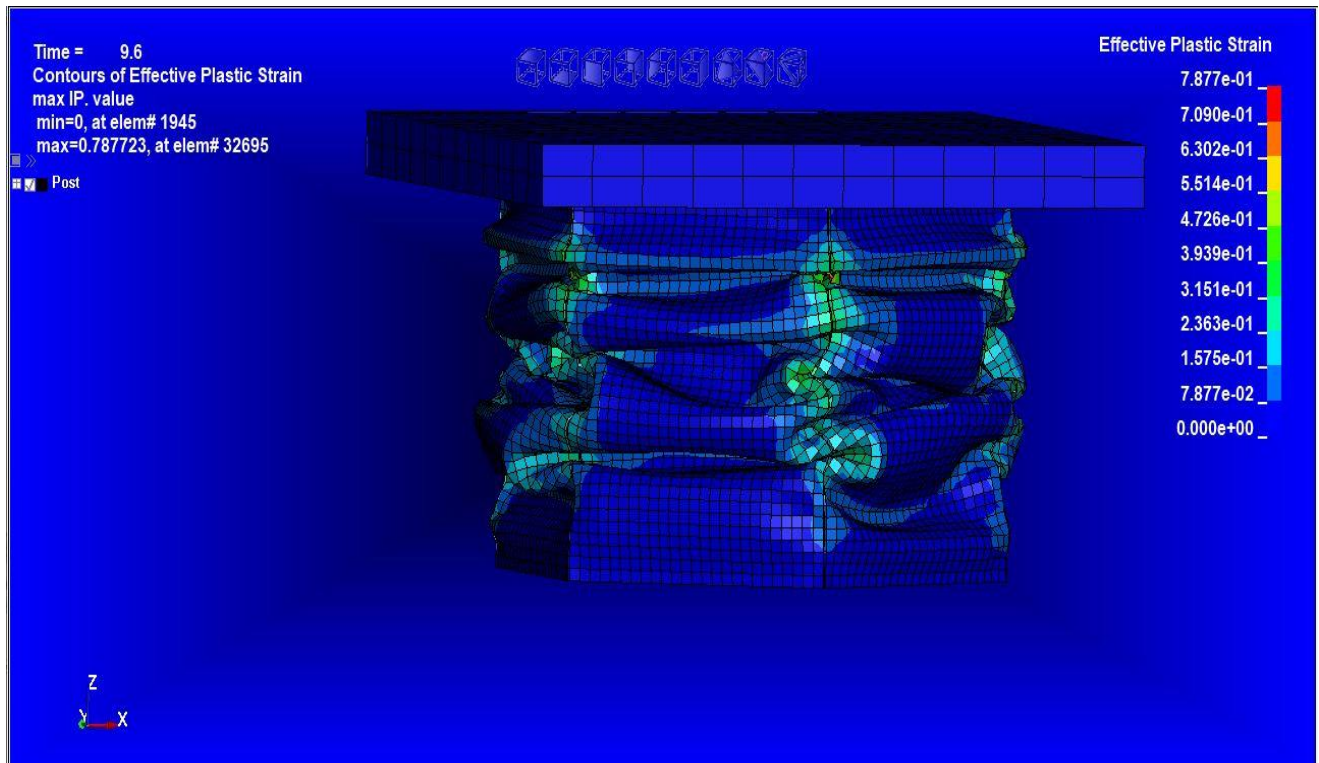
3. Deformation mode for design concept p-1 (SC-OHT)



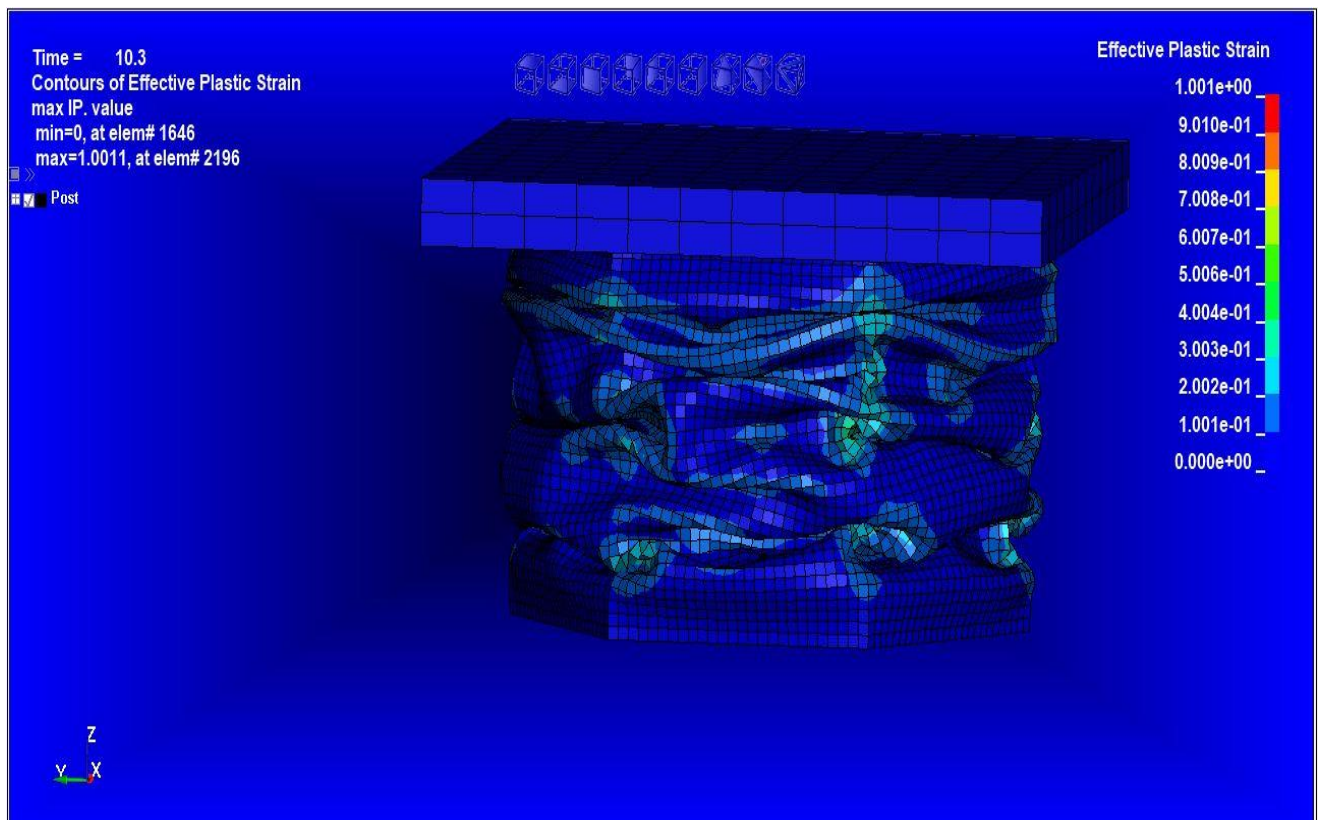
4. Deformation mode for design concept p-1 (SC-OHT)



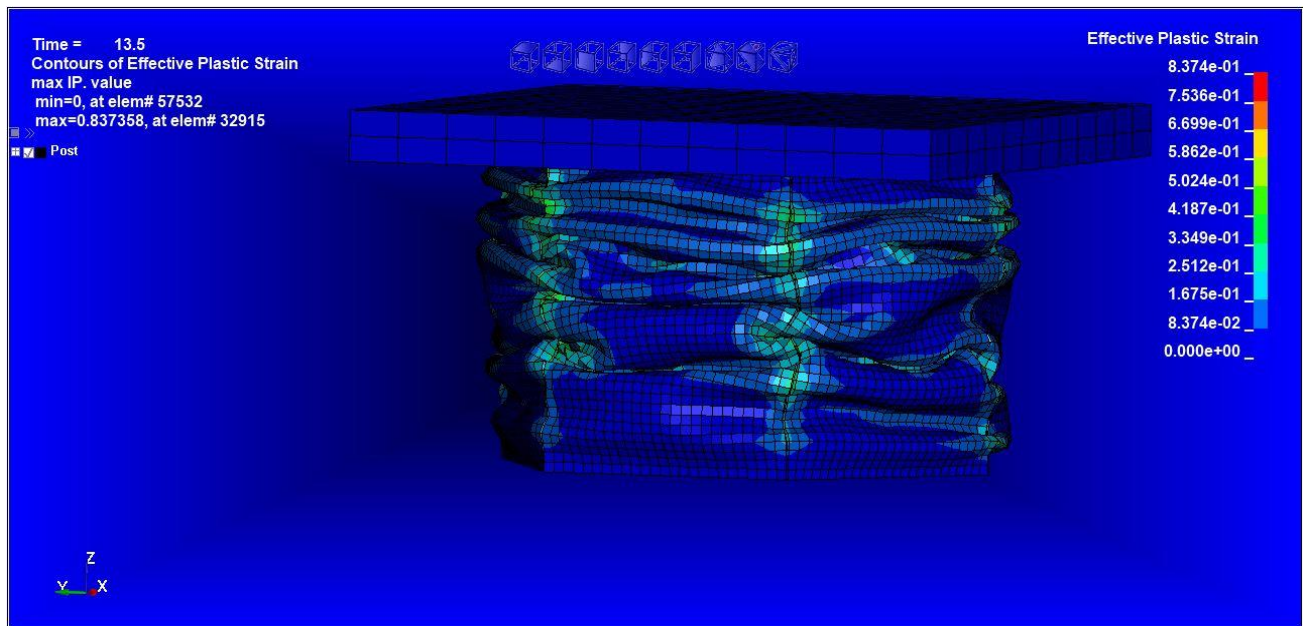
5. Deformation mode for design concept p-1 (SC-OHT)



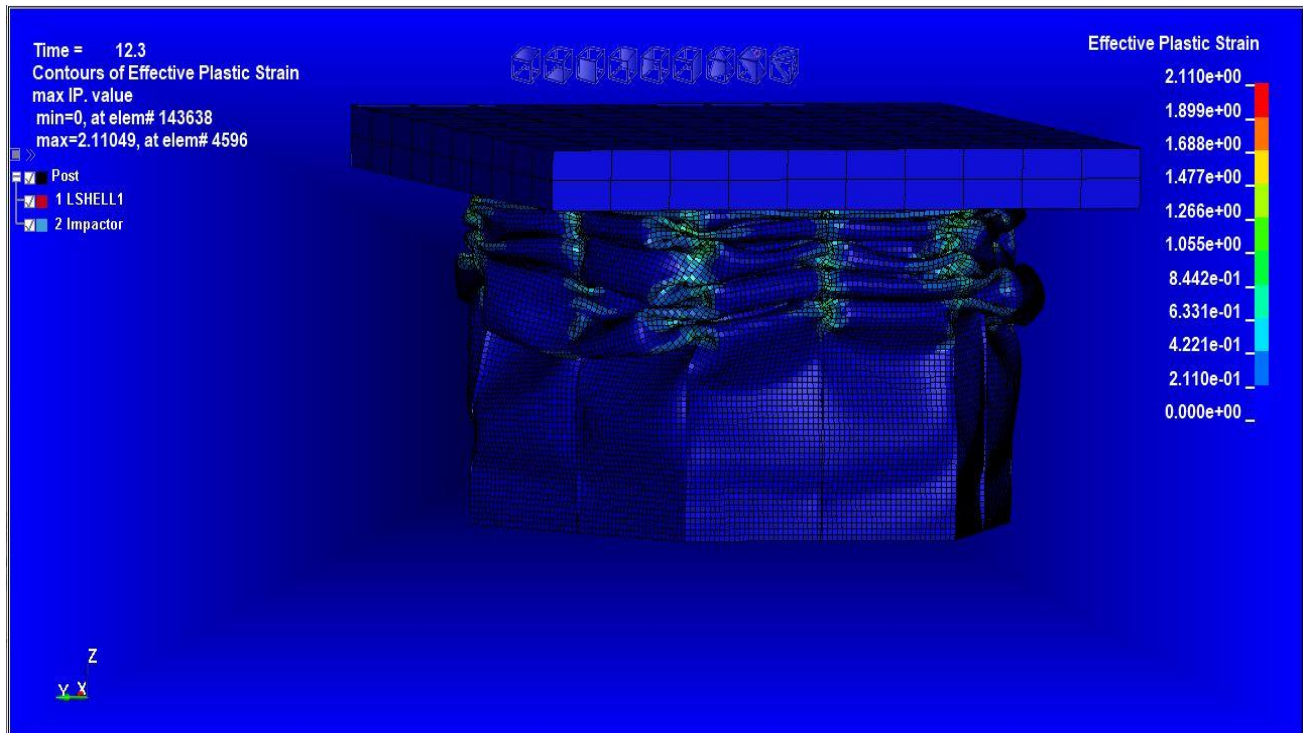
6. Deformation mode for design concept p-1 (SC-OHT)



7. Deformation mode for design concept p-1 (SC-OHT)



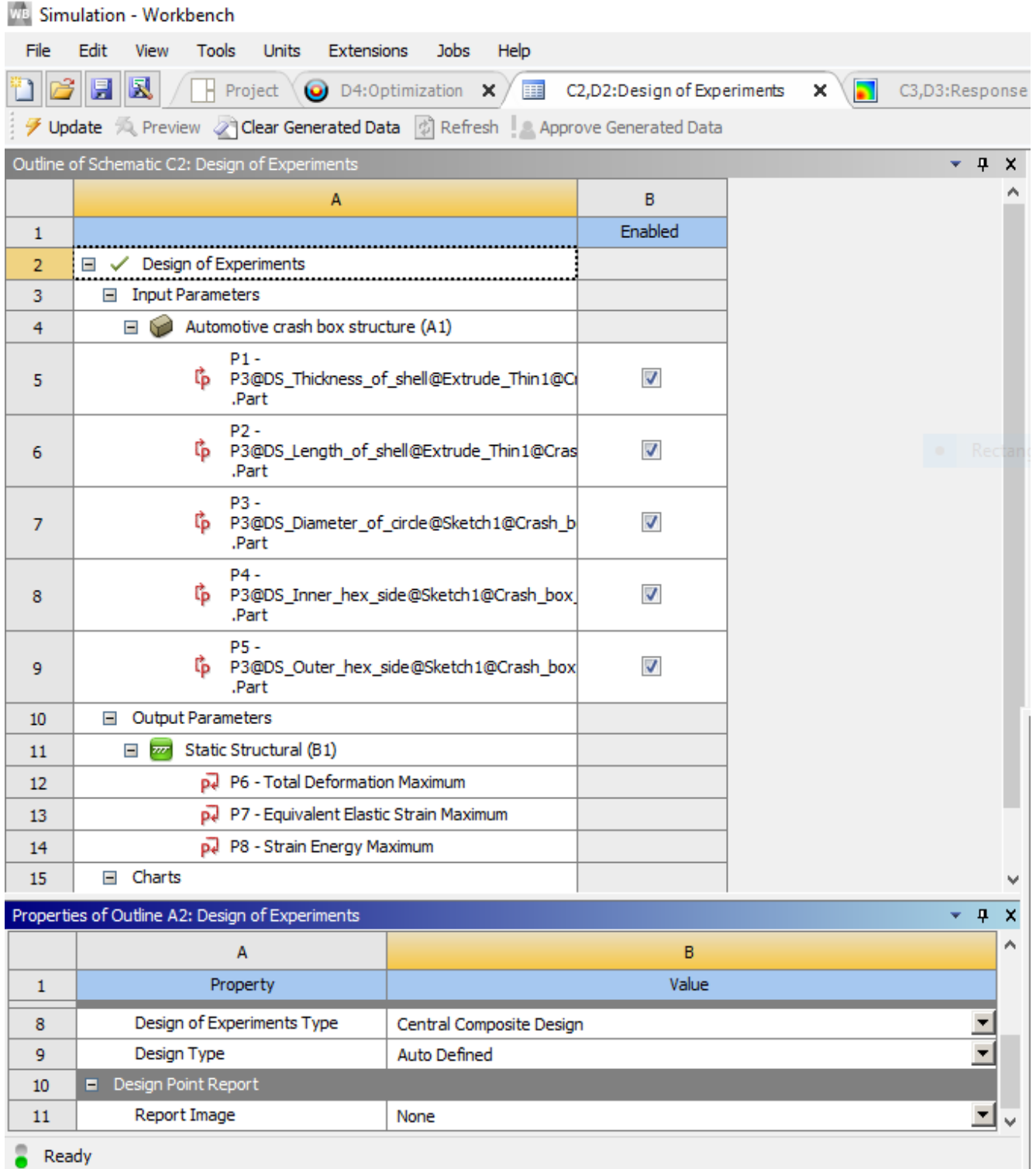
8. Deformation mode for design concept p-1 (SC-OHT)



## APPENDIX D

### DESIGNXPLORER(DX)

1. Response surface analysis with designXplorer.



## 2. Outline of schematic B2 design of experiment

Simulation - Workbench

File View Tools Units Extensions Jobs Help

Project C2,D2:Design of Experiments C3,D3:Response Surface

Update Preview Clear Generated Data Refresh Approve Generated Data

Outline of Schematic C2: Design of Experiments

	A	B
1		Enabled
2		
3	Design of Experiments	
4	Automotive crash box structure (A1)	
5	P1 - P3@DS_Thickness_of_shell@Extrude_Thin1@Crash_Box.Part	<input checked="" type="checkbox"/>
6	P2 - P3@DS_Length_of_shell@Extrude_Thin1@Crash_Box.Part	<input checked="" type="checkbox"/>
7	P3 - P3@DS_Diameter_of_circle@Sketch1@Crash_Box.Part	<input checked="" type="checkbox"/>
8	P4 - P3@DS_Inner_hex_side@Sketch1@Crash_Box.Part	<input checked="" type="checkbox"/>
9	P5 - P3@DS_Outer_hex_side@Sketch1@Crash_Box.Part	<input checked="" type="checkbox"/>
10	Output Parameters	
11	Static Structural (S1)	
12	P6 - Total Deformation Maximum	
13	P7 - Equivalent Elastic Strain Maximum	
14	P8 - Strain Energy Maximum	
15	Charts	
16	Parameters Parallel	<input checked="" type="checkbox"/>
17	Design Points vs Parameter	<input checked="" type="checkbox"/>

Table of Outline A2: Design Points of Design of Experiments

	A	B	C	D
1	Name	P1 - P3@DS_Thickness_of_shell@Extrude_Thin1@Crash_Box.Part	P2 - P3@DS_Length_of_shell@Extrude_Thin1@Crash_Box.Part	P3@DS_Diameter_of_circle@Sketch1@Crash_Box.Part
2	1	0.9	240	60
3	2	1.1	240	60
4	3	1	240	60
5	4	1	216	60
6	5	1	264	60
7	6	1	240	54
8	7	1	240	66
9	8	1	240	60
10	9	1	240	60
11	10	1	240	60
12	11	1	240	60
13	12	0.97167	233.2	58.3
14	13	1.0283	233.2	58.3
15	14	0.97167	246.8	58.3
16	15	1.0283	246.8	58.3
17	16	0.97167	233.2	61.7
18	17	1.0283	233.2	61.7
19	18	0.97167	246.8	61.7
20	19	1.0283	246.8	61.7
21	20	0.97167	233.2	58.3
22	21	1.0283	233.2	58.3
23	22	0.97167	246.8	58.3
24	23	1.0283	246.8	58.3
25	24	0.97167	233.2	61.7
26	25	1.0283	233.2	61.7
27	26	0.97167	246.8	61.7
28	27	1.0283	246.8	61.7

Properties of Outline A2: Design of Experiments

Ready

Chart: No data

## 3. Sample chart of the schematic response surface

Simulation - Workbench

File Edit View Tools Units Extensions Jobs Help

Project C2,D2:Design of Experiments C3,D3:Response Surface D4:Optimization

Update Clear Generated Data Refresh Send Study to DPS Project

Outline of Schematic D4: Optimization

	A	B	C	D
1				
2	Optimization Study			
3	Maximize P6	Goal, Maximize P6 (Default importance)		
4	Maximize P7	Goal, Maximize P7 (Default importance)		
5	Maximize P8	Goal, Maximize P8 (Default importance)		
6	Optimization Method			
7	MOGA	The MOGA method (Multi-Objective Genetic Algorithm) is a variant of the popular NSGA-II (Non-dominated Sorted Genetic Algorithm-II) based on controlled elitism concepts. It supports multiple objectives and constraints and aims at finding the global optimum.		
8	Configuration	Generate 5000 samples initially, 1000 samples per iteration and find 3 candidates in a maximum of 20 iterations.		
9	Status	Converged after 8811 evaluations.		
10	Candidate Points			
11		Candidate Point 1	Candidate Point 2	Candidate Point 3
12	P1 - P3@DS_Thickness_of_shell@Extrude_Thin1@Crash_Box.Model.Part	1.007	1.000	1.004

Parameter Relationships

Convergence Criteria

Results

Candidate Points

Tradeoff

Samples

Sensitivities

Properties of Outline : Samples

	A	C
1	Property	Enable
2	Coloring method	
3		
4		
5		
6		
7	Input Parameters	
8	P1 - P3@DS_Thickness_of_shell@Extrude_Thin1@Crash_Box.Part	<input checked="" type="checkbox"/>
9	P2 - P3@DS_Length_of_shell@Extrude_Thin1@Crash_Box.Part	<input checked="" type="checkbox"/>
10	P3 - P3@DS_Diameter_of_circle@Sketch1@Crash_Box.Part	<input checked="" type="checkbox"/>
11	P4 - P3@DS_Inner_hex_side@Sketch1@Crash_Box.Part	<input checked="" type="checkbox"/>
12	P5 - P3@DS_Outer_hex_side@Sketch1@Crash_Box.Part	<input checked="" type="checkbox"/>

Samples Chart

1.1 264 66.001 77.001 110 3.3068 2.812 7.5709

0.89999 216 53.999 62.999 89.999 2.7045 2.5706 5.4994

P1 P2 P3 P4 P5 P6 (x10<sup>-1</sup>) [m] P7 (x10<sup>-1</sup>) [m<sup>-1</sup>] P8 (x10<sup>-1</sup>) [J]

Ready

Job Monitor... No DPS Connection Show Progress Show 0 Messages

## 4. Goodness of Fit

